

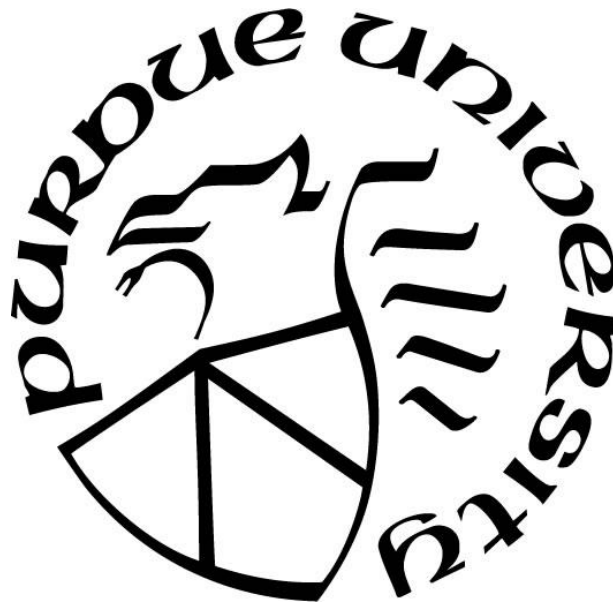
# **INVESTIGATION OF FIRE SAFETY CHARACTERISTICS OF ALTERNATIVE AVIATION FUELS**

by  
**Vikrant Goyal**

**A Dissertation**

*Submitted to the Faculty of Purdue University  
In Partial Fulfillment of the Requirements for the degree of*

**Doctor of Philosophy**



School of Mechanical Engineering  
West Lafayette, Indiana  
December 2019

**THE PURDUE UNIVERSITY GRADUATE SCHOOL**  
**STATEMENT OF COMMITTEE APPROVAL**

**Dr. Jay P. Gore, Chair**

School of Mechanical Engineering

**Dr. Robert P. Lucht**

School of Mechanical Engineering

**Dr. Li Qiao**

School of Aeronautics and Astronautics

**Dr. Gozdem Kilaz**

School of Engineering Technology

**Approved by:**

Dr. Jay P. Gore

*Dedication to  
My grandparents, parents, siblings, and friends*

## ACKNOWLEDGMENTS

Firstly, I would like to express my gratitude to Prof. Jay Gore for his constant support and guidance throughout my graduate program. Prof. Gore has always inspired me and encouraged me to perform well. I not only found an advisor in Prof. Gore, but also a friend, who has been a constant pillar of motivation and support. His deep insights in the field of combustion and about life, in general, have helped me to grow as a person. I am also very thankful to Prof. Li Qiao for being on my committee. My sincere thanks to Prof. Gozdem Kilaz for being on my committee and sharing her knowledge of fuel chemistry. I am also very thankful to Prof. Robert Lucht for constant support during various stages of work and also for being on my committee.

I want to thank all my research group members, especially Yerbatty Tursyn, Rathziel Roncancio, Raju Hasti, Jupyong Kim, Abhishek Navarkar, and Seunghyun Jo, for their constant support. They have been very helpful in completing the project targets.

I am deeply indebted to my grandparents, parents, siblings, and friends for always being there. Without them, none of this would have been possible. They have always supported me and have been a source of my inspiration.

I am thankful to the Federal Aviation Administration for supporting the projects for a major part of my graduate studies. I am also indebted to the School of Mechanical Engineering, Purdue University for its support.

# TABLE OF CONTENTS

LIST OF TABLES .....	7
LIST OF FIGURES .....	9
LIST OF ABBREVIATIONS .....	13
ABSTRACT.....	14
1. HOT SURFACE IGNITION - INTRODUCTION.....	16
1.1 Background .....	16
1.2 Objective .....	20
2. HOT SURFACE IGNITION APPARATUS .....	21
2.1 Apparatus overview .....	21
2.2 Apparatus Design Characteristics .....	22
2.3 Test matrix & Data acquisition .....	25
2.4 Data analysis .....	27
3. HOT SURFACE IGNITION RESULTS .....	30
3.1 Turbine engine fuels.....	30
3.1.1 Effect of Drop Height .....	30
3.1.2 Effect of Surface Curvature .....	33
3.1.3 HSIT Comparison.....	35
3.2 Piston Engine Fuels.....	37
3.2.1 Baseline Fuel – Avgas 100LL .....	37
3.2.2 Test Fuel A .....	40
3.2.3 Test Fuel B.....	46
3.2.4 Test Fuel C .....	52
3.2.5 Test Fuel D .....	57
4. POOL FIRE - INTRODUCTION.....	63
4.1 Objective .....	63
4.2 Background .....	64
5. POOL FIRE APPARATUS .....	74
5.1 Apparatus Overview .....	74
5.2 Apparatus Design Characteristics .....	78

5.2.1	Testing pan.....	78
5.2.2	Re-circulator heater .....	80
5.2.3	Fuel heating vessel.....	80
5.2.4	Fuel ignition system.....	81
5.2.5	Fire extinguishment methods.....	82
5.2.5.1	Lid-actuation System .....	83
5.2.5.2	CO <sub>2</sub> Extinguishment System .....	83
6.	FLAME SPREAD RATE .....	84
6.1	HEFA-50.....	89
6.2	Jet-A.....	98
6.3	Fischer Tropsch-IPK (FT-IPK).....	100
6.4	Synthetic Iso-paraffin (SIP) .....	100
7.	FLAME PROPAGATION ANALYSIS .....	105
7.1	Critical Transition Temperatures .....	105
7.2	Precursor Blue flame and Main Yellow flame.....	109
8.	CONCLUSION.....	111
	REFERENCES .....	113
	PUBLICATIONS.....	116
	APPENDIX A – HSI EXPERIMENTAL APPARATUS DESIGN .....	117
	APPENDIX B – HSI TEST PROCEDURES .....	121
	APPENDIX C – ADDITIONAL TEST DATA: HSI .....	123
	APPENDIX D – POOL FIRE APPARATUS DESIGN FILES .....	128
	APPENDIX E – Pool Fire Experiment Test Procedures .....	134

## LIST OF TABLES

Table 2-1: Comparison between current and past experimental apparatus of HSIT .....	24
Table 2-2: Test matrix .....	25
Table 2-3: Results for n-heptane .....	28
Table 2-4: n-heptane HSITs and logistic regression coefficients .....	29
Table 3-1: Test fuels properties .....	30
Table 3-2: Comparison of HSIT of n-heptane and Jet-A at 30cm and 25cm drop height .....	32
Table 3-3: Comparison of HSIT of JP-8 and Jet-A at flat and cylindrical surfaces .....	34
Table 3-4: Comparison of HSIT of test fuels .....	35
Table 3-5: Results for the Avgas 100LL .....	37
Table 3-6: Results for Test Fuel A .....	40
Table 3-7: Data comparison of the test fuel A with the baseline fuel .....	44
Table 3-8: Results for the Test Fuel B .....	46
Table 3-9: Data comparison of the test fuel B with the baseline fuel .....	50
Table 3-10: Results for the test fuel C .....	52
Table 3-11: Data comparison of the test fuel C with the Avgas 100LL .....	55
Table 3-12: Results for the test fuel D .....	57
Table 3-13: Comparison of the test fuel D with the baseline fuel .....	61
Table 4-1: Key experimental studies of flame spread rate over liquid fuels since 1994 .....	64
Table 5-1: Laser Specifications .....	81
Table 6-1: Fuel properties .....	84
Table 6-2: Jet-A composition [31-32] .....	85
Table 6-3: HEFA-50 composition [31-32] .....	85
Table 6-4: FT-IPK Composition [31-32] .....	86
Table 6-5: SIP composition [31-32] .....	86
Table 6-6: Test matrix for fuel initial temperature above flashpoint .....	88
Table 6-7: Flame arrival time for HEFA-50 at 80°C initial temperature .....	89
Table 6-8: Infrared camera filter specifications .....	91

Table 7-1: Test matrix to determine the critical transition temperature .....	107
Table 7-2: Critical Transition Fuel Initial Temperatures .....	109



## LIST OF FIGURES

Figure 1-1: Flammability and ignition regimes as a function of temperature and fuel vapor pressure [2].....	16
Figure 1-2: Auto-ignition apparatus [1].....	17
Figure 1-3: Experimental arrangement used by Colwell & Reza [2] .....	18
Figure 1-4: Experimental arrangement used by Davis et al. [5] .....	19
Figure 2-1: Hot surface ignition apparatus .....	21
Figure 2-2: Stainless steel plate bolted to the copper plate assembly containing five 1000 W cartridge heaters .....	22
Figure 2-3: Fiberglass insulation .....	23
Figure 2-4: Syringe pump configuration.....	23
Figure 2-5: Temperature variations (°C) as a function of time (seconds) inside the stainless steel plate at 750°C set temperature .....	26
Figure 2-6: Ignition probability curve of n-heptane as a function of temperatures (°C) .....	29
Figure 3-1: HSI apparatus illustrating drop height (H).....	31
Figure 3-2: Ignition probability of n-heptane, Jet-A and JP-8 as a function of surface temperature (°C) and drop height (H) .....	31
Figure 3-3: Ignition event over the cylinder .....	33
Figure 3-4: Comparison of ignition probability curves of Jet-A and JP-8 .....	33
Figure 3-5: Comparison of ignition probability curves of Heptane, JP-8, Jet-A, and JP-5 .....	35
Figure 3-6: Comparison of HSIT range of n-heptane and turbine engine fuels against their respective AIT.....	36
Figure 3-7: Ignition probability curve of Avgas 100LL as a function of surface temperature (°C) .....	38
Figure 3-8: Baseline fuel flame image at 810°C set temperature .....	39
Figure 3-9: High-speed camera images of the baseline fuel at 810°C set temperature .....	39
Figure 3-10: Ignition probability curve of Test Fuel A as a function of temperature (°C).....	41
Figure 3-11: Point ignition at 890°C surface temperature .....	42
Figure 3-12: Distributed ignition at 900°C surface temperature .....	42
Figure 3-13: High-speed camera images of flame propagation at 890°C set temperature .....	43

Figure 3-14: Comparison of ignition probability curve of Test Fuel A against Avgas 100LL ....	43
Figure 3-15: Plate after ignition tests – baseline fuel ( <i>top</i> ) and test fuel ( <i>bottom</i> ) .....	45
Figure 3-16: Ignition probability curve of the test fuel B as a function of temperature (°C) .....	47
Figure 3-17: Test fuel flame image – distributed ignition at 770°C set temperature .....	48
Figure 3-18: High speed camera images of the test fuel B at 740°C set temperature .....	49
Figure 3-19: Comparison of ignition probability curve of the test fuel B against the baseline fuel .....	49
Figure 3-20: Plate after ignition tests – baseline fuel 100 LL Avgas .....	51
Figure 3-21: Plate after ignition tests – test fuel B .....	51
Figure 3-22: Ignition probability curve of the test fuel C as a function of temperature (°C) .....	53
Figure 3-23: Test fuel flame image – distributed ignition at 840°C set temperature .....	54
Figure 3-24: High speed camera images for the test fuel C at 840°C set temperature .....	54
Figure 3-25: Comparison of ignition probability curve of the test fuel C against the baseline fuel .....	55
Figure 3-26: Plate after ignition tests – baseline fuel ( <i>top</i> ) and test fuel C ( <i>bottom</i> ).....	56
Figure 3-27: Ignition probability curve of the test fuel D as a function of temperature (°C) .....	58
Figure 3-28: Test fuel D flame image – distributed ignition at 810°C set temperature.....	59
Figure 3-29: High speed camera images of the test fuel D at 810°C set temperature .....	60
Figure 3-30: Comparison of ignition probability curve of the test fuel D against Avgas 100LL.	60
Figure 3-31: Plate after ignition tests – baseline fuel Avgas 100LL .....	61
Figure 3-32: Plate after ignition tests – and test fuel D .....	62
Figure 4-1: Experimental apparatus for determining the flame spread rate by White et. al. [11]	66
Figure 4-2: Flame spread rates of JP-5 (left) and JP-8 (right) fuels as a function of initial fuel temperature [11].....	66
Figure 4-3: Experimental apparatus by Li et al. for determining the flame spread rate [4] .....	67
Figure 4-4: Flame spread rates of 0#diesel and RP5 fuels as a function of initial fuel temperature [11-15].....	68
Figure 4-5: Effect of the pan width ( <i>left</i> ) and pan depth ( <i>right</i> ) on the flame spread rate [26] ....	69
Figure 4-6: Effect of the pan length to the flame spread rate [26].....	70
Figure 4-7: Flame spread regimes for methanol described by Akita [29]. .....	71

Figure 4-8: Schematic of the flame spread along the fuel surface below the flashpoint by Mackinven [26] .....	71
Figure 4-9: Schematic representation of flame propagation over the fuel maintained at a temperature below its flashpoint [15] .....	72
Figure 5-1: CAD image of the experimental apparatus .....	75
Figure 5-2: Complete experimental apparatus .....	76
Figure 5-3: P&ID of the experimental apparatus .....	77
Figure 5-4: Isometric view of the rectangular pool .....	78
Figure 5-5: Front view of the rectangular pool .....	79
Figure 5-6: CAD models of top test pan ( <i>top</i> ) and bottom ( <i>bottom</i> ) pan .....	79
Figure 5-7: Re-circulator heater .....	80
Figure 5-8: Fuel heating vessel .....	80
Figure 5-9: Ray diagram for laser ignition .....	81
Figure 5-10: Laser Ignition and flame-spread process overheated Jet-A pool .....	82
Figure 5-11: Lid-Actuation system .....	83
Figure 5-12: CO <sub>2</sub> fire extinguisher system .....	83
Figure 6-1: Gas-phase thermocouple locations .....	87
Figure 6-2: Pairs of high-speed ( <i>top</i> ) and regular ( <i>bottom</i> ) at identical times for HEFA-50 at 80°C .....	90
Figure 6-3: Infrared camera images showing flame propagation at few specific thermocouple locations for HEFA-50 at initial temperature 80°C .....	91
Figure 6-4: Liquid phase thermocouple responses for HEFA-50 fuel at 80°C .....	92
Figure 6-5: Gas phase thermocouple responses for HEFA-50 fuel at 80°C .....	93
Figure 6-6: Liquid phase thermocouple responses for HEFA-50 fuel at room temperature .....	94
Figure 6-7: Gas-phase thermocouple responses for HEFA-50 fuel at room temperature .....	94
Figure 6-8: Regular ( <i>left</i> ) and high-speed ( <i>right</i> ) camera video frames for HEFA-50 fuel at initial temperature 25°C and time-steps between 0 to 25 seconds .....	95
Figure 6-9: High-speed video frames of flame propagation over HEFA-50 fuel surface for different initial temperatures at 0.8 seconds .....	96
Figure 6-10: Flame spread rate for HEFA-50 fuel for different initial fuel temperatures .....	97
Figure 6-11: Pairs of high-speed ( <i>top</i> ) and regular ( <i>bottom</i> ) frames at identical times of flame propagation over Jet-A at initial temperature of 80°C .....	98

Figure 6-12: Flame spread rate for Jet-A fuel for different initial fuel temperatures .....	99
Figure 6-13: Flame spread rate comparison of Jet-A with JP-8 (White et al.) .....	99
Figure 6-14: Flame spread rate for FT-IPK fuel for different initial fuel temperatures .....	100
Figure 6-15: Flame spread rate for SIP fuel for different initial fuel temperatures .....	101
Figure 6-16: Flame spread rates for Jet-A, HEFA-50, FT-IPK and SIP fuels at different initial temperatures .....	102
Figure 6-17: Flame-spread regimes based on initial fuel temperatures .....	103
Figure 6-18: Liquid phase controlled flame propagation .....	103
Figure 6-19: Gas-phase controlled flame propagation.....	104
Figure 7-1: Critical transition temperature range for all fuels .....	105
Figure 7-2: Blue flame front image frames for different initial fuel temperatures at same location .....	106
Figure 7-3: Flame front image for 70°C ( <i>left</i> ) and 90°C ( <i>right</i> ) initial HEFA-50 fuel temperatures at identical times .....	108
Figure 7-4: Yellow flame and blue flame spread rate over all test fuels .....	110

## LIST OF ABBREVIATIONS

AIT	Auto-ignition temperature
FT-IPK	Fischer-Tropsch-IPK
HSI	Hot surface ignition
HSIT	Hot surface ignition temperature
HEFA	Hydro-processed esters and fatty acids
IR	Infrared
NFPA	National Fire Protection Association
SIP	Synthetic Iso-paraffin
$T_{i-1}$	Starting temperature for hot surface ignition test, K
$T_{ign-1}$	Temperature corresponding to 1 <sup>st</sup> visually observed temperature, K
$T_{ign-50}$	50% ignition probability temperature, K
$T_{ign-100}$	100% ignition probability temperature, K
TC	Thermocouple

## ABSTRACT

Due to the depletion of fossil fuel reserves and emission challenges associated with its usage, there is a need for alternative aviation fuels for future propulsion. The alternative fuels with handling, storage and combustion characteristics similar to conventional fuels can be used as “drop-in” fuels without significant changes to the existing aviation infrastructure. Fire safety characteristics of alternative aviation fuels have not been studied intensively and therefore research is needed to understand these characteristics. In this study, fire safety characteristics namely hot surface ignition (HSI) and flame spread phenomena are investigated for alternative aviation fuels.

HSI is defined as the process of a flammable liquid coming in contact with a hot surface and evaporating, mixing and reacting with the surrounding oxidizer with self-supporting heat release (combustion). If all the conditions are adequate, the fuel may completely turn into combustion products following the ignition process. This work presents results from more than 5000 ignition tests using a newly developed reproducible test apparatus. A uniform surface temperature stainless steel plate simulating the wall of a typical exhaust manifold of an aircraft engine is used as the hot surface. Ignition tests confirmed that the ignition event is transient and initiates at randomly distributed locations on the hot surface. The results show many significant differences and some similarities in the ignition characteristics and temperatures of the different fuels. In this work, hot surface ignition temperatures (HSITs) are measured for nine hydrocarbon liquids. Five of these fuels are piston engine based, three fuels are turbine-engine based and one fuel is a pure liquid, heptane. The piston engine based fuels are given by FAA and are confidential and hence labeled as test fuels A, B, C, D for this study. The HSITs of these fuels are measured and compared against a baseline fuel 100 LL aviation gasoline (100LL Avgas). HSITs of conventional turbine engine based fuels namely Jet-A, JP-8, and JP-5 are also measured.

Flame spread along liquid fuel has been one of the important combustion phenomena that still requires more in-depth research and analysis for the deep understanding of the chemical processes involved. Flame spread rate determines how fast the flame spreads along the fuel surface and it is an important parameter to study for fire safety purposes. For the flame spread rates study, a novel experimental apparatus is designed and fabricated. The experimental apparatus consists of a

rectangular pan, a fuel heating system, an autonomous lid actuation system, a CO<sub>2</sub> fire extinguisher system, and a laser ignition system. The flame spread phenomenon is studied for conventional aviation fuel, namely, Jet-A and three alternative aviation fuels, namely, hydro-processed ester fatty acids (HEFA-50), Fischer-Tropsch – IPK (FT-IPK) and synthetic iso-paraffin (SIP). The experiments are conducted for a wide range of initial fuel temperatures ranging from 25°-100°C for Jet-A, HEFA-50, FT-IPK and from 80-140°C for SIP as the flash-point of SIP is 110°C and is ~3 times higher than that of other three fuels. The flame spread rate of all fuels increases exponentially with increasing fuel's initial temperature. Flame spread rate is as low as ~5 cm/sec for Jet-A, HEFA-50, FT-IPK for 25°C initial fuel temperature and goes to as high as 160 cm/sec for 80°C initial fuel temperature. For SIP based jet fuel, flame spread rate is ~160 cm/sec for initial fuel temperature of 140°C. Additionally, it was also found that the flame propagation consists of two types of flames: a precursor blue flame located ahead of the main yellow flame. These flames are more evident over the fuels' surface with initial fuel temperatures higher than their respective flash-points. The precursor blue flame propagates like a premixed flame and the main yellow flame propagates like diffusion combustion.

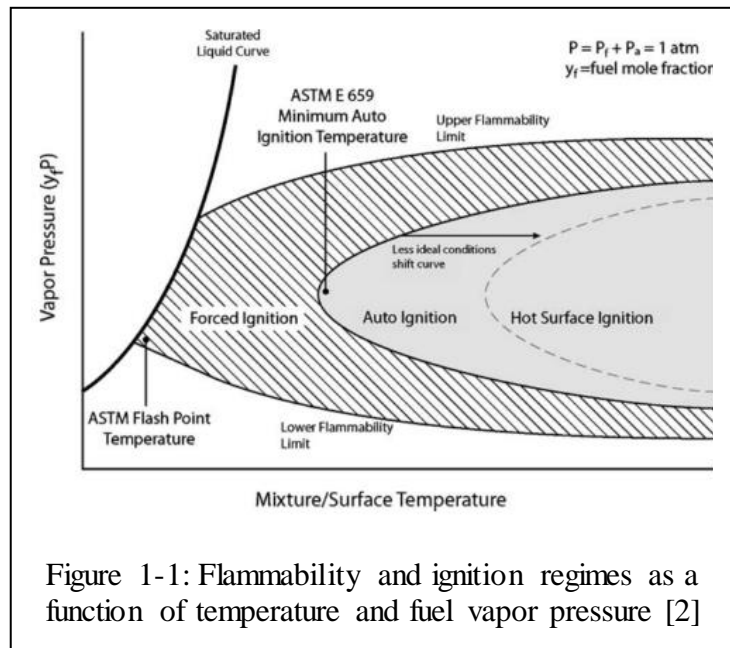
This dissertation includes eight chapters. Chapter 1 gives an overview of the work done until now in the field of hot surface ignition. Following this review, the experimental apparatus designed and fabricated for this study are discussed in Chapter 2. This chapter also talks about the test matrix, data acquisition tools and concludes with the data analysis method. In Chapter-3, HSITs of 3 turbine engine based fuels and 5 piston engine based fuels are reported. This chapter also discusses the effect of drop height and curvature (flat v/s cylindrical) for two fuels, Jet-A, and heptane. This concludes the work done in the field of HSI in this dissertation. Chapter 4 talks about the past work reported by various researchers in the field of flame spread phenomenon and key learnings from their work. Chapter 5 discusses the experimental apparatus designed and fabricated for flame spread phenomenon study. In chapter-6, flame spread rates of 4 alternative aviation fuels are reported. This chapter also discusses the flame spread mechanism associated with slower (liquid-phase controlled) and faster (gas-phase controlled) flame propagation. Chapter 7 discusses flame propagation which consists two types of flames: a precursor blue flame and a main yellow flame. Chapter 8 concludes the key findings of the hot surface ignition and flame spread phenomenon study in this research work.

# 1. HOT SURFACE IGNITION - INTRODUCTION

## 1.1 Background

U.S. fire departments reported 287,000 vehicle fires on an average per year from 2003-2007 [1]. These fires lead to an average of 480 civilian deaths, 1,525 civilian injuries, and \$1.3 billion in direct property damage [1]. And 29% of vehicle fires began with the ignition of flammable or combustible liquids, and 2% of these vehicle fires (~6600) originate from the heat sources which are very close to the flammables and combustibles [1]. There were 310 aircraft fires per year in 2003-2007, which accounted for 29 civilian deaths, 21 civilian injuries and \$44 million direct property damage [1]. Aircraft fires accounted for less than 1% of the total vehicle fires, but 6% of the associated deaths and 4.4% in direct property damage [1]. Hot surface ignition is, therefore, a phenomenon relevant to both automobile and aviation industries. Hot surface ignition is defined as the process of a flammable liquid encountering a hot surface and evaporating, mixing and reacting with the surrounding oxidizer with self-supporting heat release (combustion). If all the conditions are adequate, the fuel may completely turn into combustion products following the ignition process. The initiation and sustenance of the exothermic process depend on the heat of vaporization, mixing rate with the surrounding air, balance between the energy released during the initiation reactions and the rate of heat

loss. Among the various parameters, one of the most important parameters determining the probability of successful ignition is the temperature of the hot surface. Figure 1-1 shows how the mixing/surface temperature and the fuel vapor pressure (or fuel mole fraction) relate to the different ignition regimes, i.e. forced ignition, auto ignition, and hot surface ignition regime. From figure 1-1, it can also be



seen that if a less ideal condition such as a surface to which heat is lost, upon initiation of the



reaction, exists then higher temperatures are required for sustainable ignition. It can also be seen that the hot surface ignition temperatures are always higher than the auto-ignition temperatures. The auto-ignition temperature, as defined by the ASTM, is the temperature of a fuel-air mixture at which the mixture ignites at atmospheric pressure without an external source.

The NFPA (National Fire Protection Association) guidelines suggest that the HSIT of liquids in the open air is approximately 200°C (360°F) higher than the auto-ignition temperatures [3]. Auto-ignition temperatures of flammable liquids are obtained by using standardized tests such as ASTM E 659, shown in Figure 1-2. In the ASTM E 659 test, 100  $\mu$ L of fluid is dropped into a uniformly heated 500 mL glass flask containing air at a predetermined temperature. The liquid on entering the container evaporates and mixes with the surrounding air. The fuel and air mixture is then observed for 10 minutes or until auto-ignition occurs. As seen in figure 1-1, the mixing/surface temperature is a function of the mole fraction (represented by the partial vapor pressure of the fuel). Several tests are thus performed with different mole fractions until minimum auto-ignition temperature is obtained, as described in the test procedures followed for the ASTM E 659 test [2].

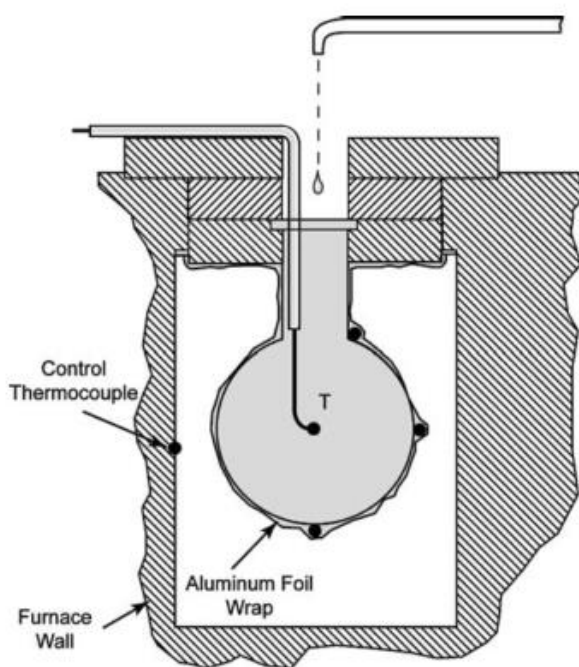


Figure 1-2: Auto-ignition apparatus [1]

As hot surfaces are often exposed, natural convection and forced airflows dilute and cool the flammable vapor requiring a higher supply of energy from the hot surface for a sustained reaction.

The additional energy can only be supplied by a hotter surface leading to an increase in the temperature necessary to achieve ignition. An improved understanding of the hot surface ignition processes is of significant interest to ensure the safety and integrity of aircraft engines and other components.

The research work described in this dissertation draws on the methods and measurements of the hot surface ignition temperatures for different aviation and automobile fuels, as reported by Colwell et al. [4] and Davis et al. [5]. They both measured the hot surface ignition temperatures for different aviation and automobile fuels. Colwell et al. used an experimental arrangement schematically shown in Figure 1-3. A single drop of fuel is delivered on to the hot surface every 15 seconds by using a 2 mL pipette [4].

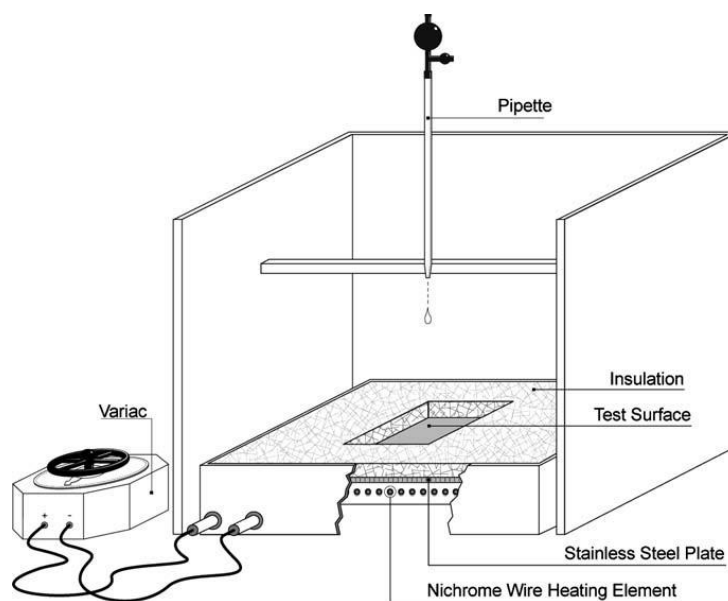


Figure 1-3: Experimental arrangement used by Colwell & Reza [2]

Colwell et al. concluded that the hot surface ignition phenomenon is a probabilistic event. Results showed that for all the liquids tested, hot surface ignition temperatures are always higher than their respective auto-ignition temperatures [4]. The experiment conducted by Davis et al. [5] involved spraying a constant volume of fuel (0.25 mL) onto a hot surface in a quiescent environment. The tested fuels are high octane leaded gasoline, methanol, and nitromethane. Electrical heating elements are used to supply energy to a stainless-steel plate, surrounded by insulation in order to prevent excessive heat loss. The arrangement is shown in Figure 1-4.

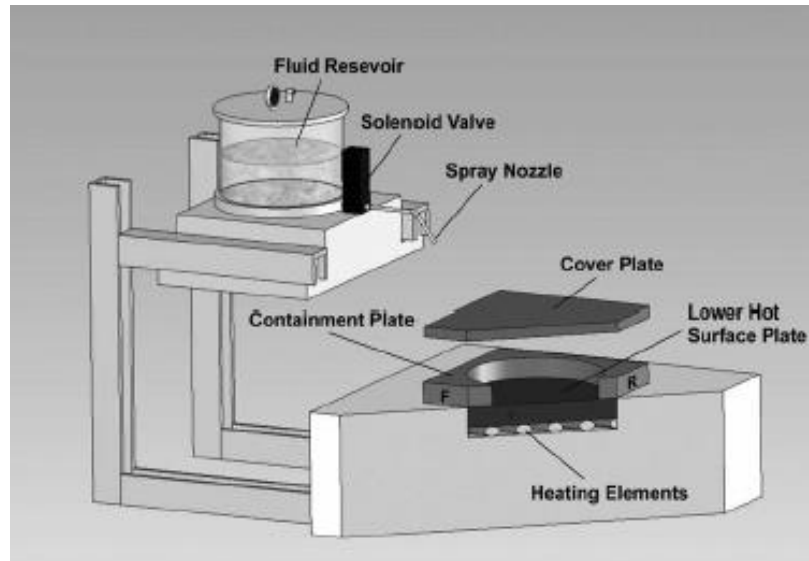


Figure 1-4: Experimental arrangement used by Davis et al. [5]

The hot surface plate is heated to an initial temperature of 200°C and then heated in steps of 10°C following five successive sprays of the liquid fuel in 1-minute intervals. The heating and spraying steps are repeated until the temperature reaches a value at which five successive ignitions representing a 100% probability of ignition over a sample size of 5 sprays are observed. The repeatability of the tests is checked by repeating the procedure and averaging the outcome over the 10 sprays at each surface temperature [5]. Davis et al. [5] found that hot surface ignition occurs over a range of temperatures with the probability of ignition increasing monotonically with temperature. The authors confirmed that the HSIT for all fuels is higher than the corresponding auto-ignition temperatures. Davis et al. [5] emphasized that certain fuels may have a lower auto-ignition temperature but a higher hot surface ignition temperature than the corresponding quantities for other fuels.

Johnson et al. measured the minimum hot surface ignition temperatures of five aircraft fluids, MIL-H-5606, MIL-H-83282, MIL-L-7806, JP-4 and JP-8. They used an air-heated bleed-air duct in a high realism test article [6]. For JP-8, minimum HSIT was found to be 1100°F when sprayed at 8 ml/second with 2 ft/second ventilation airflow [5]. Johnson et al. also found that heating ventilation airflow reduces the minimum HSIT.

In another study, Somandepalli et al. [8] measured the HSIT of ethanol, gasoline, E-85, diesel, and E-diesel. In studies [3-8], it was found that hot surface ignition occurs over a range of temperatures with the probability of ignition increasing monotonically with temperature. The authors confirmed that the HSIT for all fuels is higher than the corresponding auto-ignition temperatures. Davis et al. [5] emphasized that certain fuels may have a lower auto-ignition temperature but a higher hot surface ignition temperature than the corresponding quantities for other fuels. This observation confirms the need for the HSIT tests for the conventional and alternative aviation fuels described in the present study.

## **1.2 Objective**

- Design and fabricate an experimental apparatus to investigate the hot surface ignition temperature (HSIT) of a pure liquid n-heptane, three turbine engine fuels and five piston engine fuels.
- Compare the HSIT of alternative piston engine fuels with that of the baseline fuel.
- Study the effect of drop height (H) and surface curvature (flat v/s cylindrical) on the HSIT of turbine engine fuels.
- Visually assess the presence of residue following the ignition tests.

In the present study, an experimental apparatus consisting of a hot stainless-steel plate surface with controlled uniform surface temperature is employed to investigate the HSIT of the test fuels. The experimental apparatus designed for the present tests represents an improvement in the uniformity as well as repeatability of the temperature of the surface of the hot plate as discussed in the following sections.

## 2. HOT SURFACE IGNITION APPARATUS

### 2.1 Apparatus overview

A photograph of the experimental arrangement used in the present study is shown in Figure 2-1: Hot surface ignition apparatus.

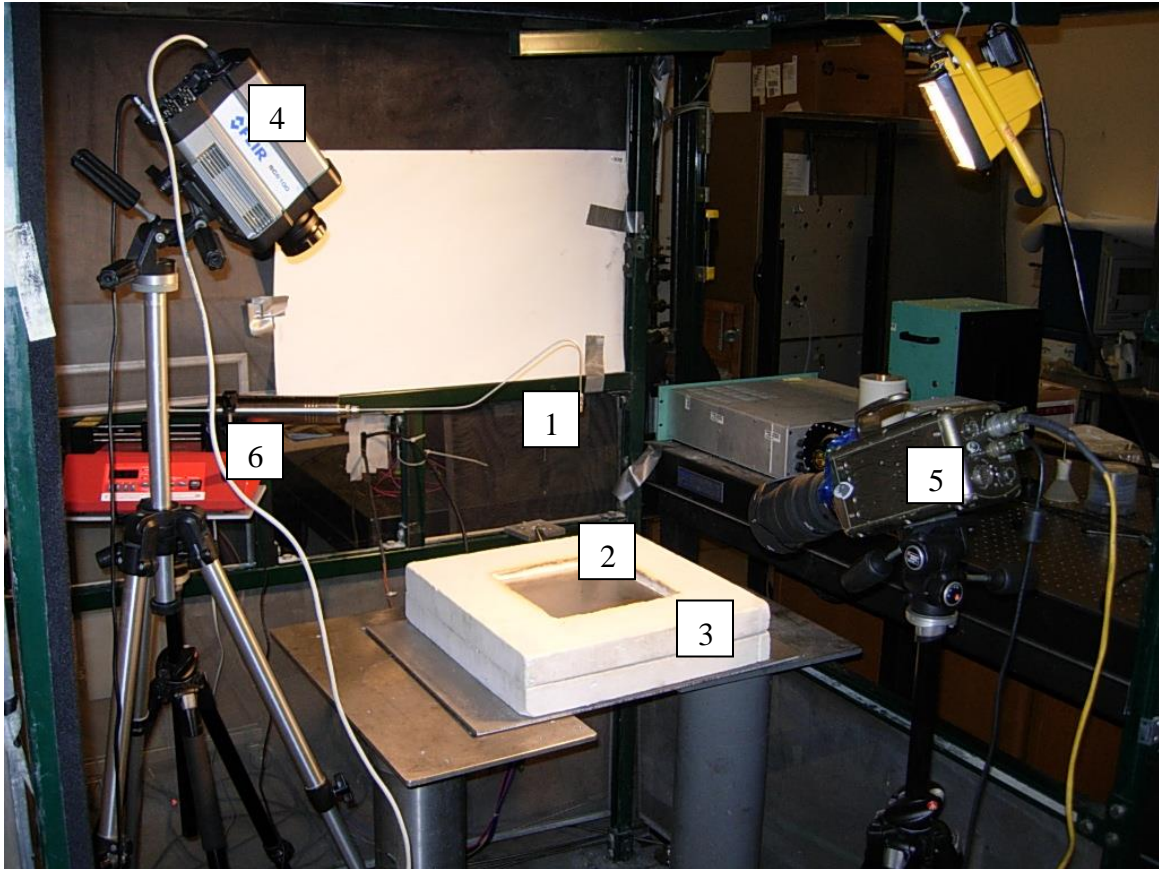


Figure 2-1: Hot surface ignition apparatus

The numbered components shown in figure 5 are as follows:

- 1) Fuel nozzle
- 2) Hot Surface plate (stainless steel plate)
- 3) High-temperature ceramic insulation
- 4) Infrared Camera
- 5) High-Speed Camera
- 6) Programmable syringe pump

## 2.2 Apparatus Design Characteristics

Figure 2-2 depicts the removable stainless-steel plate bolted to a copper plate assembly containing electrical heaters. A separate plate is manufactured for each individual fuel to avoid the potential effects of contamination of the surfaces on the measurements. The main components of the apparatus include a stainless steel plate, copper plate, cartridge heaters, temperature controller, and high-temperature ceramic insulation. The purpose of all rig components is discussed in this section. Five cartridge heaters are inserted into the high thermal conductivity copper plate (101) of 23 cm x 23 cm x 2.5 cm (9" x 9" x 1") size, each of them delivering 1000 Watts of power. Five K-type thermocouples are located along with these heating elements in order to provide feedback on the copper plate temperature and adjust the plate temperature using a temperature controller. The exposed hot surface is made of a 23 cm x 23 cm x 2.5 cm 304-stainless steel plate simulating the wall of a typical exhaust manifold of an aircraft engine. Five thermocouples are embedded in the hot surface plate and are accessible from the bottom of the two-plate assembly. These thermocouples give feedback on the stainless-steel plate temperature. The measured temperatures are estimated to be less than 5°C of the actual surface temperature since the junction of each thermocouple is only 0.25 cm below the surface of the plate.



Figure 2-2: Stainless steel plate bolted to the copper plate assembly containing five 1000 W cartridge heaters

The two plates are bolted with four 0.635 cm (0.25") black-oxide alloy steel bolts in order to ensure that the apparatus is secure and there is minimum contact resistance between the plates. A fiberglass insulation of 10.16 cm (4") thickness, shown in Figure 2-3, is placed around the two plates to reduce the heat losses due to convection and radiation.

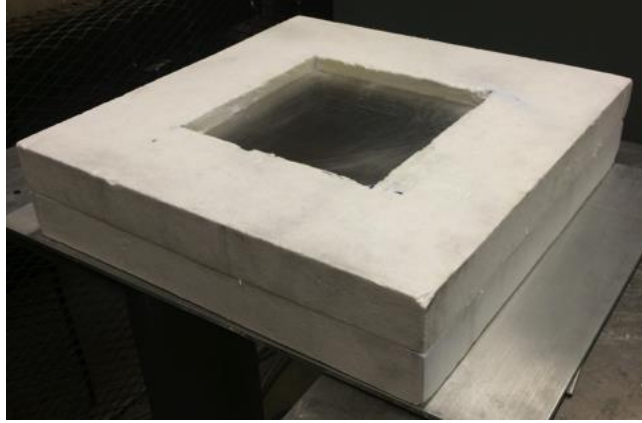


Figure 2-3: Fiberglass insulation

A 4.47 cm diameter, 200 mL stainless-steel syringe is chosen to ensure that there is sufficient fuel during the test as shown in Figure 2-4. A programmable syringe pump capable of applying 200 pounds of linear force is used to dispense the fuels onto the hot surface. Perfluoropolyether (PFPE) based lubricant is used for lubricating the stainless-steel syringe plunger O-rings. This lubricant was used because of its chemical inertness, thermal stability and non-flammability characteristics [5]. A bent stainless-steel tube is used to ensure vertical droplet orientation and to avoid trapped air in the syringe. A Swagelok fitting with a 0.32 cm (1/8") orifice diameter is used as a nozzle to dispense the fuel drop.

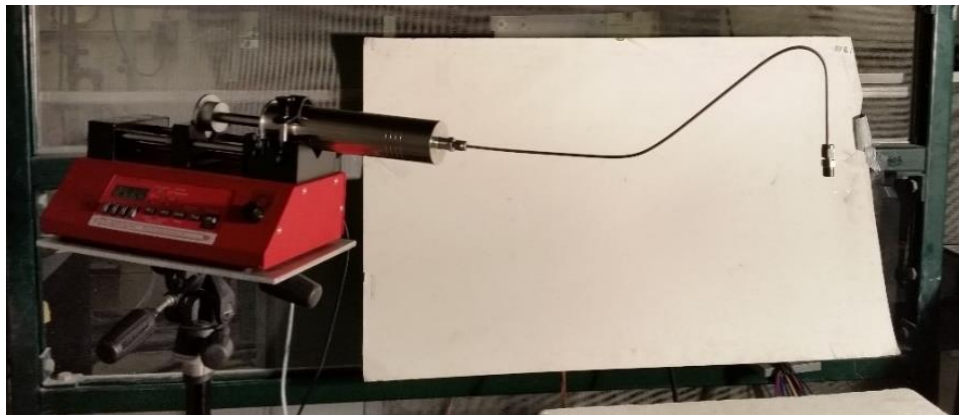


Figure 2-4: Syringe pump configuration

Data are acquired from 5 thermocouples each in the copper plate and the stainless-steel plate. A high-speed camera is also used to observe the origin and propagation of the ignition event on the hot surface. Table 2-1 shows a comparison between measurements of HSIT in the present study

and in prior studies. Future studies for assessing the dependence of the statistics of the HSIT on drop size, initial dispensation height, and velocity and the theoretical basis for these are highly recommended.

Table 2-1: Comparison between current and past experimental apparatus of HSIT

	<b>Davis et al. [4]</b>	<b>Colwell &amp; Reza [2]</b>	<b>Present study</b>
<b>Hot surface dimensions</b>	9" x 9" x 0.5" 304-stainless steel	18.9" x 18.9" x 0.2" 304-stainless steel	9" x 9" x 0.5" 304-stainless steel
<b>Fluid delivery System</b>	Nitrogen pressurized reservoir; an inline solenoid valve and a spray nozzle	2 mL pipette	Programmable syringe pump capable of dispensing desired fuel volume precisely
<b>Volume of fuel drop, <math>\mu\text{L}</math></b>	–	~ 20-30	~ 25
<b>Physical form/number of drops</b>	Spray/5 tests performed twice	200 drops	20 drops at each temperature
<b>Drop height</b>	–	25 cm	30 cm
<b>Temperature intervals between consecutive drop tests</b>	10°C	10°C	10°C
<b>Time interval between consecutive drops in a single drop test</b>	1 minute	15 seconds	10 seconds
<b>Temperature distribution near center of plate</b>	$\pm 20^\circ\text{C}$	$\pm 18^\circ\text{C}$	$\pm 5^\circ\text{C}$
<b>Hot surface covered between drop events?</b>	Yes	No	No



### 2.3 Test matrix & Data acquisition

The objective of the test is to determine the hot surface ignition temperature of the fuel. Hot surface ignition being a probabilistic event, the temperature is increased gradually until 100% ignition probability is observed. The number of ignitions is counted by visual observation of a luminous flame and is recorded using a DSLR and a high speed camera. Table 2-2: Test matrix below shows the test matrix developed for this study.

Table 2-2: Test matrix

	Set temperature in the copper plate	Temperature increment	Number of drops	Observation	Final Decision Point
<b>Test Phase #1</b>	$T_{i,1} = 400^{\circ}\text{C}$ $T_{f,1} = T_{\text{ign},i}$	$50^{\circ}\text{C}$	20 drops every 10 seconds at each set temperature	Report the temperature corresponding to the first ignition, $T_{\text{ign},i}$	Test phase is complete once the first ignition is observed
<b>Test Phase #2</b>	$T_{i,2} = T_{\text{ign},i} - 40^{\circ}\text{C}$ $T_{f,2} = T_{\text{ign},f}$ at 1 <sup>st</sup> Max. probability ignition temperature	$10^{\circ}\text{C}$		Report the temperatures corresponding to the different ignition probabilities	Test phase is complete once 20 successive ignitions are observed at two consecutive temperatures

A single experiment consists of two phases. Phase 1 testing determines the initial ignition temperature. Here,  $T_{i,1}$  is the starting temperature of the fuel test and is  $400^{\circ}\text{C}$  for all the fuels. Temperature is then increased by  $50^{\circ}\text{C}$  until the first ignition is observed, and the corresponding temperature,  $T_{\text{ign},i}$ , is recorded. Phase 2 testing begins by decreasing the set temperature to  $T_{\text{ign},i} - 40^{\circ}\text{C}$ , and then incrementing the set temperature by  $10^{\circ}\text{C}$ . Phase 2 concludes once 20 successive ignitions are observed at two consecutive temperatures and the temperature corresponding to 1<sup>st</sup> maximum probability ignition temperature,  $T_{\text{ign},f}$ , is recorded. The temperature of the copper plate is monitored and controlled using a six-zone On/Off-PID (proportional, integral and derivative) temperature controller. In the current experiment, binary (On-Off) control is used and the temperatures in the copper plate are monitored via the controller display. The controller is microprocessor-based and is connected to the signals from the five k-type thermocouples embedded in the copper plate along the cartridge heaters. The power to each cartridge heater is

automatically controlled to ensure plate temperatures remain uniform and within the user-defined control limits of the set temperature. The data acquisition is performed using a LabVIEW GUI that reports the temperature recorded by the five thermocouples placed in the stainless steel plate. The temperature difference between the stainless steel surface and the copper plate increases as the set temperature increases as heat losses due to conduction and radiation are higher at higher temperatures. For example, at the 400°C set temperature, the difference between the plate temperatures is 4°C, but at the 800°C set temperature, this difference increases to 12°C.

The temperatures recorded by the thermocouples located in the stainless steel plate are shown in Figure 2-5 as a function of time in seconds. The temperature variation with time is in the  $\pm 5^\circ\text{C}$  range for all thermocouple locations. As depicted in Appendix A1 – two thermocouples, TC1 and TC4, which are near the edge, showed lower temperatures than the three thermocouples, TC2, TC3, and TC5, which are near the center of the stainless steel plate. This is caused by the heat loss through the edges of the plates to the insulation. The temperature readings of the thermocouples in the stainless-steel plate are assumed to be close to the actual surface temperature since the junction of each thermocouple is 0.25 cm (0.1”) below the stainless steel plate surface. Most of the ignitions are initiated near the center of the hot surface and thus the average of the temperature readings recorded by the thermocouples placed near the center of plate, TC2, TC3, and TC5, are considered to be the stainless-steel surface temperatures for the data analysis described in the next section.

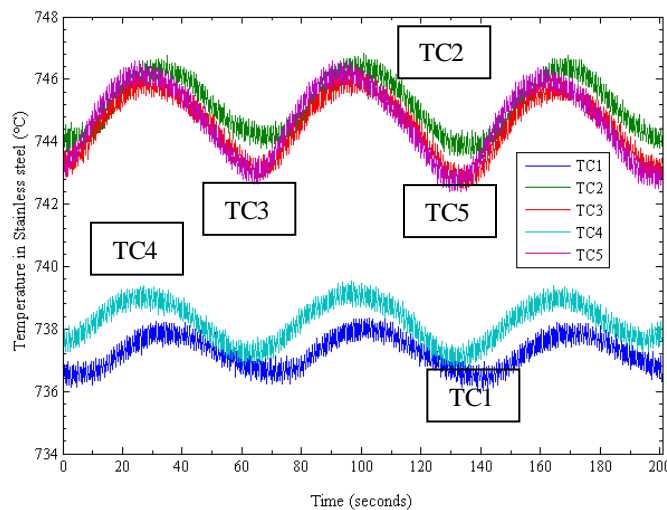


Figure 2-5: Temperature variations ( $^\circ\text{C}$ ) as a function of time (seconds) inside the stainless steel plate at 750°C set temperature

## 2.4 Data analysis

The hot surface ignition phenomenon is a probabilistic event. Ignition probability is defined as a ratio of the number of ignitions and the total number of drops. Ignitions count is recorded by the visual presence of a luminous flame. A curve fit is plotted in which the probabilities of ignition are defined as a function of the hot surface temperature using a Logistic function whose two parameters are evaluated using the lowest maximum and the highest minimum temperatures for ignition. The Logistic function is given by the following expression,

$$P(I) = \frac{\exp(b_0 + b_1 T)}{1 + \exp(b_0 + b_1 T)} \quad (1)$$

where,  $P(I)$  is the ignition probability corresponding to the measured temperature,  $T(^{\circ}\text{C})$  and  $b_0$  and  $b_1 (^{\circ}\text{C}^{-1})$  are the coefficients determined empirically by using the temperatures corresponding to the lowest measured probability of ignition ( $> 0$ ) and the highest measured probability of ignition ( $< 1$ ).

Each of the present experiments for the fuel leads to the following deliverables:

- Temperature corresponding to the minimum ignition probability point,  $T_{\text{ign,min}}$ ;
- Temperature corresponding to a 50% ignition probability point,  $T_{\text{ign,50}}$ ;
- Temperature corresponding to a maximum ignition probability point,  $T_{\text{ign,max}}$ ;
- Coefficients of the logistic regression curve fit  $b_0$  and  $b_1$ ;
- A plot of the ignition probability as a function of temperature; and
- A comparison of the ignition characteristics of an alternative fuel with those of the baseline fuel.

A test is performed with n-heptane in order to validate the test matrix and the test procedures used for this experiment. The properties of n-heptane supplied with the MSDS sheet are as follows:

- Density (at  $15^{\circ}\text{C}$ ) =  $680 \text{ kg/m}^3$
- AIT =  $204^{\circ}\text{C}$
- Flash-point =  $-4^{\circ}\text{C}$
- Relative vapor density (air = 1) = 3.5
- Boiling point =  $98.4^{\circ}\text{C}$

The results are shown in Table 2-3.

Table 2-3: Results for n-heptane

<b>Set temperature in the copper plate (°C)</b>	<b>Mean temperature in the stainless-steel plate (°C)</b>	<b># of Ignitions</b>	<b>P(I)</b>
400	398	0	0.00
500	496	0	0.00
600	597	0	0.00
650	646	0	0.00
660	668	0	0.00
670	662	0	0.00
680	671	0	0.00
690	679	1	0.05
700	686	3	0.15
710	691	4	0.20
720	699	9	0.45
730	706	16	0.80
740	713	17	0.85
750	721	20	1.00
760	729	20	1.00

In the table above, the “set temperature” is the temperature set on the temperature controller. The “mean temperature” is the average temperature recorded by the thermocouples, TC2, TC3 and TC5, which are near the center in the stainless-steel plate. The “# of ignitions” is the number of drops that ignited out of the 20 drops dropped on the hot surface and P(I) is the ignition probability.

From table 2-3, it can be seen that the first ignition is observed at a measured plate temperature of 679°C and 100% ignition probability is observed at 721°C. Ignition probability data along with a logistic curve fit as a function of temperature (°C) in Figure 2-6. A logistic fit 0.05 - 0.85 is plotted by using 5% ignition probability point corresponding to 679°C and 85% ignition probability corresponding to 713°C. The estimated temperature interval error bounds are shown as bars and

represent the highest and the lowest temperatures read by the thermocouples embedded in the stainless-steel plate. The results of the n-heptane tests are shown in table 2-4.

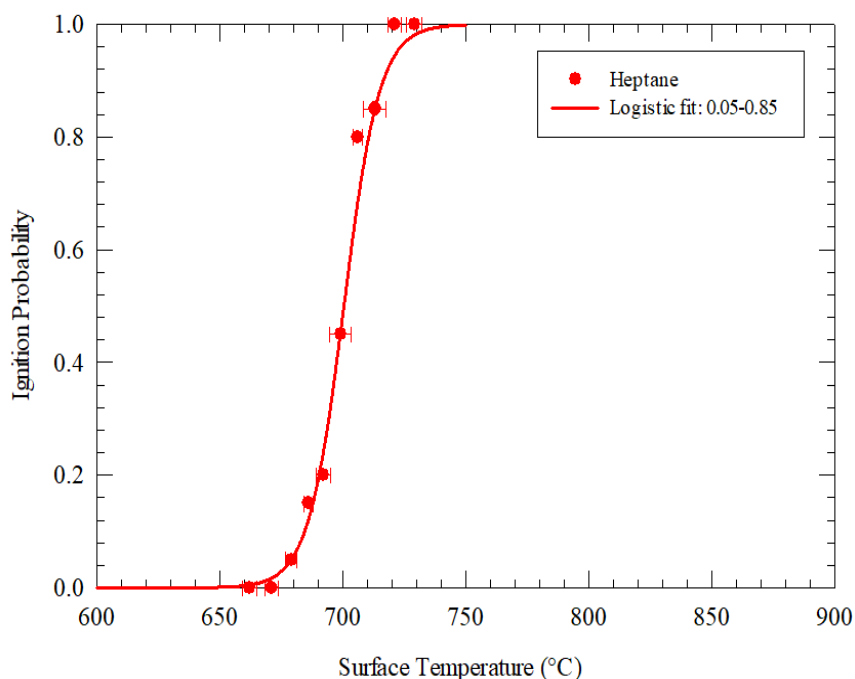


Figure 2-6: Ignition probability curve of n-heptane as a function of temperatures (°C)

Table 2-4 compares the temperature corresponding to the min. and max. ignition probability point against the ignition temperatures predicted by the logistic fit 0.05 - 0.85. As stated above, the logistic fit is plotted by using 5% ignition probability point corresponding to 679°C and 85% ignition probability corresponding to 713°C.

Table 2-4: n-heptane HSITs and logistic regression coefficients

Parameter	HSIT	
	Data	Logistic fit
Min. ignition probability temperature (°C)	679	679
50% ignition probability temperature (°C)	-	701
Max. ignition probability temperature (°C)	728	728
Logistic curve regression coefficients	$b_0 = -68.39$ ; $b_1 = 0.10^{\circ\text{C}^{-1}}$	

### 3. HOT SURFACE IGNITION RESULTS

#### 3.1 Turbine engine fuels

Hot surface ignition temperatures are measured for turbine engine based fuels namely Jet-A, JP-8, and JP-5. JP-8 and JP-5 are military-grade aviation kerosene fuels. More than 2600 ignition tests are conducted for these fuels. Properties of these fuels are listed in Table 3-1: Test fuels properties\*.

Table 3-1: Test fuels properties\*

<b>Fuel</b>	<b>Density (@ 15°C) kg/m<sup>3</sup></b>	<b>AIT (°C)</b>	<b>Flash Point (°C)</b>	<b>Relative Vapor Density (Air =1)</b>	<b>Boiling temperature (°C)</b>
Jet-A	775	210	37.8	4.5	149-300
JP-8	775	210	38	4.5	140-300
JP-5	800	246	> 60	4.5	140-300

*\*Source: Fuel Suppliers*

From the table 3-1, it should be noticed that AIT of Jet-A, JP-8, and JP-5 is ~200°C. Higher AIT implies higher minimum hot surface ignition temperature. HSIT measurements of the abovementioned liquids are conducted in three phases and are reported in this section. In the first phase, 800 ignition tests are conducted with n-heptane and Jet-A to study the effect of drop height on ignition probability. In the second phase, 800 ignition tests of JP-8 and Jet-A are conducted to study the effect of curvature (flat vs cylindrical) on HSIT. In the third phase, 1000 ignition tests are conducted to measure and compare the HSIT of all test fuels.

##### 3.1.1 Effect of Drop Height

The distance between the hot surface and the fuel nozzle is an important variable and defined as drop height (Figure 3-1: HSI apparatus illustrating drop height (H)). The number of secondary droplets formed after primary droplet impingement on the hot surface strongly depends on the drop height. Preliminary tests are conducted with 15 cm drop height and it showed flame stabilization

on the fuel nozzle. For a safe and reproducible ignition results, HSIT of Jet-A, and JP-8 are measured and compared against the HSIT of pure liquid n-heptane at 25 cm and 30 cm drop height.

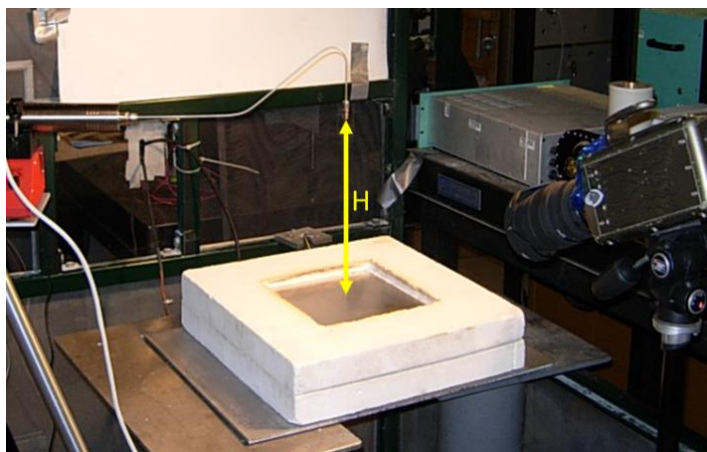


Figure 3-1: HSI apparatus illustrating drop height (H)

At each surface temperature, 20 drops are injected onto the hot surface and ignition is recorded by the visual presence of the flame. Figure 3-2 shows the ignition probability data along with a logistic curve fit corresponding to both drop heights are plotted as a function of surface temperature ( $^{\circ}\text{C}$ ).

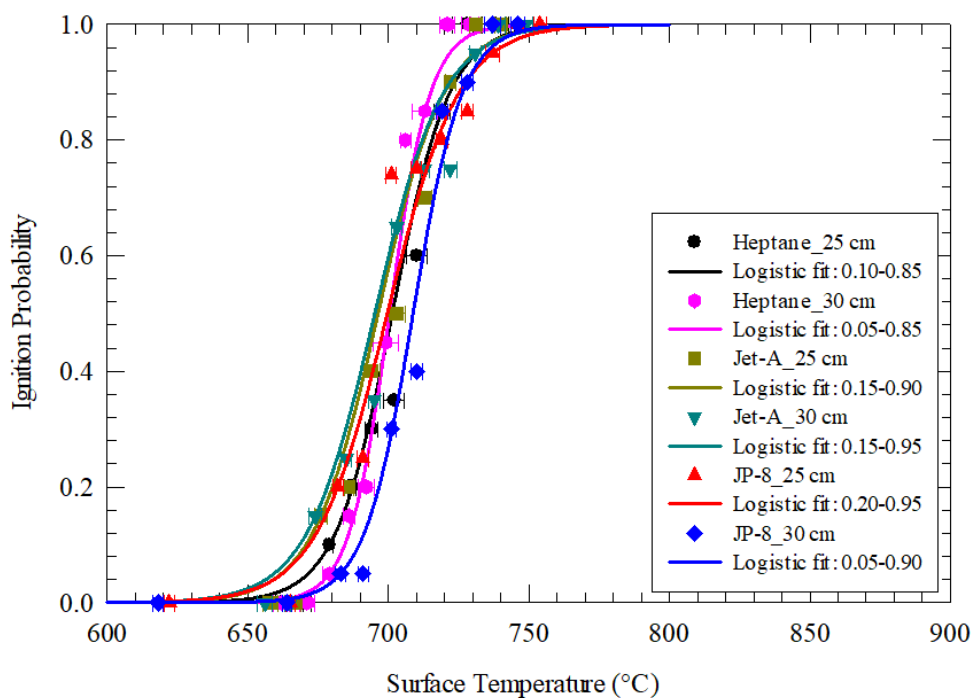


Figure 3-2: Ignition probability of n-heptane, Jet-A and JP-8 as a function of surface temperature ( $^{\circ}\text{C}$ ) and drop height (H)

For n-heptane at 25 cm drop height, a logistic fit 0.10 - 0.85 is plotted by using 10% ignition probability point corresponding to 679°C and 85% ignition probability corresponding to 719°C. At 30 cm drop height, a logistic fit 0.05 - 0.85 is plotted by using 5% ignition probability point corresponding to 679°C and 85% ignition probability corresponding to 713°C.

For Jet-A at 25 cm drop height, a logistic fit 0.15 - 0.90 is plotted by using a 15% ignition probability point corresponding to 676°C and 90% ignition probability corresponding to 722°C. At 30 cm drop height, a logistic fit 0.15 - 0.95 is plotted by using 15% ignition probability point corresponding to 674°C and 95% ignition probability corresponding to 731°C.

For JP-8 at 25 cm drop height, a logistic fit 0.20 - 0.95 is plotted by using a 20% ignition probability point corresponding to 682°C and 95% ignition probability corresponding to 737°C. For 30 cm drop height, a logistic fit 0.05 - 0.90 is plotted by using 5% ignition probability point corresponding to 683°C and 90% ignition probability corresponding to 728°C.

Table 3-2: Comparison of HSIT of n-heptane and Jet-A at 30cm and 25cm drop height

<b>Fuel</b>	<b>n-heptane</b>		<b>Jet-A</b>	
<b>Drop height (H)</b>	<b>30 cm</b>	<b>25 cm</b>	<b>30 cm</b>	<b>25 cm</b>
Min. probability ignition temperature (°C)	679	679	674	676
Max. probability ignition temperature (°C)	721	728	739	731
Logistic curve regression coefficients	$b_0 = -96.39$ $b_1 = 0.14 \text{ } ^\circ\text{C}^{-1}$	$b_0 = -68.94$ $b_1 = 0.10 \text{ } ^\circ\text{C}^{-1}$	$b_0 = -57.06$ $b_1 = 0.082 \text{ } ^\circ\text{C}^{-1}$	$b_0 = -59.51$ $b_1 = 0.085 \text{ } ^\circ\text{C}^{-1}$

From Table 3-2, it can be concluded that the distance between the nozzle and the surface does not significantly affect the present comparison between the HSIT of different liquids. To prevent damage to the fuel nozzle and to ensure a repeatable fuel injection condition, a drop height of 30 cm is selected for all the tests. Drop height range from 15 cm to 30 cm is also consistent with prior HSIT experiments in the literature.



### 3.1.2 Effect of Surface Curvature

The effect of surface curvature is studied in this section. Hot surface ignition tests with JP-8 and Jet-A are performed on the flat and cylindrical surfaces with 30 cm drop height. A stainless steel 304 cylinder with a 3-inch diameter and 6-inch length is used for this comparative study. The cylinder is heated using a 1 kW cartridge heater inserted along the center annulus of the cylinder. Figure 3-4 shows the ignition event as JP-8 is dispensed onto the hot cylinder maintained at 850°C set temperature.

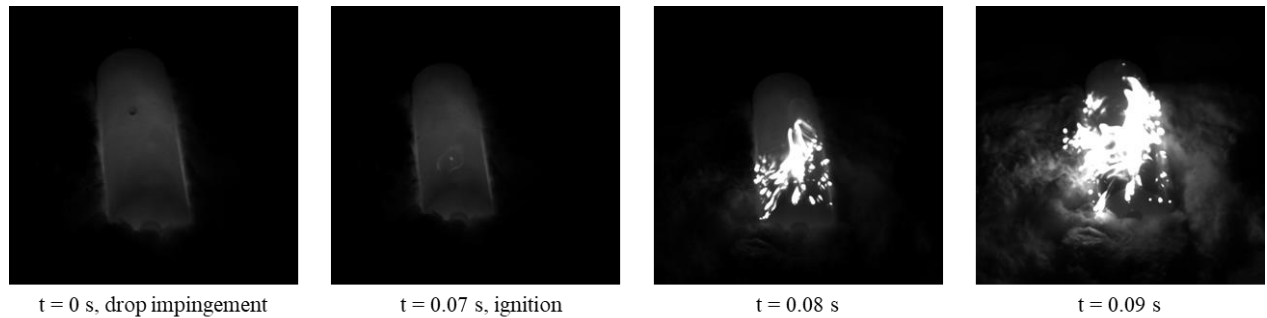


Figure 3-3: Ignition event over the cylinder

Ignition probability data along with a logistic curve fit corresponding to both surfaces are plotted as a function of temperature (°C) in figure 3-4.

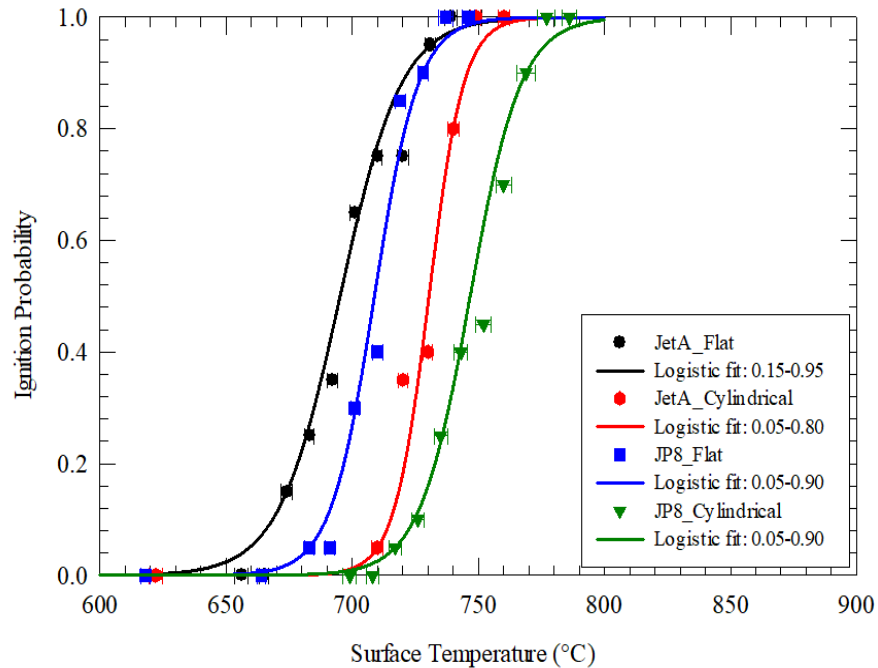


Figure 3-4: Comparison of ignition probability curves of Jet-A and JP-8

For JP-8 injection onto the flat surface, a logistic fit 0.05 - 0.90 is plotted by using a 5% ignition probability point corresponding to 683°C and 90% ignition probability corresponding to 728°C. For JP-8 injection onto the cylindrical surface, a logistic fit 0.05 - 0.90 is plotted by using a 10% ignition probability point corresponding to 717°C and 90% ignition probability corresponding to 769°C. For Jet-A injection onto the flat surface, a logistic fit 0.15 - 0.95 is plotted by using 15% ignition probability point corresponding to 674°C and 95% ignition probability corresponding to 731°C and for cylindrical surface, a logistic fit 0.05 - 0.80 is plotted by using 5% ignition probability point corresponding to 710°C and 80% ignition probability corresponding to 740°C.

Table 3-3: Comparison of HSIT of JP-8 and Jet-A at flat and cylindrical surfaces

<b>Fuel</b>	<b>JP-8</b>				<b>Jet-A</b>			
<b>Curvature type</b>	<b>Flat</b>		<b>Cylindrical</b>		<b>Flat</b>		<b>Cylindrical</b>	
	Data	Logistic fit	Data	Logistic fit	Data	Logistic fit	Data	Logistic fit
Min. probability ignition temperature (°C)	683	683	717	717	674	674	710	710
50% probability ignition temperature (°C)	-	709	-	747	-	695	-	730
Max. probability ignition temperature (°C)	737	737	777	777	739	739	749	749
Logistic curve regression coefficients	$b_0 = -80.98$ $b_1 = 0.114 \text{ } ^\circ\text{C}^{-1}$		$b_0 = -73.84$ $b_1 = 0.099 \text{ } ^\circ\text{C}^{-1}$		$b_0 = -57.06$ $b_1 = 0.082 \text{ } ^\circ\text{C}^{-1}$		$b_0 = -105.44$ $b_1 = 0.144 \text{ } ^\circ\text{C}^{-1}$	

From Table 3-3, it can be seen that curvature has a substantial effect on first hot ignition temperature. For JP8, there is a difference of 34°C between their respective first hot surface ignition temperatures and for Jet-A, there is a difference of 36°C between the respective minimum hot surface ignition temperatures.

### 3.1.3 HSIT Comparison

Ignition probability data along with logistic curve fit for all fuels are plotted in Figure 3-5: Comparison of ignition probability curves of Heptane, JP-8, Jet-A, and JP-5. For heptane, JP-8 and Jet-A, logistics curves were plotted in the same manner as discussed in the sections above. For JP5, a logistic fit 0.05 - 0.95 is plotted by using a 5% ignition probability point corresponding to 667°C and 95% ignition probability corresponding to 749°C.

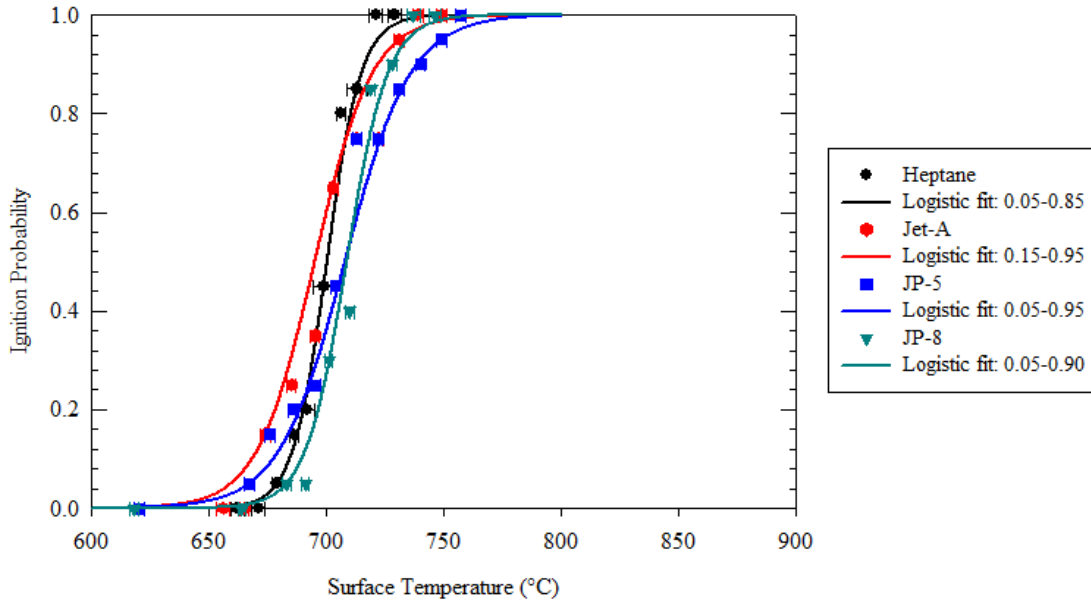


Figure 3-5: Comparison of ignition probability curves of Heptane, JP-8, Jet-A, and JP-5

Deliverables from testing of all fuels are tabulated below,

Table 3-4: Comparison of HSIT of test fuels

<b>Fuel</b>	<b>Heptane</b>	<b>JP-8</b>	<b>Jet-A</b>	<b>JP-5</b>
Min. probability ignition temperature (°C)	679	683	674	667
Max. probability ignition temperature (°C)	721	737	739	757
Logistic curve regression coefficients	$b_0 = -96.39$ $b_1 = 0.14^{\circ}\text{C}^{-1}$	$b_0 = -80.98$ $b_1 = 0.114^{\circ}\text{C}^{-1}$	$b_0 = -57.06$ $b_1 = 0.082^{\circ}\text{C}^{-1}$	$b_0 = -50.84$ $b_1 = 0.072^{\circ}\text{C}^{-1}$
AIT (°C)	204	210	210	246

From Table 3-4, it can be concluded that minimum and maximum probability ignition temperature for n-heptane and turbine engine fuels, Jet-A, JP5, and JP8 is in the range of 665-680°C and 720-760°C respectively. Also, the minimum ignition temperatures for these fuels are significantly (400°C-450°C) higher than their respective auto-ignition temperatures.

Figure 3-6 compares the HSIT range of n-heptane and turbine engine fuels against their respective auto-ignition temperature (AIT). HSIT range is defined as the temperature range where the lowest temperature corresponds to the min. ignition probability temperature and highest temperature corresponds to the max. ignition probability temperature.

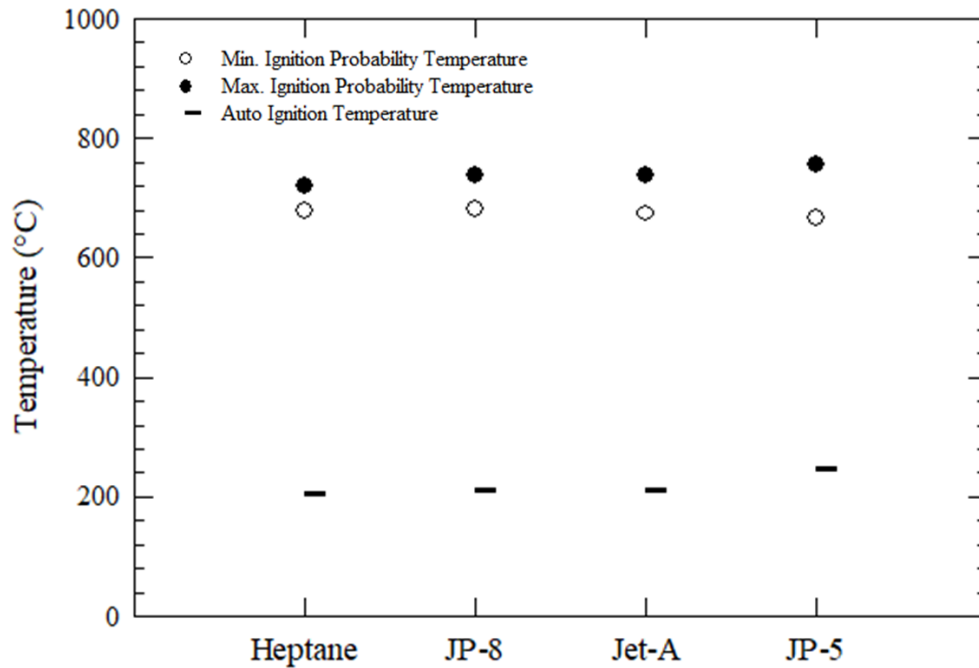


Figure 3-6: Comparison of HSIT range of n-heptane and turbine engine fuels against their respective AIT

From the figure above, it should be noted that ignition range of n-heptane is 42°C, for JP-8 it is 54°C, for Jet-A it is 65°C, and for JP-5 it is 90°C. The HSIT range of JP-5 is significantly higher in comparison to other fuels. This is probably linked to fuel composition which ultimately affects its chemical and physical properties. In the literature, the HSIT range is higher for the fuels with higher density and higher dynamic viscosity [4].

### 3.2 Piston Engine Fuels

In this section, the HSIT of four new alternative piston engine fuels is reported and compared against the HSIT of the baseline fuel Avgas 100LL. The test fuels provided by the FAA were confidential and hence are labeled as Test fuel A, B, C, and D. In the following sections, HSIT of each test fuel is discussed and compared against the HSITs of the baseline fuel.

#### 3.2.1 Baseline Fuel – Avgas 100LL

The baseline fuel properties as per the safety data sheets (SDS) are as follows:

- Density (at 15°C): 0.725 g/cm<sup>3</sup>
- Auto-Ignition Temperature: 430°C / 806°F
- Vapor density (Air = 1): 3 at 101 kPa

The test results of the baseline fuel are shown in Table 3-5.

Table 3-5: Results for the Avgas 100LL

<b>Set Temperature in the copper plate (°C)</b>	<b>Mean Temperature in the stainless steel plate (°C)</b>	<b># of Ignitions</b>	<b>P(I)</b>
400	396	0	0.00
500	495	0	0.00
600	592	0	0.00
700	691	0	0.00
750	741	0	0.00
760	748	0	0.00
770	758	0	0.00
780	768	3	0.15
790	778	5	0.25
800	788	14	0.70
810	797	17	0.85
820	806	20	1.00
830	815	20	1.00

In Table 3-5, the “set temperature” is the temperature set on the temperature controller. The “mean temperature” is the average temperature recorded by the thermocouples, TC2, TC3 and TC5, which are near the center in the stainless-steel plate. The “# of ignitions” is the number of drops that ignited out of the 20 drops dropped on the hot surface and P(I) is the ignition probability. From table 3-5, the min. ignition probability temperature is observed at 768°C and max, ignition probability temperature is observed at 806°C.

Ignition probability data along with the logistic curve fit are plotted as a function of temperature (°C) in Figure 3-7. The logistic fit 0.15 - 0.85 is plotted by using the 15% ignition probability point corresponding to the measured temperature of 768°C and the 85% ignition probability point corresponding to the measured temperature of 797°C.

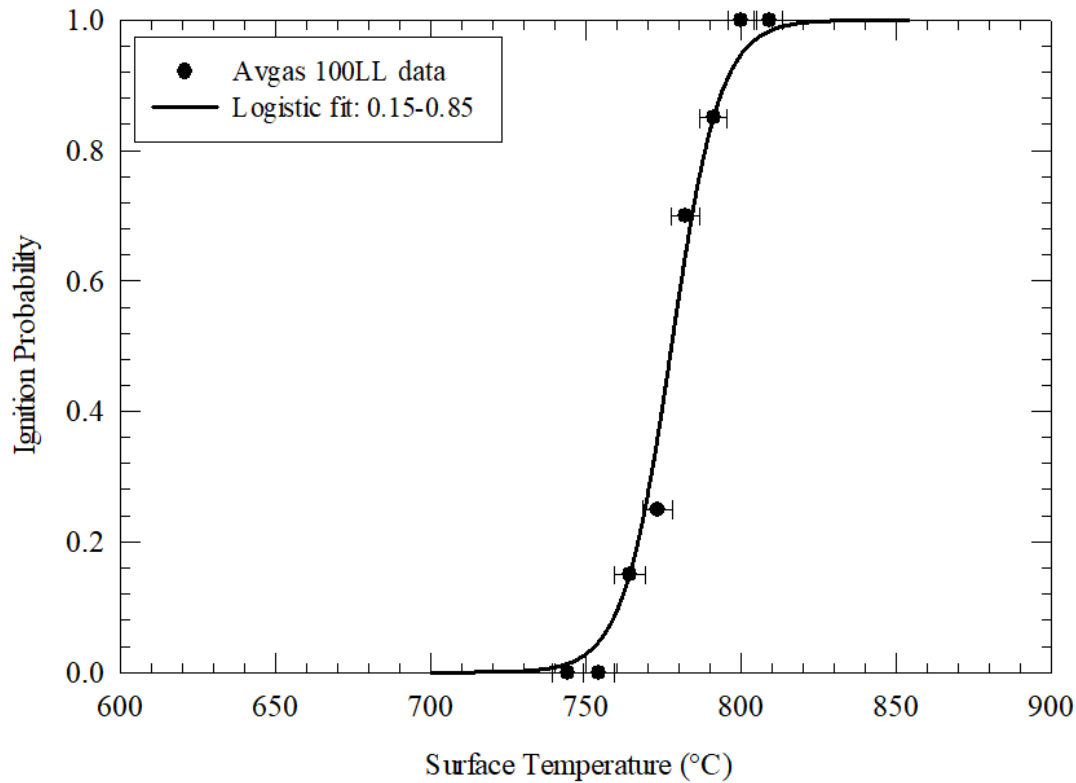


Figure 3-7: Ignition probability curve of Avgas 100LL as a function of surface temperature (°C)

The estimated temperature interval error bounds are shown as bars and represent the highest and the lowest temperatures read by the thermocouples TC2, TC3, and TC5 embedded in the stainless-steel plate. The following data are derived from the baseline fuel tests:

- Temperature corresponding to the first ignition:  $T = 768^{\circ}\text{C}$
- Temperature corresponding to a 50% ignition probability:  $T = 782^{\circ}\text{C}$  (interpolated from the logistic curve)
- Temperature corresponding to a 100% ignition probability:  $T = 806^{\circ}\text{C}$
- Coefficients of the logistics curve fit:  $b_0 = -93.609$ ;  $b_1 = 0.119^{\circ}\text{C}^{-1}$

A photograph of the flame following the ignition of a drop of the baseline fuel is depicted in Figure 3-8. The drop on impingement with the hot surface broke-up into multiple daughter droplets. The visible flames result from burning of these multiple daughter drops and last only for a few seconds and are worthy of future experimental and theoretical studies.



Figure 3-8: Baseline fuel flame image at 810°C set temperature

High-speed camera images are recorded at each temperature in order to qualitatively study the initiation and propagation of the ignition events. The images are recorded with a frame rate of 5000 Hz. Sample images separated by 25 ms to 100 ms are shown in figure 3-9.

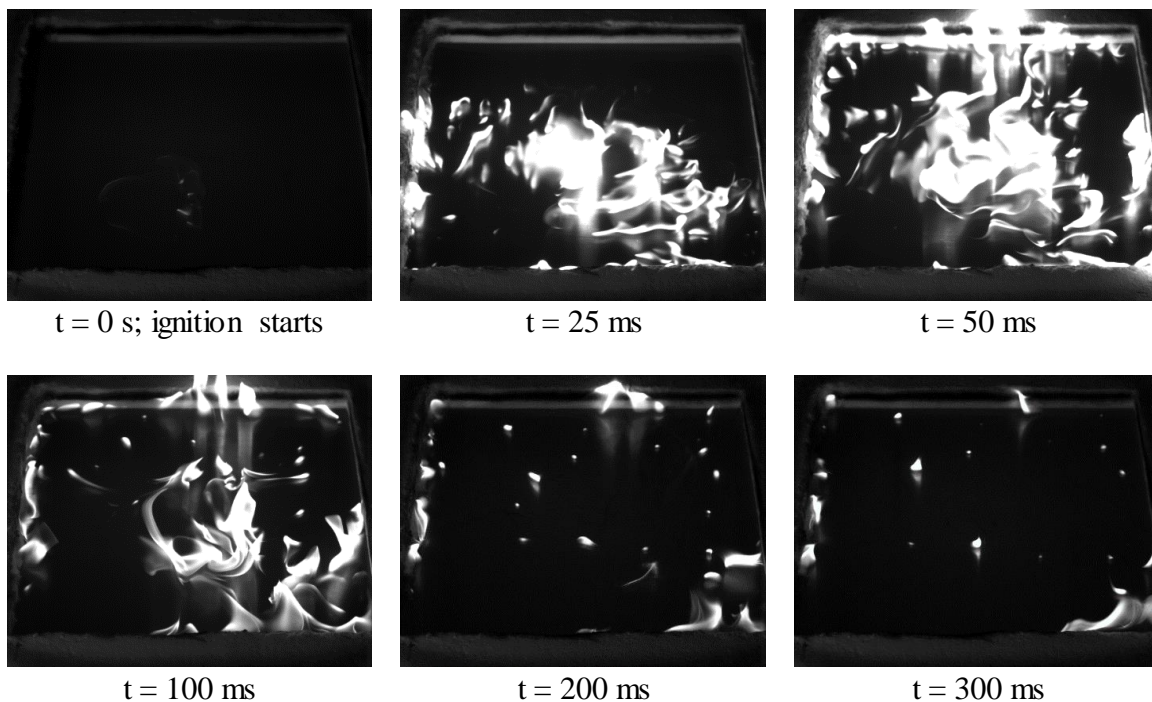


Figure 3-9: High-speed camera images of the baseline fuel at 810°C set temperature

### 3.2.2 Test Fuel A

The properties of the fuel for blind testing supplied with the MSDS sheet are as follows:

- Density (at 15° C): 0.769 g/cm<sup>3</sup>
- Auto-Ignition Temperature: 440°C / 824°F
- Vapor density (Air = 1): >1 at 101 kPa
- Boiling point range: 24-180°C

The test results are shown in Table 3-6.

Table 3-6: Results for Test Fuel A

<b>Set temperature in the copper plate (°C)</b>	<b>Mean temperature in the stainless-steel plate (°C)</b>	<b># of Ignitions</b>	<b>P(I)</b>
300	299	0	0.00
500	494	0	0.00
700	688	0	0.00
750	738	0	0.00
800	789	0	0.00
820	807	0	0.00
840	827	0	0.00
850	834	1	0.05
860	842	6	0.30
870	851	8	0.40
880	858	11	0.55
890	866	17	0.85
900	874	20	1.00
910	882	20	1.00

In Table 3-6, the “set temperature” is the temperature set on the temperature controller. The “mean temperature” is the average temperature recorded by the thermocouples, TC2, TC3 and TC5, which are near the center in the stainless-steel plate. The “# of ignitions” is the number of drops that ignited out of the 20 drops dropped on the hot surface and P(I) is the ignition probability. From Table 3-6, it can be seen that first ignition is observed at 834°C and 100% ignition probability is observed at 874°C. Ignition probability data along with logistic curve fit are plotted as a function of temperature (°C) in Figure 3-10. The Logistic fit 0.05-0.85 is plotted by using the 15% ignition probability point corresponding to a measured temperature of 834°C and the 85% ignition probability corresponding to a measured temperature of 866°C.



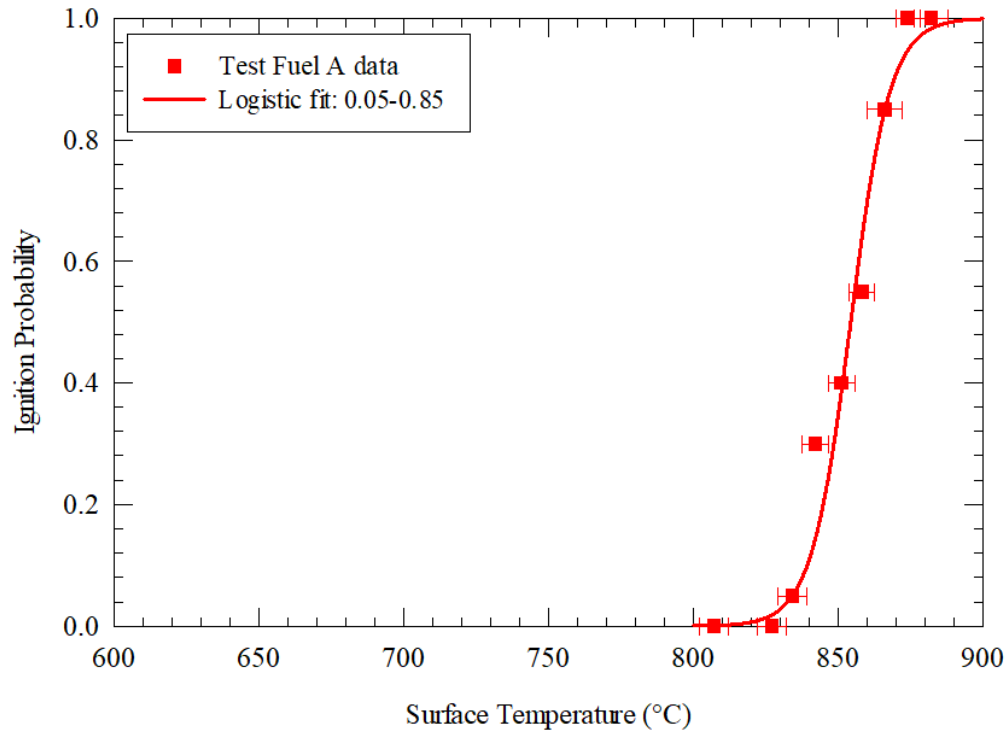


Figure 3-10: Ignition probability curve of Test Fuel A as a function of temperature (°C)

The estimated temperature interval error bounds are shown as bars and represent the highest and the lowest temperatures read by the thermocouples TC2, TC3 and TC5 embedded in the stainless-steel plate. The following data are derived from the tests involving the test fuel:

- Temperature corresponding to the first ignition:  $T = 834^{\circ}\text{C}$
- Temperature corresponding to a 50% ignition probability:  $T = 854^{\circ}\text{C}$  (interpolated from logistics curve)
- Temperature corresponding to a 100% ignition probability:  $T = 874^{\circ}\text{C}$
- Coefficients of the logistics regression curve fit:  $b_0 = -124.89$ ;  $b_1 = 0.1462^{\circ}\text{C}^{-1}$

The drops collided and broke up by impinging on the surface with or without ignition. The flame propagated in two ways, namely point ignition, as if the ignition event occurred at few discrete locations, and distributed ignition, as if the ignition event is distributed across the plate. Point ignition is observed for ignition temperatures up to  $890^{\circ}\text{C}$  and distributed ignition is observed for temperatures above  $890^{\circ}\text{C}$ . This different ignition characteristic doesn't significantly impact

ignition onset temperature and 100% ignition temperature. Figure 3-11 and Figure 3-12 show the resulting flame for point ignition and distributed ignition respectively.



Figure 3-11: Point ignition at 890°C surface temperature



Figure 3-12: Distributed ignition at 900°C surface temperature

High speed camera images are recorded at each temperature in order to qualitatively study the initiation and propagation of the ignition events. The images are recorded with a frame rate of 5000 Hz. Sample images separated by 25 ms to 100 ms are shown in Figure 3-13.

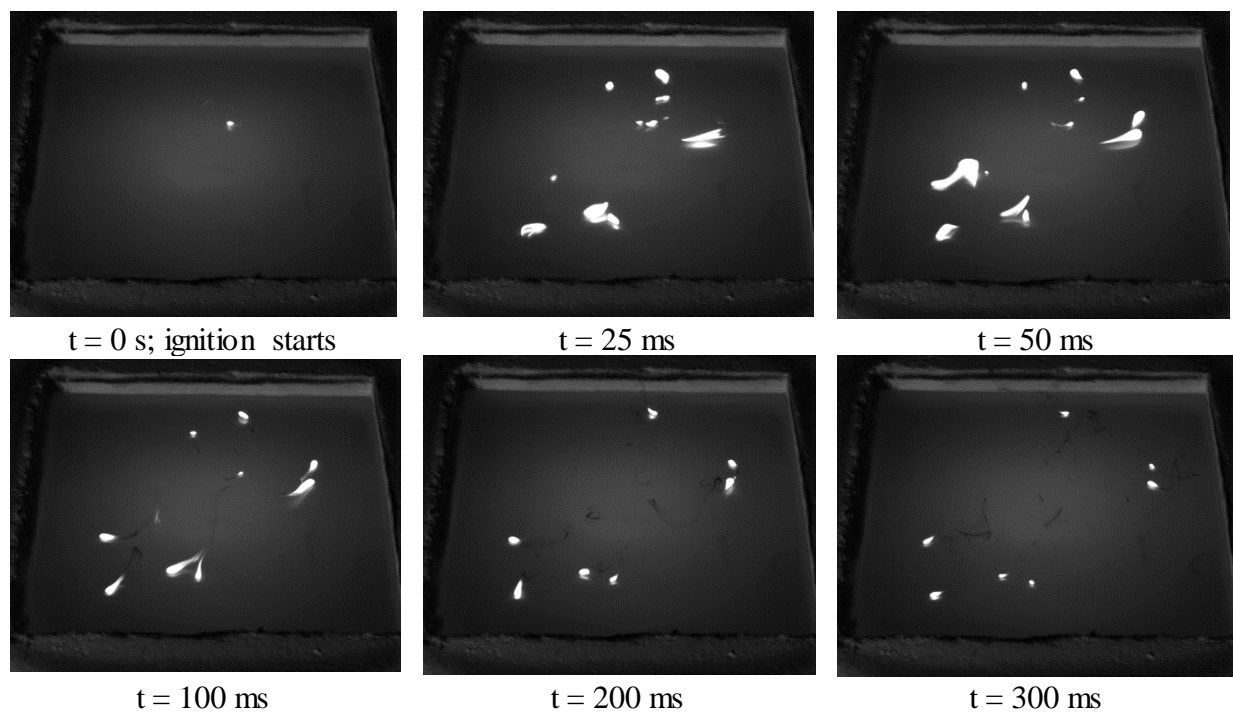


Figure 3-13: High-speed camera images of flame propagation at 890°C set temperature

The test fuel ignition data is plotted compared with the baseline fuel and as shown in Figure 3-14.

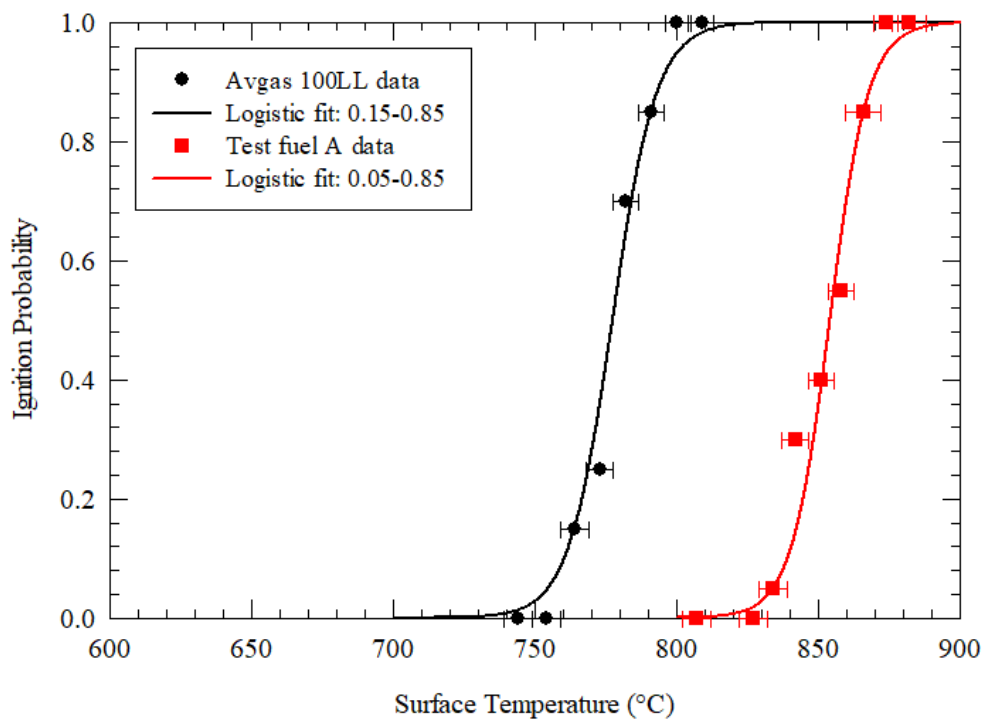


Figure 3-14: Comparison of ignition probability curve of Test Fuel A against Avgas 100LL

From figure 3-15 it should be noticed that the HSIT of the test fuel A is significantly higher in comparison to the HSIT of the baseline fuel. This is probably due to higher density of the test fuel in comparison to the baseline fuel. Table 3-7 compares the HSITs of the test fuel with the baseline fuel (Avgas 100LL).

Table 3-7: Data comparison of the test fuel A with the Avgas 100LL

	<b>Avgas 100LL</b>		<b>Test Fuel A</b>	
	<b>Data</b>	<b>Logistic fit 0.15-0.85</b>	<b>Data</b>	<b>Logistic fit 0.05-0.85</b>
<b>Min. ignition probability temperature</b>	768°C	768°C	834°C	834°C
<b>50% ignition probability temperature</b>	-	782°C	-	854°C
<b>100% (99.9%) ignition probability temperature</b>	806°C	823°C	874°C	888°C
<b>Regression Coefficients</b>	$b_0 = -93.609$ $b_1 = 0.119 \text{ } ^\circ\text{C}^{-1}$		$b_0 = -124.89$ $b_1 = 0.1462 \text{ } ^\circ\text{C}^{-1}$	

The first ignition temperature of the test fuel is higher by ~65°C in comparison to the baseline fuel. The 50% ignition probability temperature of test fuel is ~70°C higher than that of the baseline fuel. The ignition range of both test fuel and baseline fuel is the same, ~40°C. The temperature corresponding to the 100% ignition probability for the test fuel is higher by ~70°C in comparison to the baseline fuel.

### Fuel Residue Deposits

The stainless-steel plates used for each of the fuels are visually assessed after the ignition tests. Figure 3-15 below shows the visible photographs of the plates.

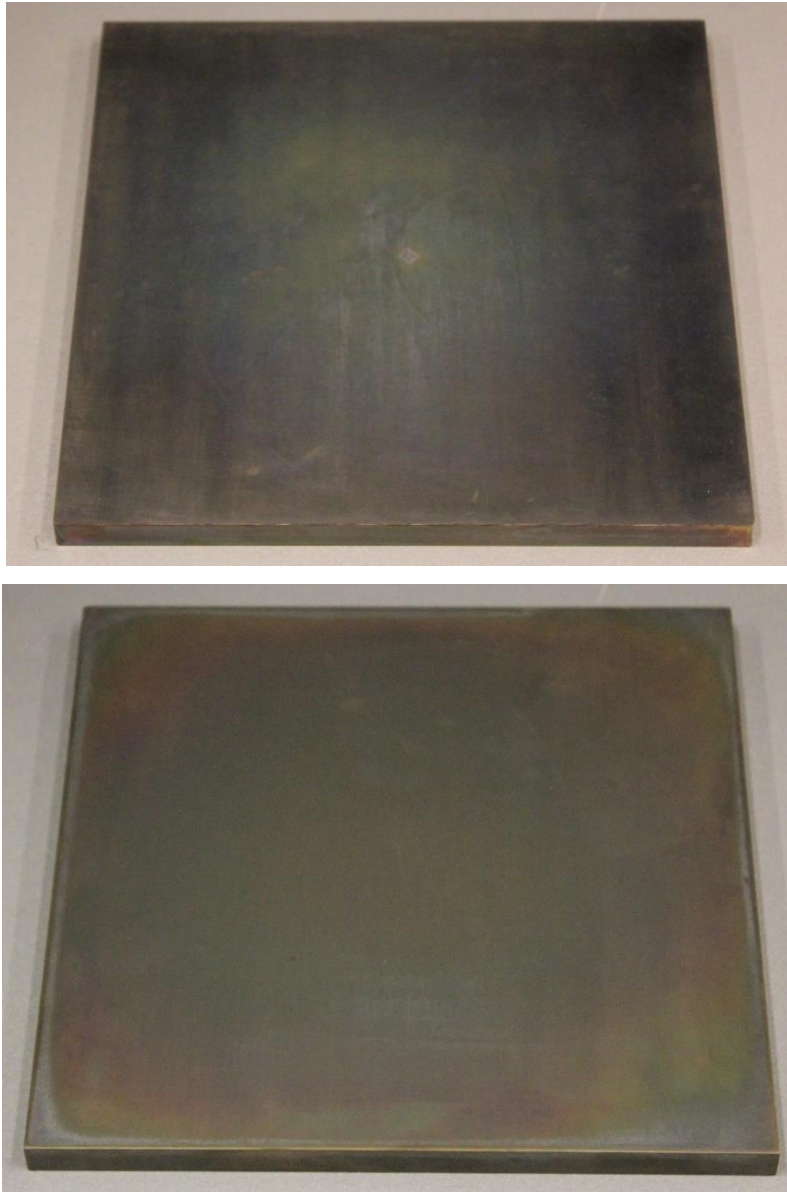


Figure 3-15: Plate after ignition tests – baseline fuel (*top*) and test fuel (*bottom*)

Qualitatively, the baseline fuel appears to have produced slightly higher residues than those produced by the test fuel. However, neither fuel produced measurable residues for the present test conditions. Most likely this is due to the elevated temperatures at which 100% ignition occurred.

### 3.2.3 Test Fuel B

The properties of the fuel for blind testing supplied with the MSDS sheet are as follows:

- Density (at 15° C): 0.70-0.72 g/cm<sup>3</sup>
- Vapor density (Air = 1): >1 at 101 kPa
- Boiling point range: 35-225°C

The test results are shown in Table 3-8.

Table 3-8: Results for the Test Fuel B

Set Temperature in the copper plate (°C)	Mean Temperature in the stainless-steel plate (°C)	# of Ignitions	P(I)
400	400	0	0.00
500	500	0	0.00
600	600	0	0.00
650	650	0	0.00
660	660	0	0.00
670	669	2	0.10
680	679	5	0.25
690	688	12	0.60
700	698	13	0.65
710	708	12	0.60
720	717	9	0.45
730	727	10	0.50
740	736	10	0.50
750	745	14	0.70
760	754	18	0.90
770	764	20	1.00
780	773	20	1.00

In Table 3-8, the “set temperature” is the temperature set on the temperature controller. The “mean temperature” is the average temperature recorded by the thermocouples, TC2, TC3 and TC5,

which are near the center in the stainless-steel plate. The “# of ignitions” is the number of drops that ignited out of the 20 drops dropped on the hot surface and  $P(I)$  is the ignition probability. From Table 3-8, it can be seen that first ignition was observed at 669°C and 100% ignition probability was observed at 764°C. Ignition probability data along with three logistic curve fits are plotted as a function of temperature (°C) in Figure 3-16.

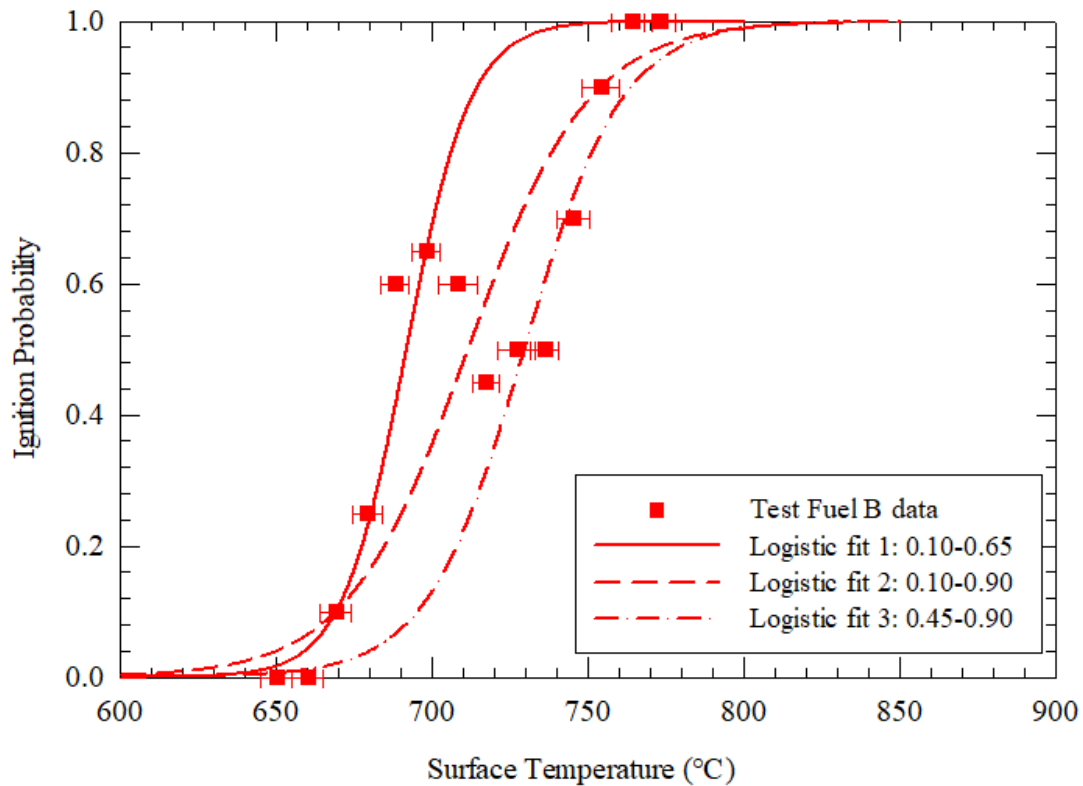


Figure 3-16: Ignition probability curve of the test fuel B as a function of temperature (°C)

The three logistics curves are plotted to address a relatively wide range of probability ignition events in the 40-70% range. The first Logistic fit 0.1 - 0.65 is plotted by using the 10% ignition probability point corresponding to a measured temperature of 669°C and the 65% ignition probability corresponding to a measured temperature of 698°C. The second Logistic fit 0.1-0.9 is plotted by using the 10% ignition probability point corresponding to a measured temperature of 669°C and the 90% ignition probability corresponding to a measured temperature of 754°C. The third Logistic fit 0.45 – 0.90 is plotted by using the 45% ignition probability point corresponding to a measured temperature of 717°C and the 90% ignition probability corresponding to a measured temperature of 754°C.



The estimated temperature interval error bounds are shown as bars and represent the highest and the lowest temperatures read by the thermocouples TC2, TC3 and TC5 embedded in the stainless-steel plate. The following data are derived from the tests involving the test fuel:

- Temperature corresponding to the first ignition:  $T = 669^{\circ}\text{C}$
- Temperature corresponding to a 50% ignition probability:  
Logistics curve fit 0.1 – 0.65:  $692^{\circ}\text{C}$   
Logistics curve fit 0.1 – 0.9:  $711^{\circ}\text{C}$   
Logistics curve fit 0.45 - 0.90:  $720^{\circ}\text{C}$
- Temperature corresponding to a 100% ignition probability:  $T = 764^{\circ}\text{C}$
- Coefficients of the logistics regression curve fit:  
Logistics curve fit 0.1 – 0.65:  $b_0 = -67.171$ ;  $b_1 = 0.0971\text{ }^{\circ}\text{C}^{-1}$   
Logistics curve fit 0.1 – 0.9:  $b_0 = -36.784$ ;  $b_1 = 0.0517\text{ }^{\circ}\text{C}^{-1}$   
Logistics curve fit 0.45 - 0.90:  $b_0 = -46.69$ ;  $b_1 = 0.0640\text{ }^{\circ}\text{C}^{-1}$

It is worth noting that this fuel demonstrated a slight reduction in ignition probability with increasing temperature in the range of  $708\text{--}736^{\circ}\text{C}$ . Due to the blind nature of the study, the reasons for this phenomenon were not investigated. Preliminary testing of this fuel showed similar behavior. This issue was navigated by using multiple logistic curve fits for regions of interest.

The drops collided and broke up into multiple daughter droplets by impinging on the surface with or without ignition. The flame propagated as if the ignition event was distributed across the plate. Figure 3-17 below shows the stainless-steel plate at  $770^{\circ}\text{C}$  set temperature (100% ignition probability) and the resulting flame respectively.



Figure 3-17: Test fuel flame image – distributed ignition at  $770^{\circ}\text{C}$  set temperature



High speed camera images are recorded at each temperature in order to qualitatively study the initiation and propagation of the ignition events. The images are recorded with a frame rate of 5000 Hz. Sample images separated by 25 ms to 100 ms are shown in figure 3-18.

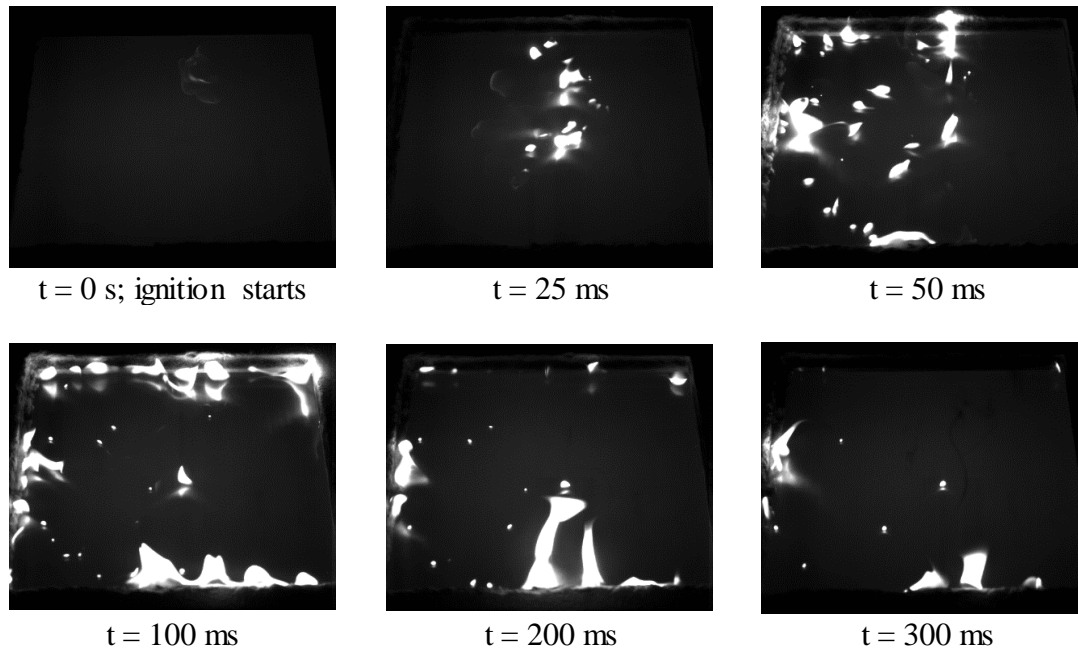


Figure 3-18: High-speed camera images of the test fuel B at 740°C set temperature

The test fuel ignition data is plotted and compared with the baseline fuel as shown in Figure 3-19.

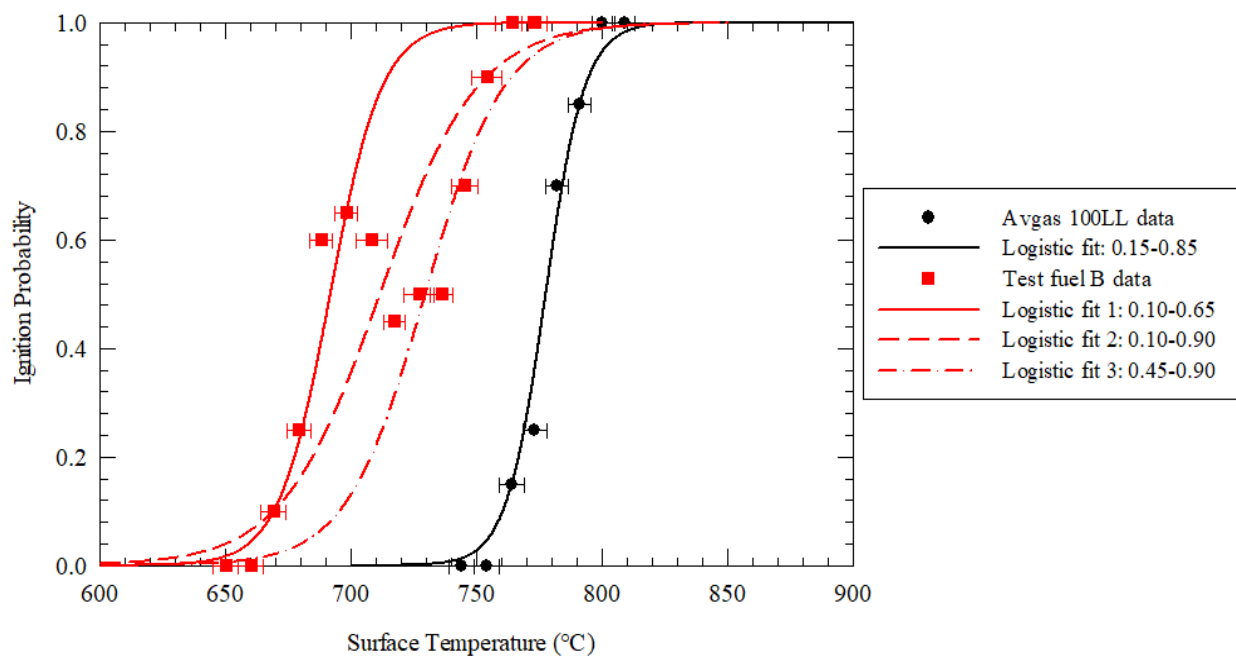


Figure 3-19: Comparison of ignition probability curve of the test fuel B against the baseline fuel

Table 3-9 compares the HSITs of the test fuel with the baseline fuel.

Table 3-9: Data comparison of the test fuel B with Avgas 100LL

	<b>Avgas 100LL</b>		<b>Test Fuel- B</b>			
	<b>Data</b>	<b>Logistic fit 0.15- 0.85</b>	<b>Data</b>	<b>Logistic fit 0.1 – 0.65</b>	<b>Logistic fit 0.1 - 0.9</b>	<b>Logistic fit 0.45 – 0.9</b>
<b>Min. ignition probability temperature</b>	768°C	768°C	669°C	669°C	669°C	669°C
<b>50% ignition probability temperature</b>	N/O	782°C	727°C and 736°C	692°C	711°C	720°C
<b>100% (99.9%) ignition probability temperature</b>	806°C	823°C	764°C	742°C	802°C	795°C
<b>Regression Coefficients</b>	$b_0 = -93.609$ $b_1 = 0.119 \text{ } ^\circ\text{C}^{-1}$		$b_0 = -67.171$ $b_1 = 0.0971 \text{ } ^\circ\text{C}^{-1}$		$b_0 = -36.784$ $b_1 = 0.0517 \text{ } ^\circ\text{C}^{-1}$	$b_0 = -46.668$ $b_1 = 0.0648 \text{ } ^\circ\text{C}^{-1}$

The first ignition temperature of the test fuel is lower by ~100°C in comparison to the baseline fuel. For the test fuel, two 50% ignition probability temperatures are obtained, 727°C and 736°C and are lower by ~50°C in comparison to the baseline fuel, 782°C. The ignition range of the test fuel is 100°C whereas for the baseline fuel it is around 40°C. The temperature for 100% ignition probability for the test fuel appears to be ~40°C lower than that of the baseline fuel.

### Fuel Residue Deposits

The stainless-steel plates used for each of the fuels are visually assessed after the ignition tests. Figure 3-20 and Figure 3-21 below shows the visible photographs of the plates.



Figure 3-20: Plate after ignition tests – baseline fuel 100 LL Avgas



Figure 3-21: Plate after ignition tests – test fuel B

Qualitatively, the baseline fuel appears to have produced slightly higher residues than those produced by the test fuel. However, the plate used for the test fuel appears visibly darker. Neither fuel produced measurable residues for the present test conditions. Most likely this is due to the elevated temperatures at which 100% ignition occur.

### 3.2.4 Test Fuel C

The properties of the fuel for blind testing supplied with the MSDS sheet are as follows:

- Density (at 15° C): 0.769 g/cm<sup>3</sup>
- Vapor density (Air = 1): >1 at 101 kPa
- Boiling point: 38°C

The results are shown in Table 3-10.

Table 3-10: Results for the test fuel C

<b>Set Temperature in the copper plate (°C)</b>	<b>Mean Temperature in the stainless-steel plate (°C)</b>	<b># of Ignitions</b>	<b>P(I)</b>
400	398	0	0.00
500	497	0	0.00
600	597	0	0.00
650	647	0	0.00
700	696	0	0.00
750	745	0	0.00
760	755	3	0.15
770	765	6	0.30
780	774	6	0.30
790	786	11	0.55
800	791	12	0.60
810	799	12	0.60
820	811	19	0.95
830	817	18	0.90
840	825	20	1.00
850	832	20	1.00

In Table 3-10, the “set temperature” is the temperature set on the temperature controller. The “mean temperature” is the average temperature recorded by the thermocouples, TC2, TC3 and TC5, which are near the center in the stainless-steel plate. The “# of ignitions” is the number of drops that ignited out of the 20 drops dropped on the hot surface and P(I) is the ignition probability.

From Table 3-10, it can be seen that first ignition was observed at 755°C and 100% ignition probability was observed at 825°C. The ignition probability data along with logistic curve fit are plotted as a function of temperature (°C) in Figure 3-22. The logistic fit 0.15 - 0.95 is plotted by

using the 15% ignition probability point corresponding to a measured temperature of 755°C and the 95% ignition probability corresponding to a measured temperature of 811°C.

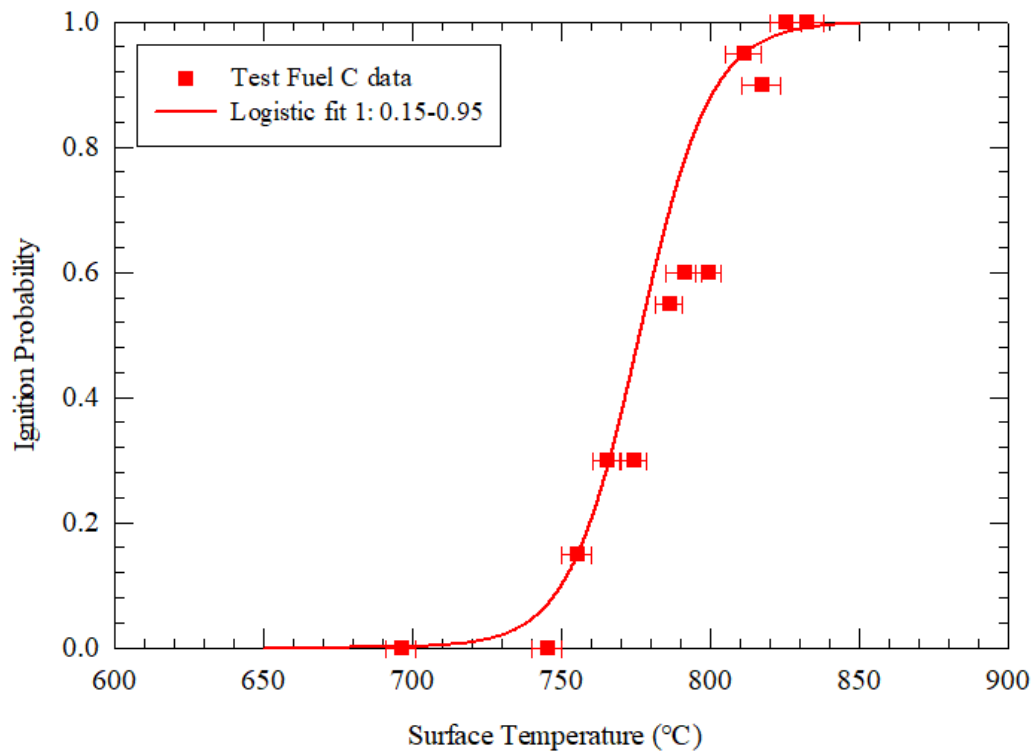


Figure 3-22: Ignition probability curve of the test fuel C as a function of temperature (°C)

The estimated temperature interval error bounds are shown as bars and represent the highest and the lowest temperatures read by the thermocouples TC2, TC3 and TC5 embedded in the stainless-steel plate.

The following data are derived from the tests involving the test fuel:

- Temperature corresponding to the first ignition:  $T = 755^{\circ}\text{C}$
- Temperature corresponding to a 50% ignition probability:  $T = 776^{\circ}\text{C}$  (interpolated from the logistics curve)
- Temperature corresponding to a 100% ignition probability:  $T = 825^{\circ}\text{C}$
- Coefficients of the logistics regression curve fit:  $b_0 = -64.82$ ;  $b_1 = 0.0835\text{ }^{\circ}\text{C}^{-1}$

The drops collided and broke up by impinging on the surface with or without ignition. The flame propagated as if the ignition event was distributed across the plate. Figure 3-23 below shows an

image of the stainless-steel plate at 840°C set temperature (100% ignition probability) and the resulting flame respectively.



Figure 3-23: Test fuel flame image – distributed ignition at 840°C set temperature

High-speed camera images are recorded at each temperature in order to qualitatively study the initiation and propagation of the ignition events. The images are recorded at a frame rate of 5000 Hz. Sample images separated by 25 ms, 50 ms, and 100 ms are shown in figure 3-24.

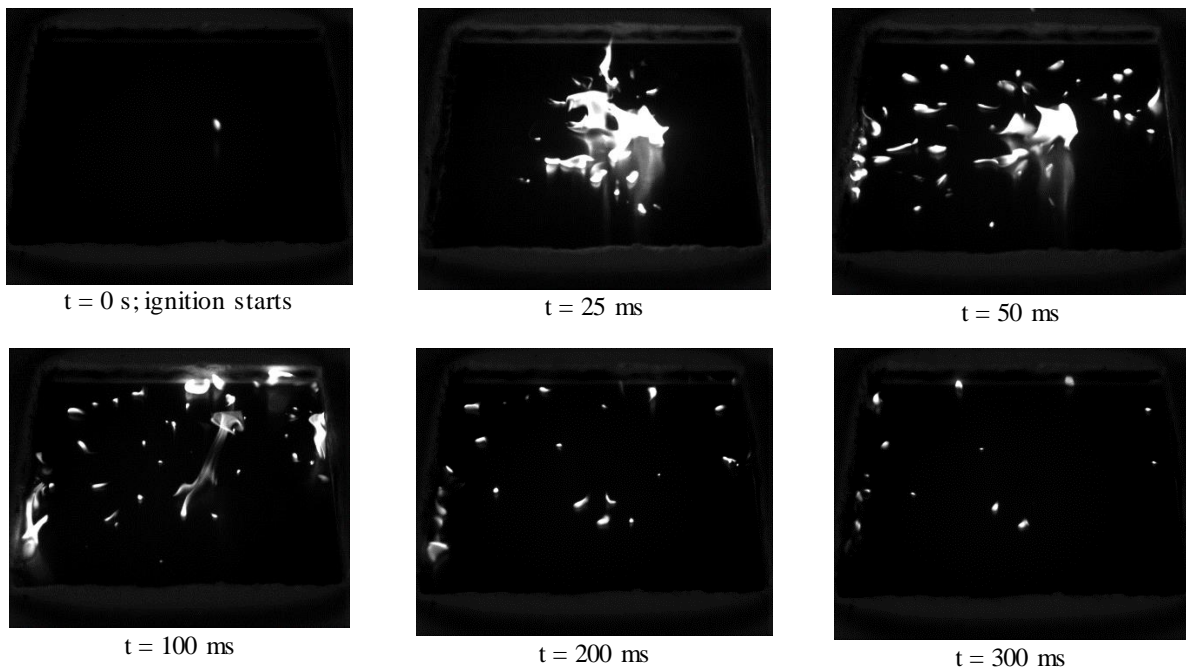


Figure 3-24: High-speed camera images for the test fuel C at 840°C set temperature

The test fuel ignition curve is compared with the baseline fuel and shown in Figure 3-25.

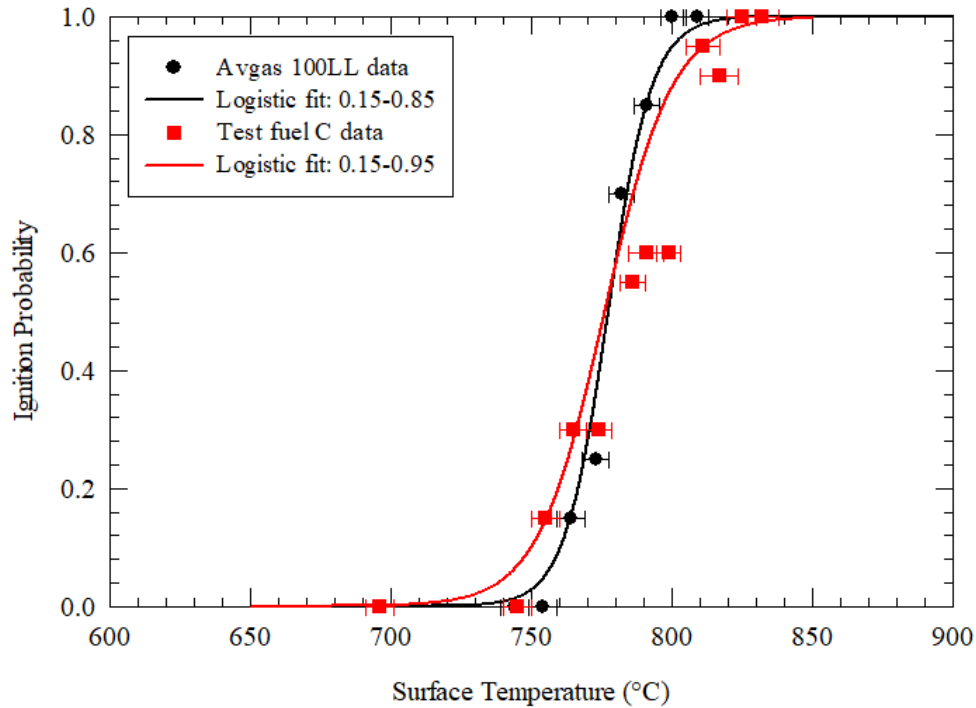


Figure 3-25: Comparison of ignition probability curve of the test fuel C against the baseline fuel  
Table 3-11 compares the HSIT of the test fuel C with the Avgas 100LL.

Table 3-11: Data comparison of the test fuel C with the Avgas 100LL

	<b>Avgas 100LL</b>		<b>Test Fuel C</b>	
	<b>Data</b>	<b>Logistic fit 0.15-0.85</b>	<b>Data</b>	<b>Logistic fit 0.15-0.95</b>
<b>Min. ignition probability temperature</b>	768°C	768°C	755°C	755°C
<b>50% ignition probability temperature</b>	N/O	782°C	N/O	776°C
<b>100% (99.9 %) ignition probability temperature</b>	806°C	823°C	825°C	837°C
<b>Regression coefficients</b>	$b_0 = -93.609$ $b_1 = 0.119 \text{ } ^\circ\text{C}^{-1}$		$b_0 = -64.82$ $b_1 = 0.0835 \text{ } ^\circ\text{C}^{-1}$	

The first ignition temperature of the test fuel is lower by  $\sim 10^\circ\text{C}$  in comparison to the baseline fuel. The 50% ignition probability temperature of the test fuel is within  $5^\circ\text{C}$  of the baseline fuel. The



ignition range of the test fuel is  $\sim 70^{\circ}\text{C}$  whereas for the baseline fuel it is  $\sim 40^{\circ}\text{C}$ . The temperature corresponding to 100% ignition probability for the test fuel appears to be within  $10^{\circ}\text{C}$  to  $20^{\circ}\text{C}$  of the baseline fuel.

### Fuel Residue Deposits

The stainless-steel plates used for each of the fuels are visually assessed after the ignition tests. Figure 3-26 below shows the visible photographs of the plates.



Figure 3-26: Plate after ignition tests – baseline fuel (*top*) and test fuel C (*bottom*)

Qualitatively, the test fuel appears to have produced slightly higher residues than those produced by the baseline fuel. However, neither fuel produced measurable residues for the present test conditions. Most likely this is due to the elevated temperatures at which 100% ignition occurred.



### 3.2.5 Test Fuel D

The properties of the fuel D for blind testing supplied with the MSDS sheet are as follows:

- Density (at 15°C): 0.720-0.755 g/cm<sup>3</sup>
- Boiling point range: 35-185°C
- Auto-ignition temperature: > 225°C/482°F

The results are shown in Table 3-12.

Table 3-12: Results for the test fuel D

<b>Set Temperature in the copper plate (°C)</b>	<b>Mean Temperature in the stainless-steel plate (°C)</b>	<b># of Ignitions</b>	<b>Ignition probability</b>
400	400	0	0.00
500	500	0	0.00
600	599	0	0.00
700	697	1	0.05
710	706	4	0.20
720	716	3	0.15
730	726	2	0.10
740	736	3	0.15
750	745	1	0.05
760	754	1	0.05
770	763	3	0.15
780	772	9	0.45
790	781	8	0.40
800	789	19	0.95
810	793	20	1.00
820	799	20	1.00

In Table 3-12, the “set temperature” is the temperature set on the temperature controller. The “mean temperature” is the average temperature recorded by the thermocouples, TC2, TC3 and TC5, which are near the center in the stainless-steel plate. The “# of ignitions” is the number of drops that ignited out of the 20 drops dropped on the hot surface and P(I) is the ignition probability. From table 5, it can be seen that the first ignition was observed at 697°C and a 100% ignition probability was observed at 793°C. Ignition probability data along with two logistic curves are plotted as a function of temperature (°C) in Figure 3-27.

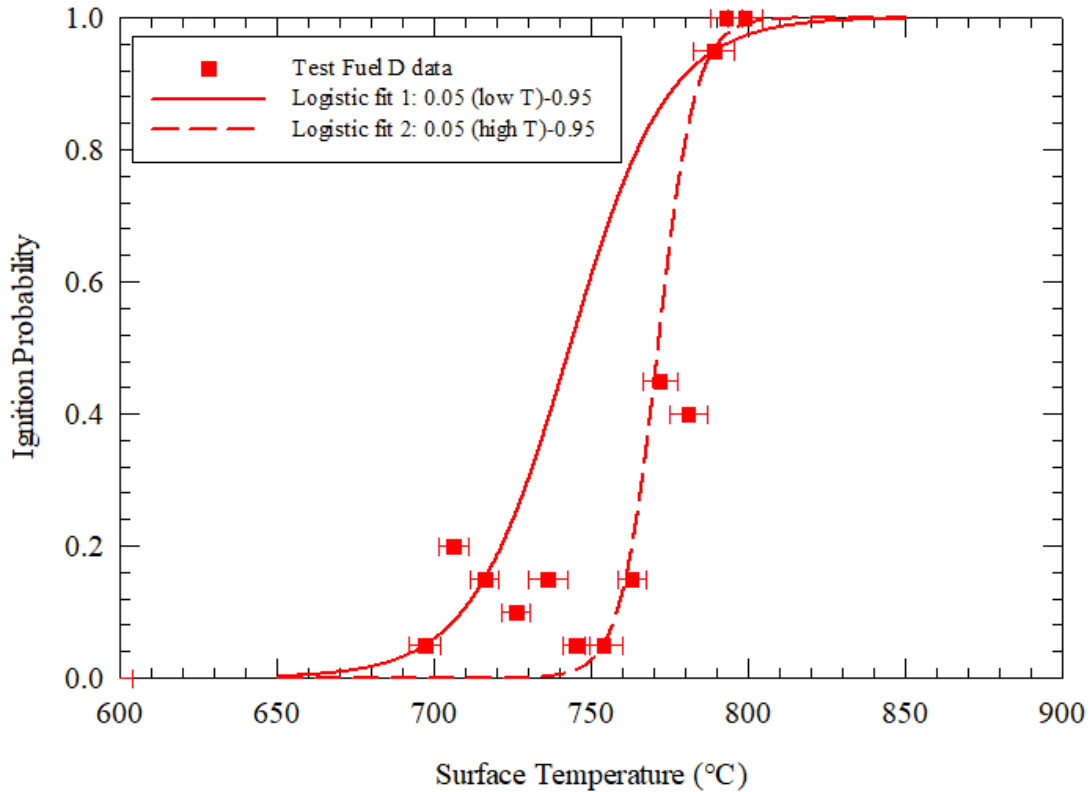


Figure 3-27: Ignition probability curve of the test fuel D as a function of temperature (°C)

The two logistics curves are plotted to address a relatively wide range of low probability ignition events in the 10-20% range. The first Logistic fit 0.05 (Low T) – 0.95 is plotted by using the low temperature 5% ignition probability point corresponding to a measured temperature of 697°C and the 95% ignition probability point corresponding to a measured temperature of 789°C. The logistic fit 0.05 (high T) – 0.95 is plotted by using the high temperature 5% ignition probability point corresponding to a measured temperature of 754°C and the 95% ignition probability point corresponding to a measured temperature of 789°C.

The estimated temperature interval error bounds are shown as bars and represent the highest and the lowest temperatures read by the thermocouples TC2, TC3 and TC5 embedded in the stainless-steel plate. The following data are derived from the tests involving the test fuel:

- Temperature corresponding to the first ignition:  $T = 697^{\circ}\text{C}$
- Temperature corresponding to a 50% ignition probability:
  - Logistics curve fit 0.05 (Low T) – 0.95:  $743^{\circ}\text{C}$
  - Logistics curve fit 0.05 (High T) – 0.95:  $771^{\circ}\text{C}$

- Temperature corresponding to a 100% ignition probability:  $T = 793^{\circ}\text{C}$
- Coefficients of the logistics regression curve fit:  
 Logistic fit 0.05 (Low T) – 0.95:  $b_0 = -47.56$ ;  $b_1 = 0.0640\text{ }^{\circ}\text{C}^{-1}$   
 Logistic fit 0.05 (High T) – 0.95:  $b_0 = -129.81$ ;  $b_1 = 0.1683\text{ }^{\circ}\text{C}^{-1}$

It is worth noting that this fuel demonstrated a slight reduction in ignition probability with increasing temperature in the range of  $716\text{--}763^{\circ}\text{C}$ . Due to the blind nature of the study, reasons for this phenomenon were not investigated. This issue was navigated by using multiple logistic curve fits for regions of interest.

The drops collided and broke up by impinging on the surface with or without ignition. The flame propagated as if the ignition event was distributed across the plate. Figure 3-28 below show an image of the stainless-steel plate at  $810^{\circ}\text{C}$  set temperature (100% ignition probability) and the resulting flame respectively.



Figure 3-28: Test fuel D flame image – distributed ignition at  $810^{\circ}\text{C}$  set temperature

High speed camera images are recorded at each temperature in order to qualitatively study the initiation and propagation of the ignition events. The images are recorded at a frame rate of 5000 Hz. Sample images separated by 25 ms, 50 ms and 100 ms are shown in Figure 3-29.

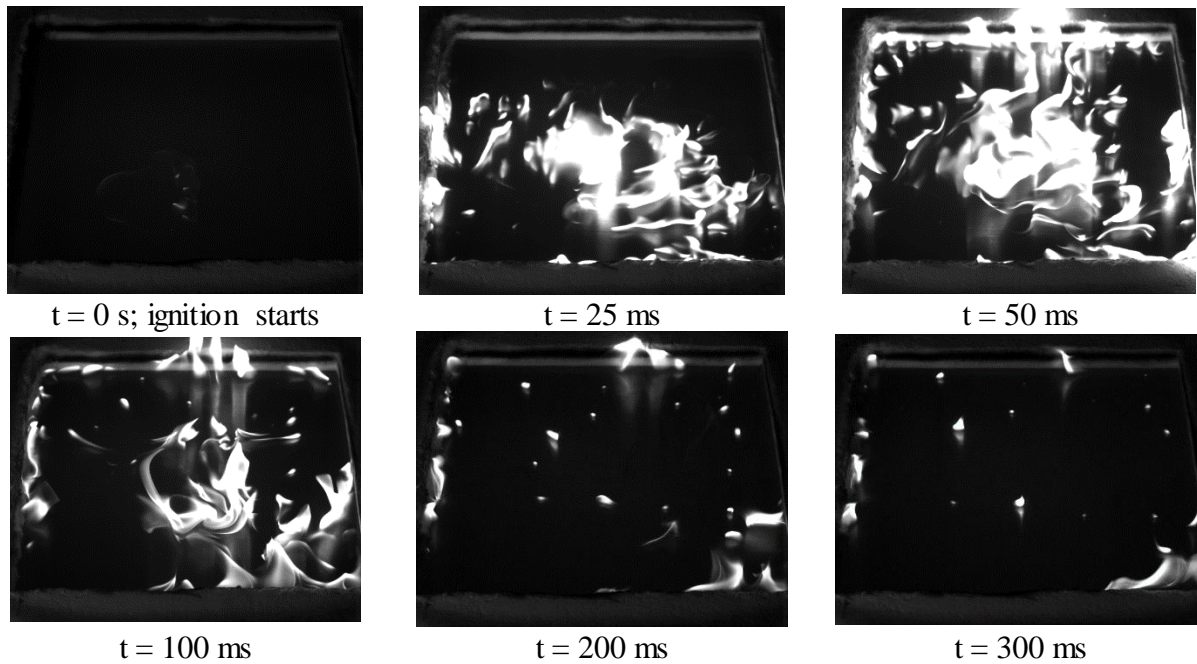


Figure 3-29: High speed camera images of the test fuel D at 810°C set temperature

The test fuel ignition data are compared with the baseline fuel in Figure 3-30.

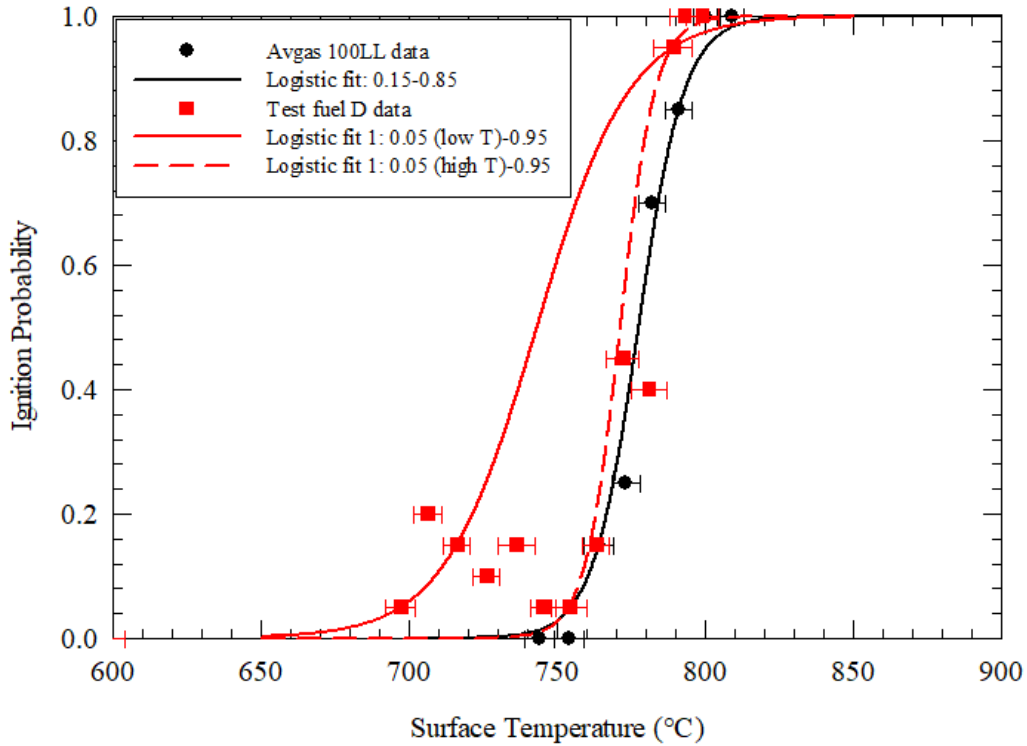


Figure 3-30: Comparison of ignition probability curve of the test fuel D against Avgas 100LL

Table 3-13: Comparison of the test fuel D with Avgas 100LL

	<b>Avgas 100LL</b>		<b>Test Fuel-D</b>		
	<b>Data</b>	<b>Logistic fit 0.15 – 0.85</b>	<b>Data</b>	<b>Logistic fit 0.05 (Low T) -0.95</b>	<b>Logistic fit 0.05 (High T) - 0.95</b>
<b>Min. ignition probability temperature (°C)</b>	768	768	697	697	697
<b>50% ignition probability temperature (°C)</b>	-	782	-	74	771
<b>100% (99.9%) ignition probability temperature (°C)</b>	806	823	793	820	801
<b>Regression coefficients</b>	$b_0 = -93.609$ $b_1 = 0.119 \text{ } ^\circ\text{C}^{-1}$		$b_0 = -47.56$ $b_1 = 0.0640 \text{ } ^\circ\text{C}^{-1}$		$b_0 = -129.81$ $b_1 = 0.1683 \text{ } ^\circ\text{C}^{-1}$

The first ignition temperature of the test fuel is lower by ~100°C in comparison to the baseline fuel. The 50% ignition probability temperature of the test fuel is between ~10°C and ~40°C lower than that of the baseline fuel. The ignition range of the test fuel is ~100°C whereas that of the baseline fuel is ~40°C. The temperature for 100% ignition probability for the test fuel appears to be within 10°C to 20°C of the baseline fuel.

### Fuel Residue Deposits

The stainless-steel plates used for each of the fuels are visually assessed after the ignition tests. Figure 3-32 and Figure 3-32 below shows the visible photographs of the plates.



Figure 3-31: Plate after ignition tests – baseline fuel Avgas 100LL



Figure 3-32: Plate after ignition tests – and test fuel D

Qualitatively, the test fuel appears to have produced slightly higher residues than those produced by the baseline fuel. However, neither fuel produced measurable residues for the present test conditions. Most likely this is due to the elevated temperatures at which 100% ignition occurred.

## **4. POOL FIRE - INTRODUCTION**

Flame spread along liquid fuel has been one of the critical combustion phenomena that still requires more in-depth research and analysis for the deep understanding of the chemical and the heat transfer processes involved. Flame spread rate determines how fast the flame spreads along the fuel surface and it is an important parameter to study for fire safety purposes. Flame spread along the fuel surface could be involved in various incidents such as after an accidental fire start in the air wing compartment of the aircraft, fuel storage tanks, or even an oil spill. Specifically, the wing compartment of the aircraft is widely used for the fuel storage purposes in conventional aircraft, which makes the airplane wings one of the most hazardous areas in the aircraft. Therefore, knowing the flame spread rate of aviation fuel is vital to prevent the fire on time. Previous works have shown that the flame spread rate is a strong function of the initial temperature of the fuel and the flashpoint temperature of the fuel [9-30]. This study focuses on understanding the flame spread phenomenon of conventional and alternative aviation fuels.

### **4.1 Objective**

To understand the complexity of the flame spread phenomena for different fuels, it is essential to design and construct an appropriate experimental apparatus and to perform multiple experiments for different fuels to verify and determine the flame spread rates and critical transition temperatures. The objectives of this study are:

1. Design and construct a reliable and accurate experimental apparatus to record the flame spread phenomena of aviation fuels for different initial temperatures.
2. Calculate and compare the flame spread rates of current conventional aviation fuel Jet-A with the alternative aviation fuels such as Fischer-Tropsch-IPK (FT-IPK) jet-fuel, synthetic iso-paraffin (SIP) jet-fuel and hydro-processed esters and fatty acids (HEFA-50) based jet fuel.
3. Study the flame spread phenomena associated with all the test fuels.
4. Determine the critical transition temperature associated with each test fuel. The critical transition temperature is the temperature at which flame spread transits from a slower spread rate to a faster spread rate.

## 4.2 Background

The flame spread rate of hydrocarbon fuels and alcohol has been reported by many researchers over the past few decades. In this section, the key outcomes of most relevant studies are summarized. Kinbara [9] performed one of the first published experiments on the flame spread along liquid fuels in 1930 and studied the flame-spreading phenomena for different types of alcohol liquids. Kinbara [9] found that the flame spread rate over alcohols increases with liquid temperature upto a maximum and then decreases. The most recent experimental studies of the flame spread were performed by White et al. [11] and Li et al. [12-17] in 1997 and 2015 respectively.

Table 4-1 shows the chronological order of the most important papers that are related to the flame spread study along with the fuels since 1994. A similar summary table of the experiments done before 1994 could be found in the review done by Howard Ross [10].

Table 4-1: Key experimental studies of flame spread rate over liquid fuels since 1994

Authors	Fuels	Pan dimensions (cm)	Initial fuel temperature range (°C)	Findings
White et. al. [11], 1997	JP-5 JP-8	163 x 20 x 2.5 stainless steel pan	10-90	Flame spread rate for JP-5 and JP-8 for various initial temperatures range. Induction time as a function of initial fuel temperature Different critical transition temperatures for JP-5 and JP-8.
Degroote et. al. [18-22], 2000-2005	Methanol Ethanol 2-propanol 1-butanol	<ul style="list-style-type: none"> <li>Two pans with different sizes were used.</li> <li>- 40 x 40 x 2.5</li> <li>- 100 x 1.5 x 3.4</li> </ul>	-11-30	Pulsation effect of different alcohols. Critical transition temperatures were determined for different flame spreading regimes.



		<ul style="list-style-type: none"> <li>Aluminum and Pyrex walls to study the wall material effect on flame spread.</li> </ul>		
Li et. al. [12-17] 2014-2017	Aviation kerosene - RP5  0# diesel	163 x 4 x 10 with Pyrex windows equipped on both sides of the middle part of the pan	~16- ~100	Flame spread rates of RP-5 and #0 diesel as a function of initial temperature, the variation of sub-surface flow length as a function of initial temperature, flame spread rate of #0 diesel at different attitudes for different initial temperatures, pulsating behavior of flame spread across n-butanol,

White et al. determined the flame spread rate over JP-5 and JP-8 fuels for varying initial fuel temperatures and is most relevant to current study. JP-5 and JP-8 are military grade kerosene fuels. The primary difference between JP-8 and JP-5 is their closed cup flash-point. JP-5 has a higher flash-point of 60°C whereas JP-8 has a flash-point of 38°C. JP-8 is similar to Jet-A but it contains anti-corrosive and anti-icing additives. Figure 4-1 shows the experimental apparatus used by White et al. White et. al. used a stainless steel pan of 163 cm length, 20 cm width and 2.5 cm depth dimensions. Six hot water channels are installed under the pan to maintain a constant temperature above 20°C. In addition, a hot water heater is used to heat the fuel to the required temperature before pumping the fuel into the pan. The flame spread event was recorded using a video camera with a capability of 30 fps and it is calculated using by utilizing frame by frame from one end of the pool to another end.

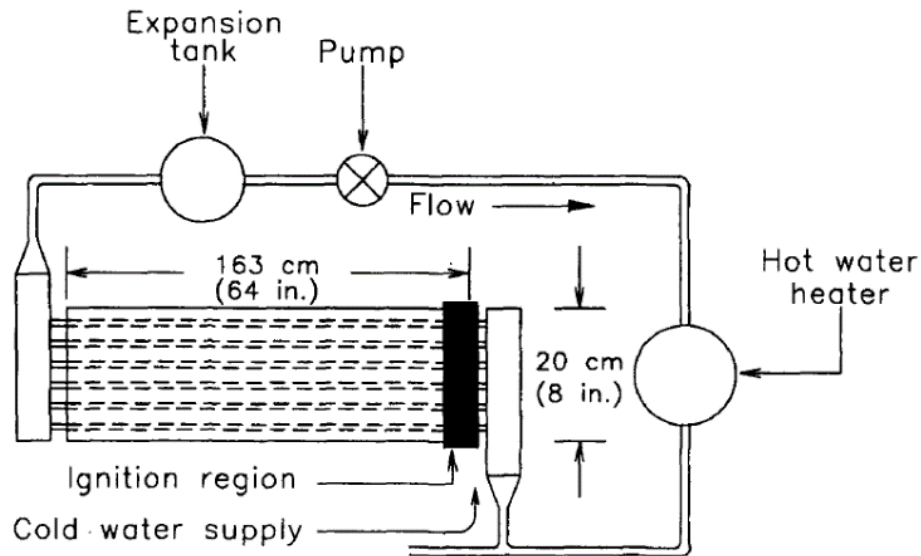


Figure 4-1: Experimental apparatus for determining the flame spread rate by White et. al. [11]

The results obtained by White et al. shows the flame spread rate for JP-5 and JP-8 for different initial temperatures. The results by White et al. are shown in Figure 4-2.

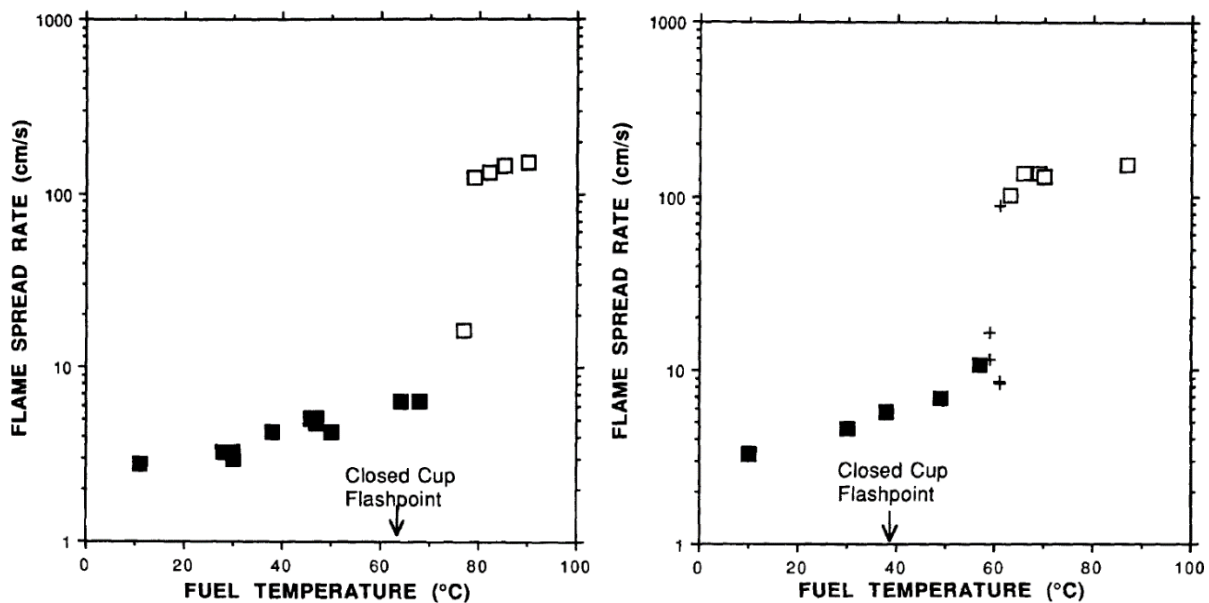


Figure 4-2: Flame spread rates of JP-5 (left) and JP-8 (right) fuels as a function of initial fuel temperature [11]

The results for JP-5 and JP-8 clearly demonstrated a dependence of flame spread rate on initial temperatures. The flame spread rate is slow and ~10 cm/s for initial fuel temperatures below the

respective flash-points and the rate increases above the flashpoint temperature of the fuel. The flame spread rate drastically increases to  $\sim 150$  cm/sec when the initial temperature of the fuel was above the flashpoint by  $\sim 15^\circ\text{C}$ . The reason for this is because below flashpoint the flame propagation is liquid phase-controlled (slower), and above flashpoint, the flame propagation is gas phase-controlled (faster). Additionally, White et al. used small size foam polystyrene tracers in the middle of the pan in order to study the movement of the liquid during the flame spread. They found that there was no liquid movement during the flame spread for the gas phase-controlled flame spread however liquid movement was observed for the liquid phase-controlled flame propagation due to strong sub-surface convective heat transfer.

Another experimental apparatus was built by Li et al. [12-17] in order to study the flame spread rates for aviation kerosene and diesel. Figure 4-3 shows the experimental apparatus designed by Li et al. The dimension of the pan is 100 cm length, 4 cm width and 10 cm depth. The liquid pool is ignited by using a small amount of heptane poured at one end of the pool. The flame propagation is recorded using a lateral CCD camera and a thermal IR camera. A thermal IR camera is used to measure surface temperature of the liquid pool.

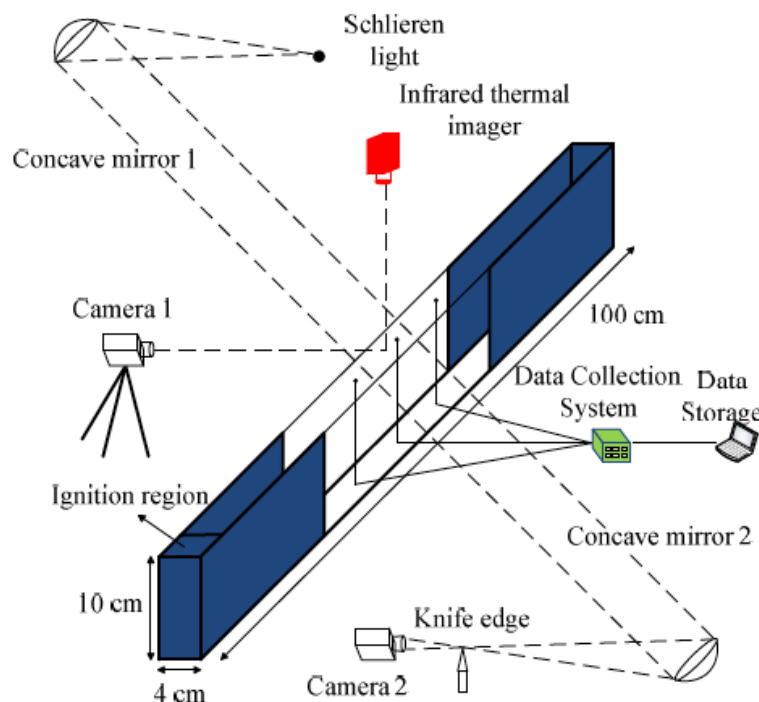


Figure 4-3: Experimental apparatus by Li et al. for determining the flame spread rate [4]

The results are shown in Figure 4-4. The same trend for the flame spread was shown in the results of RP5 and diesel as in the experimental results of White et al. for JP-5 and JP-8. The flame spread rate slowly increased from ~1 cm/s at temperatures below the flashpoint temperature of the test fuel, and drastically increased to ~100 cm/sec when the initial temperature of the fuel was above the flashpoint by around 15°C. The threshold for the transition from liquid controlled phase to the gas phase-controlled also occurred around 15°C above for the flashpoint of each fuel.

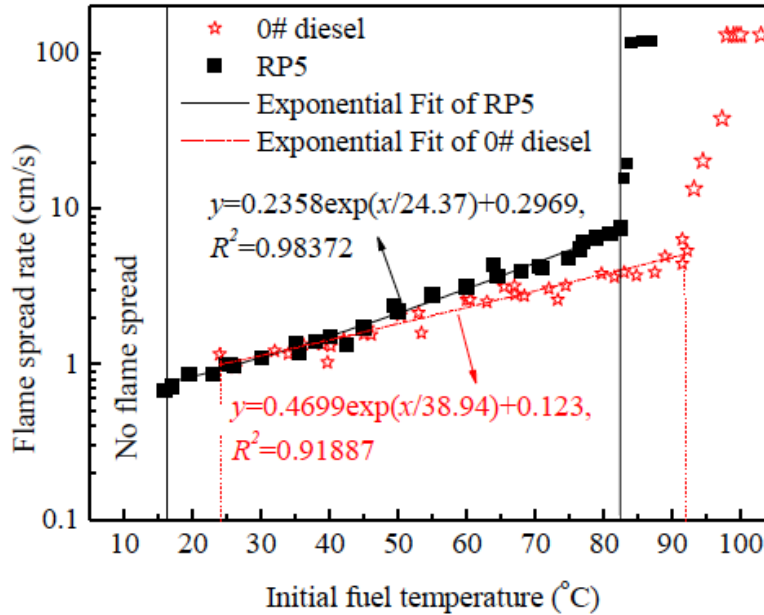


Figure 4-4: Flame spread rates of 0#diesel and RP5 fuels as a function of initial fuel temperature [11-15]

The Spanish research team, Degroote et al. [18-22] had also performed multiple experiments on flame propagation along the liquid fuels. They studied flame spread for four different aliphatic alcohols such as methanol, ethanol, 2-propanol, and 1-butanol. Two different pan sizes were used to study flame spread along those alcohols. The sizes of the testing pans were 40 cm in length, 4 cm in width and 2.5 cm in-depth, and 100 cm in length, 1.5 cm in width, and 3.4 cm in depth. Tests were performed in a quiescent environment at room temperature close to 21°C. The refrigerant circuit below the pan was used in order to control the initial temperatures of the alcohol. Degroote et al. used composite imaging technique to study the flame front propagation and 8 different thermocouples to study gas-phase flame evolution along the fuel surface.

Burgoyne and Roberts [23-25] were the first ones who studied the effects of the size of the pan on flame spread rate. They studied the flame propagation for different pan widths and fuel depths for iso-pentanol. Pan widths of 2.5 cm, 3.3 cm, and 6.3 cm were used to study the effect of pan width to flame spread rate at various initial temperatures, and it was concluded that width had no effect for higher temperatures where gas phase flame regime was observed. However, there was a difference in flame spread rate for different pan widths for lower fuel temperatures. In addition, no significant flame spread differences were reported for the fuel depths from 0.1 cm to 0.5 cm for the fuels above flashpoint. Therefore, Burgoyne and Roberts concluded that pan dimensions do not play significant role for the gas phase flame spread in determining flame spread rate; however, the effect of pan sizes for flame spread at lower fuel temperatures is needed for study.

In 1970, Mackinven et al. [26] studied effect of pool fire dimensions on the flame spread rate and used n-decane as the test fuel. Figure 4-5 shows the effect of the pan width and pan depth on the flame spread rate for different wall materials.

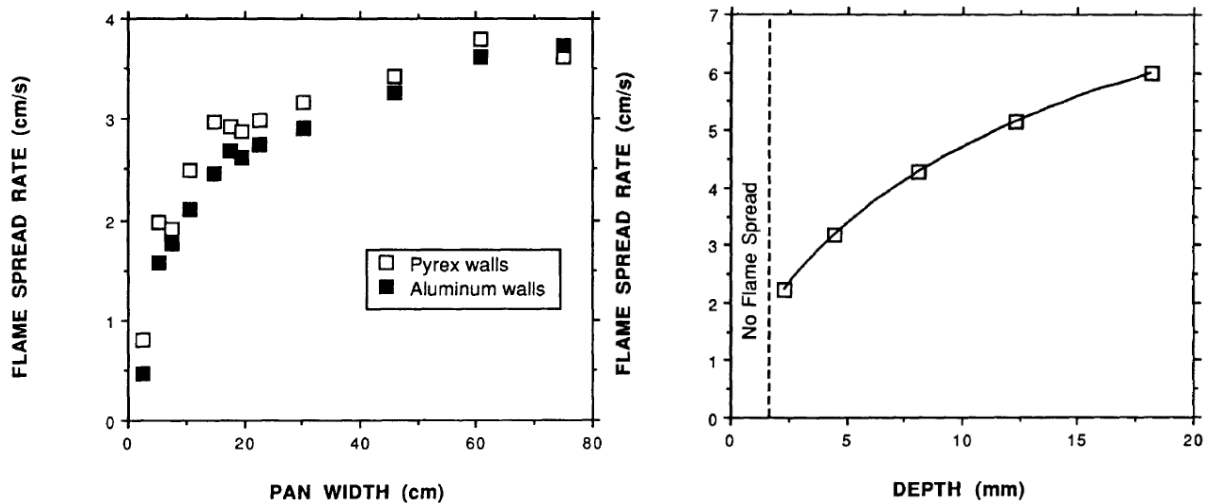


Figure 4-5: Effect of the pan width (*left*) and pan depth (*right*) on the flame spread rate [26]

Mackinven [26] determined that the width of the pan up to 20 cm had highly influenced the flame spread rate because of the viscous drag effect on the walls, and there was only a slight change in the flame spread in a 20 to 80 cm width of the pan. The effect of the different pan wall materials has also been studied as an effect on a flame spread rate. The use of aluminum walls had shown less flame spread rate than use of Pyrex walls because of the thermal conductivity difference

between both materials that affect the heat losses to the wall. experiment was repeated by Torrance [27-28] repeated the experiment, and similar results were obtained [27-28]. Results showed that the flame spread rate increased as the fuel depth increased on the pan. After 30 mm, there were not any significant changes in a flame spread rate. It has also been shown that there was no flame spread when the fuel depth was below 1.5 mm. Figure 4-6 shows the results for different pan length effects on flame spread rate, and it was found that above 180 cm there was no significant change on flame spread rate.

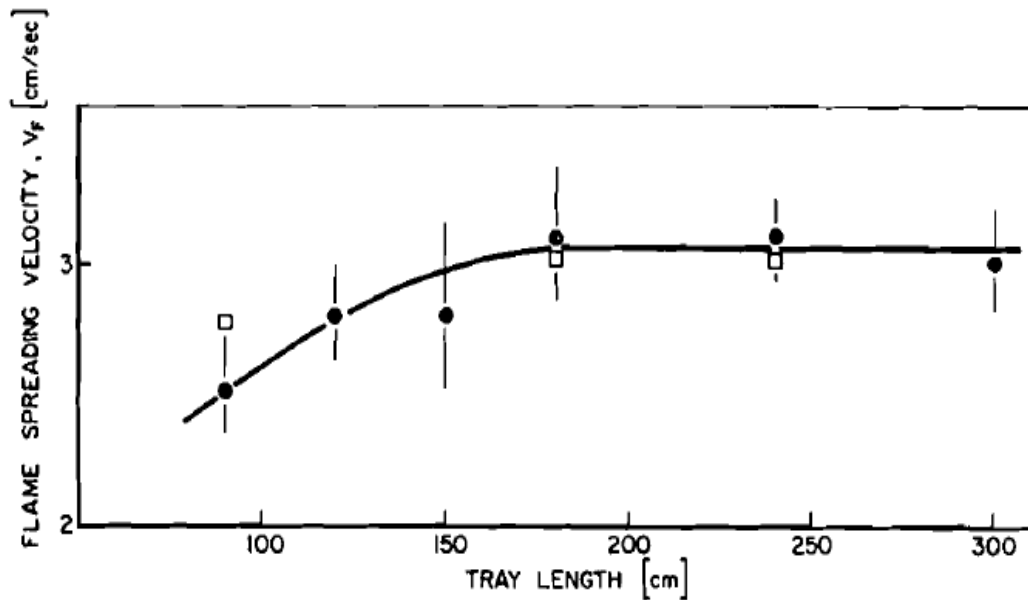


Figure 4-6: Effect of the pan length to the flame spread rate [26]

Kinbara and Burgoyne et al. divided flame spread characteristics into three regimes depending on the flame spread rates at the different initial fuels. They described first regime as a slow flame spread below the flashpoint, which was mainly driven by the preheating the fuel sub-surface, second regime was the flame spread transitioning from the liquid phase to gas phase where abrupt increase in flame spread rate was observed. The third regime was described as the region of maximum flame spread rate because of the high partial pressure of the combustible gases along the fuel surface which created almost stoichiometric mixture with the air. However, Akita [29-30] did extensive research on flame spread rate propagation along methanol and observed five different regimes for the flame spread along the methanol. Figure 4-7 shows the five regimes divided by Akita.

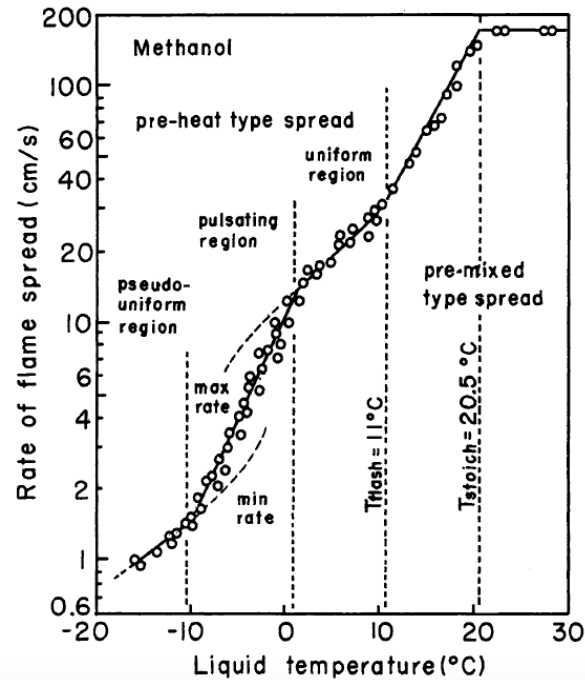


Figure 4-7: Flame spread regimes for methanol described by Akita [29].

Those regimes are pseudo-uniform, pulsating region, uniform region, transition, and pre-mixed region. The same five flames spread characteristics were observed for different liquid fuels including hydrocarbon fuels and other types of alcohols by White et al. and Li et al. in the recent experiments. Mackinven et al. have also done qualitative analysis of the flame spread below the flashpoint. They tried to explain the flame spread below the flashpoint using the schematic shown in Figure 4-8.

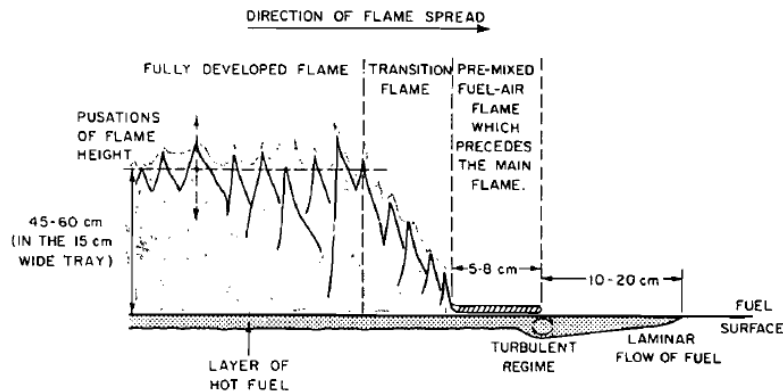


Figure 4-8: Schematic of the flame spread along the fuel surface below the flashpoint by Mackinven [26]

They observed the blue flame in front of the fuel, which they explained as a premixed fuel. The reason is that the fuel was initially below the flashpoint, and then the fuel was heated to its flashpoint from the flame behind by creating enough vapor to premix with the air. However, they also observed pulsation along the length to back and forth during the flame spread. Mackinven et al. explained the reason for the pulsation was because of the fire point and flashpoint difference of the fuel. When the fuel reached the flashpoint, the temperature of the fuel was not enough to sustain the flame along the surface, therefore, extinguished back to the transition flame. However, a steady flame spread without pulsation was observed for n-butanol fuel even though the flashpoint and fire point (a temperature enough to sustain the flame) was very close compared to other fuels. It was shown later in the experiments that the idea of fire point and flashpoint difference was not the main factor for the pulsation phenomenon as later experiments still showed pulsation using the alcohols having the same fire point and flashpoint. Therefore, the cause of the pulsation during the flame spread was explained by the creation of the gas-phase recirculation cell in front of the flame which quickly combusts and quenches back and forth as the flame spread along the fuel. The detailed schematic of the flame spread below the flashpoint by Li et al. is shown in Figure 4-9.

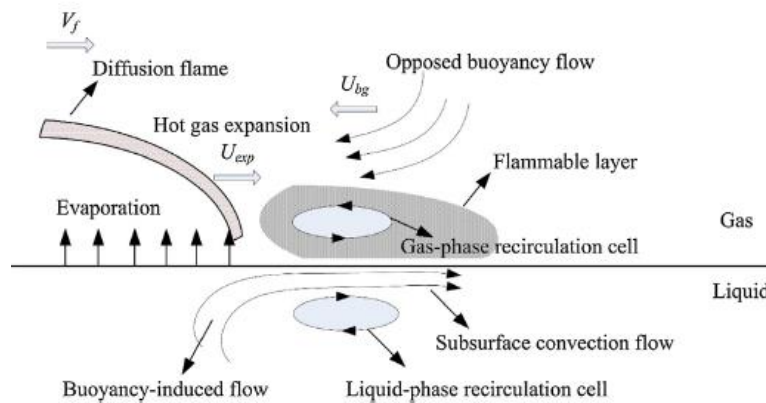


Figure 4-9: Schematic representation of flame propagation over the fuel maintained at a temperature below its flashpoint [15]

The gas-phase flame spread exists when the initial temperature of the fuel is above the flashpoint. Fuel vapor will start to be created along the surface of the fuel, thus creating fuel and air mixture along with the fuel, which would quickly combust after the ignition of the fuel. Therefore, the flame spread rate above the flashpoint would be expected to be much higher than the flame spread rate below the flashpoint. All the previous studies by Akita et al., Mackinven et al., Burgoyne et al., White et al., and Li et al. reported the gas flame spread rates between 130 to 220 cm/s.



Li et al. introduced two different types of gas-phase flame spread depending on the flame spread rate and visual differences of flame spread. Those regimes are described as super-flash lean and super-flash stoichiometric depending on the position of the main yellow flame front compared to the blue precursor flame. The main yellow flame front propagates slower compared to the blue precursor flame front during the super-flash lean regime and matches the precursor flame at the super-flash stoichiometric regime.

Based on the literature review, a study is needed to investigate the flame spread phenomenon over the alternative aviation fuels and therefore a novel experimental apparatus is designed and fabricated to measure and compare the flame spread rate of conventional aviation fuel Jet-A with the alternative aviation fuels such as Fischer-Tropsch-IPK (FT-IPK) jet-fuel, synthetic iso-paraffin (SIP) jet-fuel and hydro-processed esters and fatty acids (HEFA-50) jet fuel for varying fuel temperatures.

Following key points are withdrawn for design and fabrication of the experimental apparatus for flame spread measurements of liquid fuels at different initial temperatures,

1. The testing pan should be at least 180 cm in length, 20 cm in width, and a depth of 2.5 cm in order to measure the flame spread of the fuel without any effect from the size of the apparatus.
2. The testing pan should be able to keep the fuel contained in the pan close to a steady-state temperature during the experiment.
3. The apparatus should have the capability to heat the fuel for temperatures higher than its respective flash-point.
4. The fuel should be preheated in a specific vessel so that the light volatile components of the multi-component hydrocarbon fuels do not escape into the environment.
5. The ignition event should not have any effect on the flame spread.
6. Several flame-extinguishing methods should be installed for the safety of the experiment and personnel.
7. The initial ignition region and the end portion of the test pan should not be used for flame spread rate calculation.

In the following chapter, all components of the experimental apparatus are explained in detail.

## 5. POOL FIRE APPARATUS

### 5.1 Apparatus Overview

The experimental apparatus consists of the following main components,

1. A stainless-steel testing pan with the dimensions of 180 cm length x 25 cm width x 2.5 cm depth. The pan has the bottom three channels for the thermal fluid to keep the fuel in the pan at the required temperature during the test.
2. Fuel heating vessel that preheats the fuel to the initial test temperature before the experiment. The heating vessel is pressurized using a nitrogen cylinder during the heating in order to keep the light volatile gases from escaping the fuel heating vessel. Fuel is pumped under pressure to the stainless steel testing pan to perform the test after fuel reaches the required temperature.
3. Re-circulator heater Julabo SL-12 which heats and pumps the working thermal fluid to the bottom of the pan and to the shell of the heating vessel to heat and maintain the initial fuel temperature at the required temperature.
4. Nd: YAG laser is used to ignite the fuel for the tests with the initial temperature above the flashpoint and propane torch for the tests below the flashpoint as laser energy was not sufficient to ignite the fuel vapor-air mixture.
5. Lid-actuation system and CO<sub>2</sub> fire suppression methods are employed to extinguish the fire. The CO<sub>2</sub> fire suppression system is a secondary measure to extinguish the fire and used in a situation if shutting down the lid doesn't extinguish the fire.
6. Temperature feedback is collected from 16 K-type thermocouples that were installed along the length of the pan. Six thermocouples are used to measure the temperature of the liquid phase, and the other ten thermocouples are used to measure the temperature of the gas phase.
7. Three different cameras are used to record the flame spread phenomenon,
  - A high-speed black-white camera (5000 Hz),
  - FLIR SC6100 Infrared high-speed camera (5000 Hz), and

- Canon T3i Regular visible (30 Hz).

Figure 5-1 shows the CAD image of the experimental apparatus.

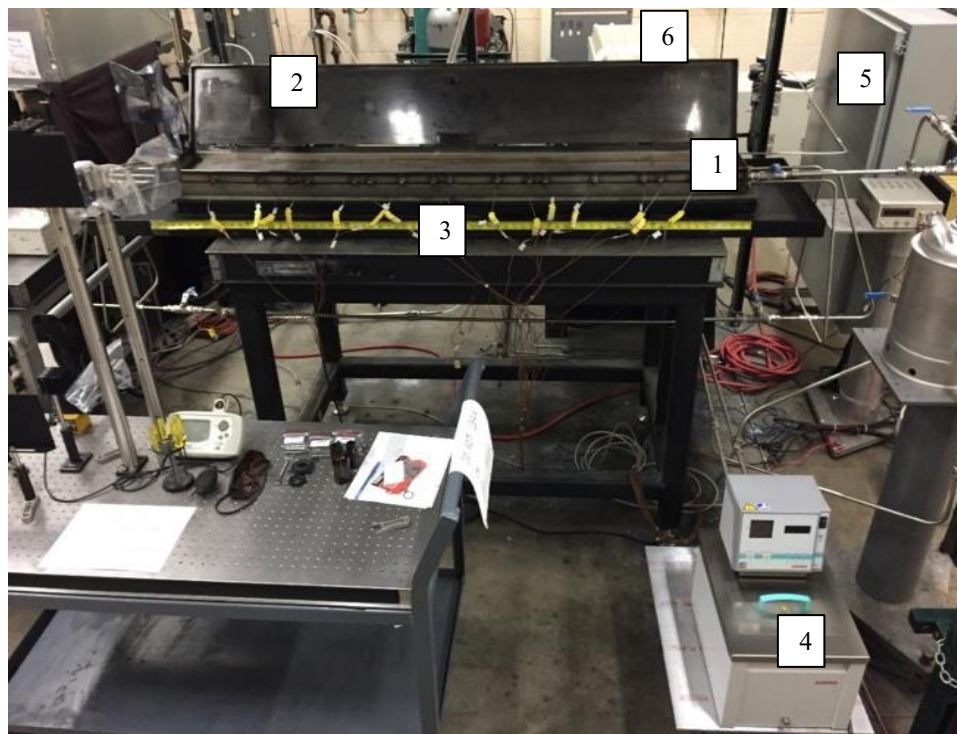


Figure 5-1: CAD image of the experimental apparatus

The numbered components in figure 5-1 are as follows,

- 1) Test pan
- 2) Lid
- 3) Thermocouples
- 4) Re-circulator heater
- 5) Fuel heating vessel
- 6) CO<sub>2</sub> fire extinguisher system
- 7) Nitrogen cylinder
- 8) Video recorders

- 1. Test pan
- 2. Lid
- 3. Thermocouples
- 4. Re-circulator heater
- 5. Data Acquisition box
- 6. Laser Head



- 7. Laser System
- 8. Fuel heating vessel
- 9. Nitrogen cylinder
- 10. Lid actuation system power control



Figure 5-2: Complete experimental apparatus

A Process and Instrumentation Diagram (P&ID) of the experimental apparatus is shown in Figure 5-3. The test pan holds 9-liters of fuel, which is maintained at a controlled temperature by a thermal fluid transfer channel with a stagnant volume of 20 liters of fluid. The thermal fluid temperature conditioning system shown within the blue rectangle is still under construction. However, the remaining apparatus has been used for the measurements reported here. The thermal fluid will be pumped into the conditioning channels by a pump that will receive the fluid from a heater and distribute it into two paths. The first path will be for conditioning the temperatures of the test pan and the second path will be for maintaining the temperature of the fuel storage tank. The system involving storage of the fuel at the test temperature and rapid delivery to the test pan will minimize the escape of fuel vapors into the test cell prior to the initiation of the ignition event.

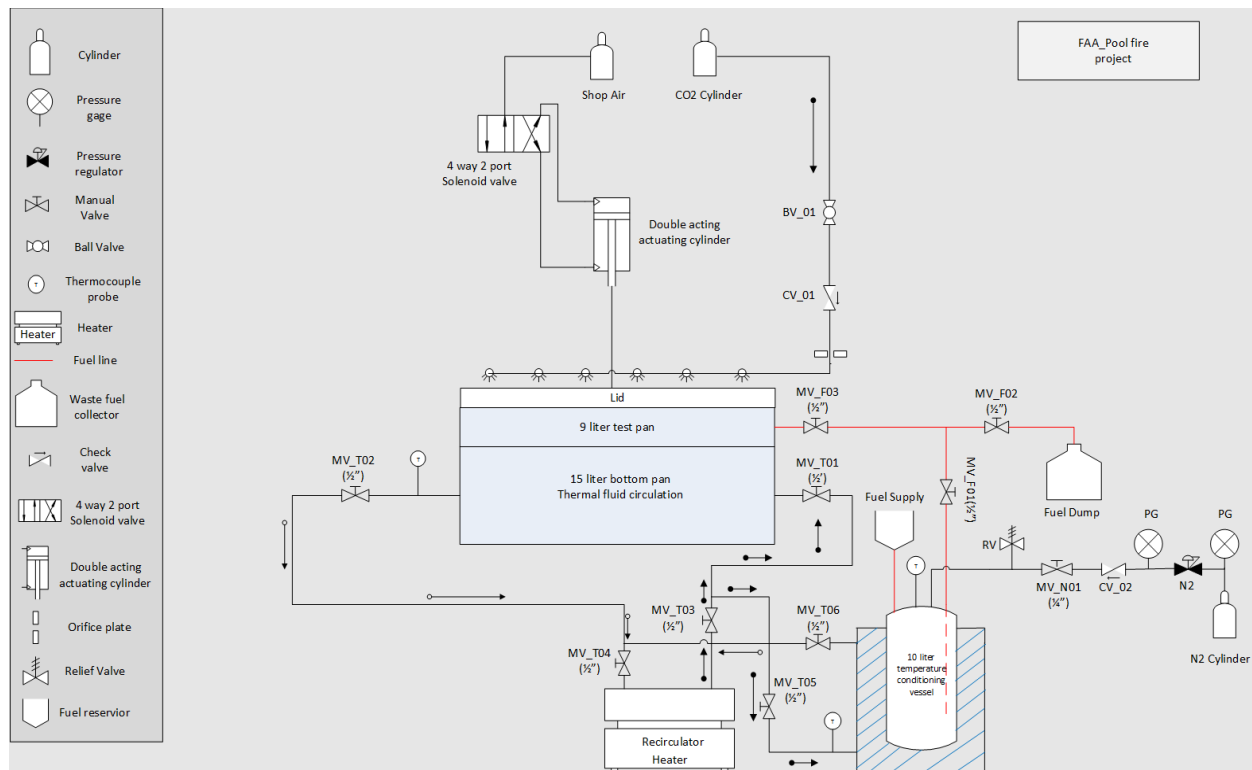


Figure 5-3: P&ID of the experimental apparatus

A lid-actuation system is installed to extinguish the fire as soon as it spreads across the pool. The lid-actuation system consists of a pneumatic double-acting cylinder connected to the lid. Air-inlet ports in the pneumatic cylinder are connected to a 4-way solenoid valve for controlling the movement of pneumatic cylinder. A CO<sub>2</sub> fire extinguisher system is installed along the x-axis of

the pool at 60 cm height to extinguish the fire in case of a failure of the lid actuation system. The CO<sub>2</sub> fire extinguisher system consists of 6 full-cone spray nozzles mounted 12" apart with 0.10" orifice diameter, a spray angle of 60°.

## 5.2 Apparatus Design Characteristics

In this section, all the major components of the apparatus are discussed in detail.

### 5.2.1 Testing pan

A rectangular stainless steel pan was designed based on literature studies and is 180 x 20 x 2.5 cm, ensuring that the resulting data is not affected by the size of the apparatus. The rectangular pool is shown in Figure 5-4. The drawings of the pan is shown in Appendix A.

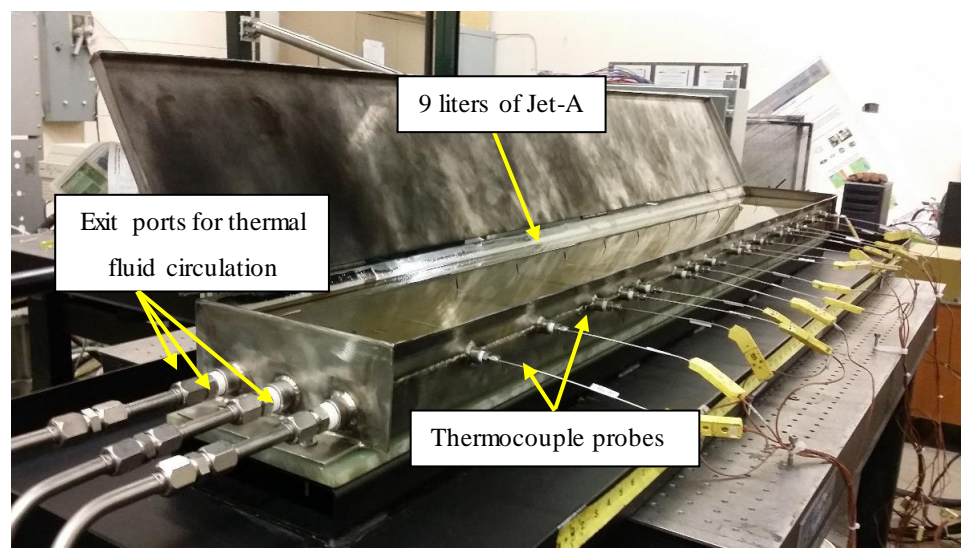


Figure 5-4: Isometric view of the rectangular pool

The length of the pool is divided into three different sections for data analysis purposes. The first 30 cm of the pan are designated to the ignition zone, and the last 30 cm of the pan has been designated to be the end zone and therefore have not been used for flame spread calculation to minimize the effects of the pool boundaries on the data.



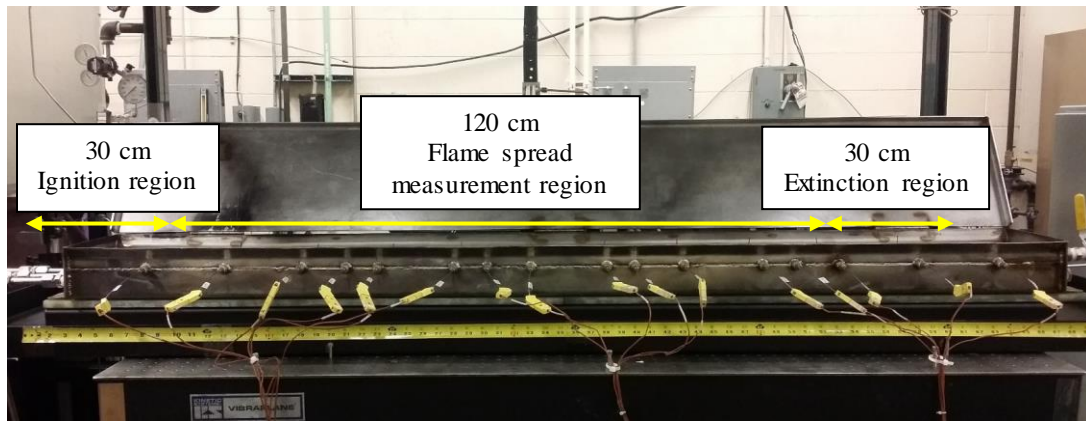


Figure 5-5: Front view of the rectangular pool

The test pan has a volume of 9 liters for the fuel, which is maintained at a controlled temperature on the top section of the pan by a thermal fluid transfer channel with a stagnant volume of 20 liters of fluid. The top and bottom sections of the pan are shown in Figure 5-6. The bottom section (thermal channel) is divided into three flow paths in order to distribute the thermal fluid uniformly along the length of the pan. The dimensions of this component of the pan are shown in APPENDIX D – .



Figure 5-6: CAD models of top test pan (*top*) and bottom (*bottom*) pan

### 5.2.2 Re-circulator heater

Thermal fluid with a high boiling point is used to control the temperature of the fuel in the pan and the fuel heating vessel. The thermal fluid is pumped into the conditioning channels by a pump that receives the fluid from the re-circulator heater and distributes it into two paths. The first path is for conditioning the temperatures of the test pan and the second path is for maintaining the temperature of the fuel storage tank. Julabo re-circulator heater is being used to meet the experiment requirements.

The Julabo re-circulator heater SL-12 can operate at temperature ranges from 20-300 °C with temperature stability of 0.01 °C. The pump flow rate capacity can vary from 22-26 liters per minute with a pump capacity flow pressure of 5.8 psi to 10.2 psi. In addition, the thermal fluid (C20S) was also ordered from Julabo which has a boiling point above 250°C and can work at temperature range 0-220 °C. Therefore, theoretical range for flame spread measurements could be done at initial temperatures from 20-220 °C.



Figure 5-7: Re-circulator heater

### 5.2.3 Fuel heating vessel

The fuel will be preheated in a jacketed stainless steel pressurized vessel in order to decrease the heating time to a certain initial temperature. The vessel is pressurized with N<sub>2</sub> so that the light fuel volatiles do not escape into the environment while the fuel is being heated. A heat transfer fluid (silicone thermal fluid C20S) is supplied to the



Figure 5-8: Fuel heating vessel




jacket surrounding the pressure vessel to heat the fuel. The heating vessel can contain up to 10 liters of fuel, which is enough to fill the pan. The image of the heating vessel is shown in Figure 5-8: Fuel heating vessel, and the drawing is attached in Appendix D6-Fuel Heating Vessel.

#### 5.2.4 Fuel ignition system

An Nd:YAG laser is used to focus 130 mJ energy per pulse at the fixed ignition location above the liquid surface for each test. The specifications of the laser are shown in Table 5-1.

Table 5-1: Laser Specifications

<b>Model</b>	Spectra-Physics Quanta-Ray GCR200 PIV400-10 (Double-head Double-pulsed Q-switch Nd:YAG laser)
<b>Energy</b>	max 400 mJ/pulse @532nm
<b>Repetition rate</b>	10 Hz
<b>Pulse duration</b>	5-10 ns
<b>Beam divergence</b>	< 0.5 mrad
<b>Beam diameter</b>	1 cm
<b>Beam shape</b>	

The ray diagram of the laser is shown in Figure 5-9.

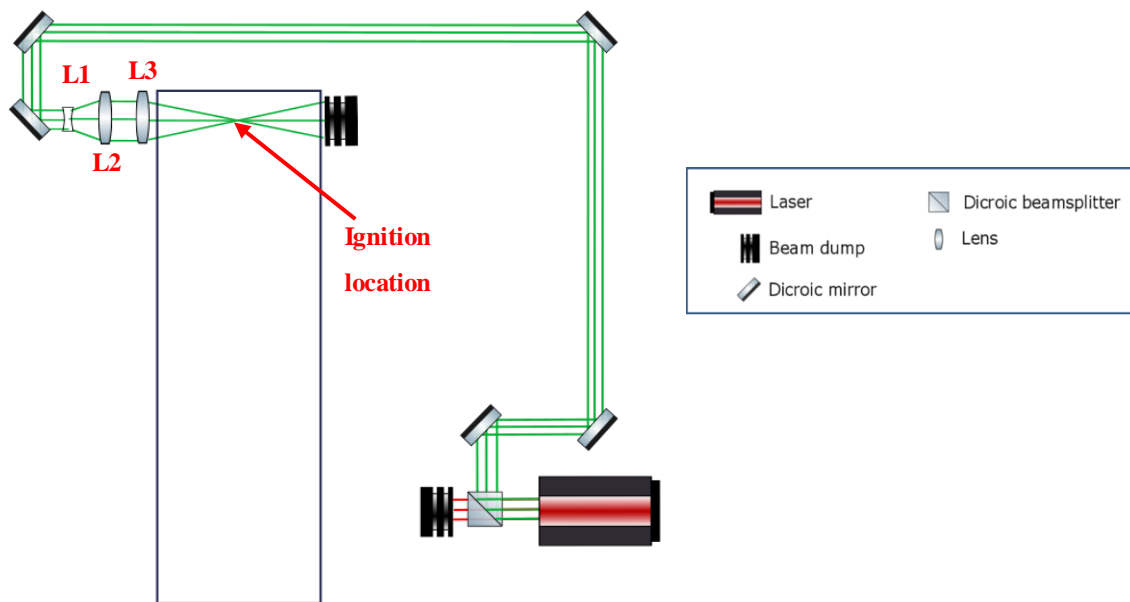


Figure 5-9: Ray diagram for laser ignition

Laser ignited a fire at various stages of development and spread are shown in Figure 5-10.

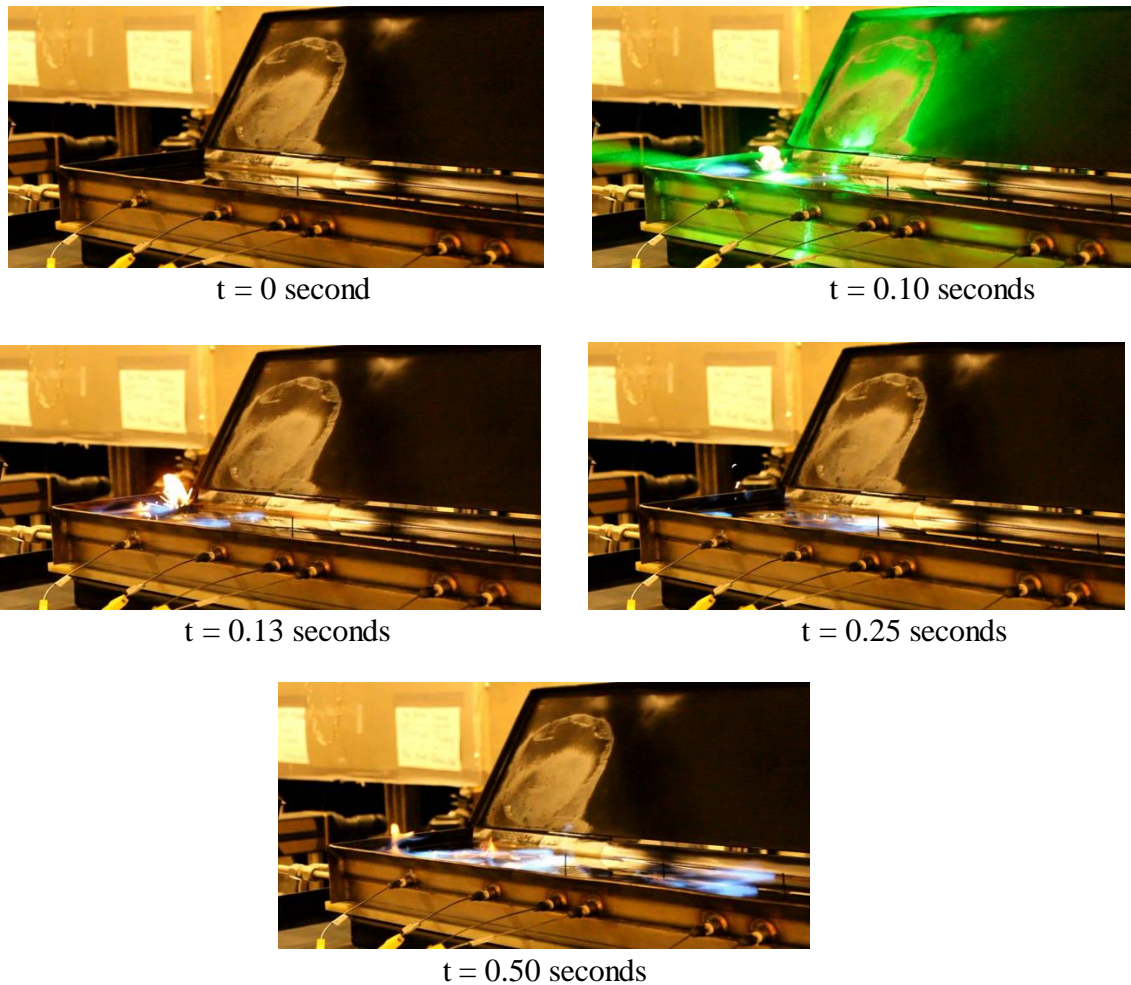


Figure 5-10: Laser Ignition and flame-spread process overhated Jet-A pool

For the test images shown in Figure 5-10, fuel's initial temperature is 60°C, and the laser beam with 158 mJ is focused at 2 mm above the liquid pool surface.

### 5.2.5 Fire extinguishment methods

Two different types of fire extinguishment methods are used for the tests. Firstly, a lid-actuation system is employed to extinguish the fire. In this system, a lid is controlled autonomously closed, once the fire reaches the other end of the pool. If the fire doesn't extinguish after closing the lid, then the CO<sub>2</sub> fire extinguishment system is used to extinguish the fire. Both fire extinguishment methods are discussed below.

### 5.2.5.1 Lid-actuation System

A lid-actuation system is installed to extinguish the flame as soon as fire spreads across the pool. A lid-actuation system shown in figure 5-11 consists of a pneumatic double-acting cylinder connected to the lid. Air-inlet ports in the pneumatic cylinder are connected to a 4-way solenoid valve to control the movement of the pneumatic cylinder.

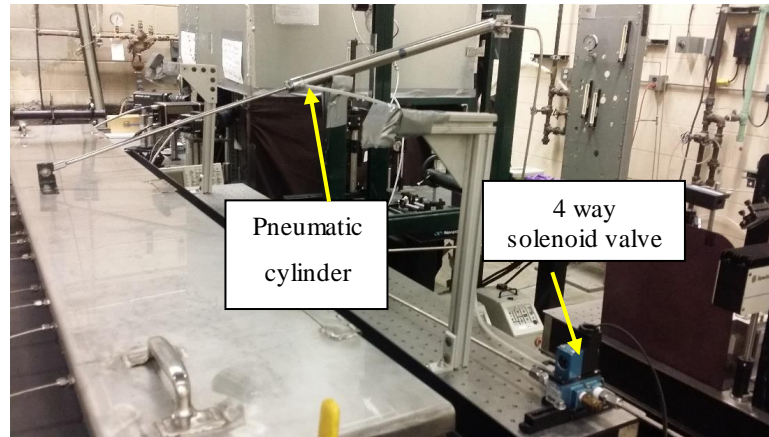


Figure 5-11: Lid-Actuation system

### 5.2.5.2 CO<sub>2</sub> Extinguishment System

The CO<sub>2</sub> fire extinguisher system shown in figure 5-12 is also installed along the x-axis of the pool at the height of 2 meters to extinguish the fire in case the fire still persists after closing the lid. The CO<sub>2</sub> fire extinguishing system consists of 6 full-cone spray nozzles with a 0.10" orifice diameter, and a spray angle of 60° and the distance between each spray nozzle is 12".

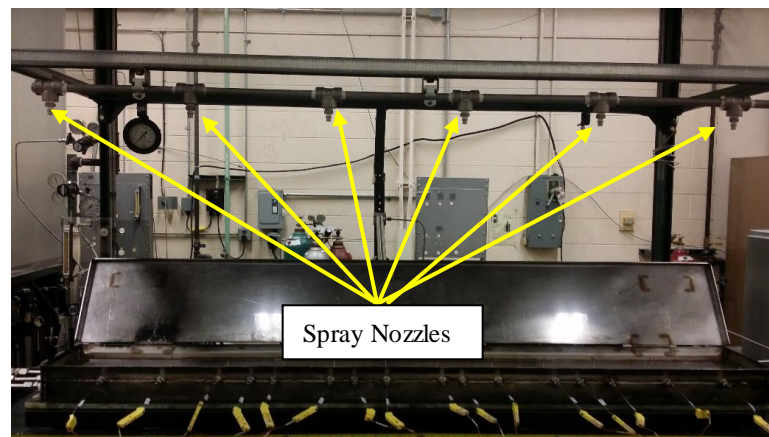


Figure 5-12: CO<sub>2</sub> fire extinguisher system

## 6. FLAME SPREAD RATE

The flame spread rates of Jet-A, Fischer-Tropsch-IPK(FT-IPK), Hydro-processed esters, and fatty acids (HEFA-50) and Synthetic Iso-paraffin (SIP) jet fuels at room temperature and temperatures above the test fuels' respective flash-point are reported. Table 6-1: Fuel properties\* below shows the properties of the fuels being tested,

Table 6-1: Fuel properties\*

Fuels	Molecular weight (kg/kmol)	Density at 15°C (kg/m <sup>3</sup> )	Flashpoint (°C/°F)	Boiling point range (°C/°F)	AIT (°C/°F)
Jet-A	167	806	43/109.4	138-300/300-572	210/410
FT-IPK	154	760	40/104	Min. 136/277	N/A**
HEFA-50	168	783	41/105.8	198 @ 14 psi/389	N/A**
SIP	212	772	>110/230	198	197/387

\* Information from fuel's safety datasheet

\*\* Not available

Jet-A is a kerosene-based fuel used in turbine-engines with flash-point of 43°C. FT-IPK is a kerosene-based fuel made from the Fischer-tropsch process. FT-IPK fuel contains C8-C16 carbon chains, branched and linear with a flash-point of 40°C. Synthetic iso-paraffin (SIP) is a farnesane (2,6,10-trimethyldodecane) derived jet fuel. The flash-point of SIP is greater than 110°C. Hydro-processed ester fatty acids-50 (HEFA-50) fuel is kerosene-based fuel derived from Camelina. HEFA-50 is a blend of 50% HEFA and 50% Jet-A by volume. The flash-point of HEFA-50 jet fuel is 41°C. It should be noticed that the flash-point of SIP is approximately 3 times of Jet-A, HEFA and FT-IPK fuels. Thus, SIP should be heated to at least 110°C, before it can be ignited. Table 6-2 shows the Jet-A composition by hydrocarbon type and should be noted it contains all main hydrocarbon types. The fuel compositions and properties are measured in LORRE lab at Purdue University using two dimensional gas chromatography with flame ionization detector (FID) and is reported by Vozka and Kilaz [32].

Table 6-2: Jet-A composition [31-32]

	Hydrocarbon type			
	n-alkanes	Iso-alkanes	Cycloalkanes	Aromatics
C7	0.01	0.20	0.36	-
C8	0.73	0.42	6.42	1.91
C9	4.54	4.27	6.52	4.80
C10	4.94	6.65	5.57	3.63
C11	3.46	4.99	3.63	2.18
C12	2.49	3.09	2.64	4.59
C13	1.94	2.90	1.44	3.90
C14	1.36	2.35	0.46	2.23
C15	0.83	1.24	0.00	0.87
C16	0.38	0.76	0.00	0.58
C17	0.13	0.17	0.02	-
C18	0.02	0.06	-	-
C19	-	0.03	-	-
<b>Total</b>	<b>20.81</b>	<b>27.11</b>	<b>27.07</b>	<b>24.69</b>

Table 6-3: HEFA-50 composition [31-32]

	Hydrocarbon type			
	n-alkanes	Iso-alkanes	Cycloalkanes	Aromatics
C7	0.05	0.04	0.07	-
C8	0.95	0.82	0.86	0.76
C9	2.84	6.77	3.17	1.93
C10	2.86	8.86	3.15	2.14
C11	2.07	7.50	3.01	2.13
C12	1.60	5.90	2.31	2.14
C13	1.32	5.71	1.98	1.53
C14	0.94	4.51	1.26	0.88
C15	0.87	3.91	0.70	0.23
C16	0.78	5.95	0.36	0.12
C17	0.14	5.97	0.11	-
C18	0.01	0.46	-	-
C19	-	0.04	-	-
<b>Total</b>	<b>14.43</b>	<b>56.42</b>	<b>16.99</b>	<b>11.86</b>

Table 6-4: FT-IPK Composition [31-32]

	Hydrocarbon type			
	n-alkanes	Iso-alkanes	Cycloalkanes	Aromatics
C7	0.00	0.00	0.06	-
C8	0.00	0.04	0.28	0.02
C9	0.08	9.23	0.53	0.08
C10	0.00	19.48	1.15	0.02
C11	0.07	24.43	1.06	0.10
C12	0.11	26.20	0.40	0.04
C13	0.07	10.88	0.00	0.05
C14	0.04	4.48	0.00	0.01
C15	0.02	1.06	0.00	0.00
C16	0.01	0.00	0.00	0.00
C17	0.00	0.00	0.00	-
C18	0.00	0.00	-	-
C19	-	0.00	-	-
<b>Total</b>	<b>0.40</b>	<b>95.80</b>	<b>3.48</b>	<b>0.32</b>

Table 6-5: SIP composition [31-32]

	Hydrocarbon type			
	n-alkanes	Iso-alkanes	Cycloalkanes	Aromatics
C7	0.00	0.00	0.27	-
C8	0.00	0.00	0.00	0.00
C9	0.00	0.00	0.00	0.00
C10	0.00	0.00	0.00	0.00
C11	0.00	0.00	0.05	0.00
C12	0.00	0.00	0.00	0.00
C13	0.00	0.00	0.00	0.00
C14	0.00	0.05	0.41	0.00
C15	0.00	99.21	0.00	0.00
C16	0.00	0.00	0.00	0.00
C17	0.00	0.00	0.00	-
C18	0.00	0.00	-	-
C19	-	0.00	-	-
<b>Total</b>	<b>0.00</b>	<b>99.27</b>	<b>0.73</b>	<b>0.00</b>

HEFA-50 composition is mentioned in table 6-3 and similar to Jet-A it contains all hydrocarbon groups, and this is due to the fact that it is a 50:50 vol% mixture with Jet-A [31-32]. Table 6-4 shows that FT-IPK is primarily composed of iso-alkanes and cycloalkanes [31-32]. Table 6-5 shows SIP composition and it should be noticed that SIP is primarily a C-15 isoalkane, namely farnesane (2,6,10-trimethyl-dodecane) [31-32].

A black and white high-speed and a DSLR video cameras are used to record the ignition and flame spread event for all the tests. A high-speed infrared camera synchronized with the black and white high speed camera is used as an additional source to record the flame spread rate. Six liquid phase temperature monitoring thermocouples and nine gas phase temperature monitoring thermocouples are used to record the time history of temperatures at various spatial locations. Figure 6-1 shows photographs of the pool fire apparatus obtained with the high-speed camera (B&W) and the low speed visible camera (color). The 9 gas phase thermocouple locations are labeled with yellow pointers in both figures.



Figure 6-1: Gas-phase thermocouple locations



The distance between the centrally placed gas phase thermocouple is 15 cm. The first 30 cm of the pan are designated as the ignition zone and the last 30 cm of the pan have been designated as the end zone and therefore have not been used for flame spread calculation to minimize the effects of the pool boundaries on the data. The flame spread rate is calculated by dividing total distance from the first gas phase thermocouple to the last (ninth) gas phase thermocouple which is 120 cm by the time it takes for the flame to spread across that distance. Table 6-6 summarizes the tests conducted for the four fuels with different initial fuel temperatures above flashpoint.

Table 6-6: Test matrix for fuel initial temperature above flashpoint

<b>Fuel (Flashpoint °C)</b>	<b>Initial Fuel Temperature (°C)</b>							
	<b>Test 1</b>	<b>Test 2</b>	<b>Test 3</b>	<b>Test 4</b>	<b>Test 5</b>	<b>Test 6</b>	<b>Test 7</b>	<b>Test 8</b>
<b>Jet-A (43°C)</b>	100	90	80	70	60	50	40	25
<b>FT-IPK (40°C)</b>	100	90	80	70	60	50	40	25
<b>HEFA(41°C)</b>	100	90	80	70	60	50	40	25
<b>SIP (&gt;110°C)</b>	140	130	120	110	100	90	80	70

The test matrix starts with a fuel temperature significantly higher than the flashpoint with stepwise reductions until a point of no ignition is reached. No ignition means that the fuel vapor cannot be ignited by consecutive sparks energized through 800 mJ laser pulses. In addition to the test matrix shown in table 3.2, every fuel was tested at the room temperature ( $T = 25^{\circ}\text{C}$ ), which is below the flashpoint, using propane torch as an ignition source. Nd-YAG laser is used to ignite the fuel pool for initial temperatures above  $60^{\circ}\text{C}$ . Details of the high-speed and low-speed videos, thermocouple measurement systems, and an interpretation of the results in terms of the flame spread rate at various initial fuel temperatures are discussed for each fuel. The procedures for all fuels are identical. The flame spread rates corresponding to different initial fuel temperatures are discussed in the following sections.



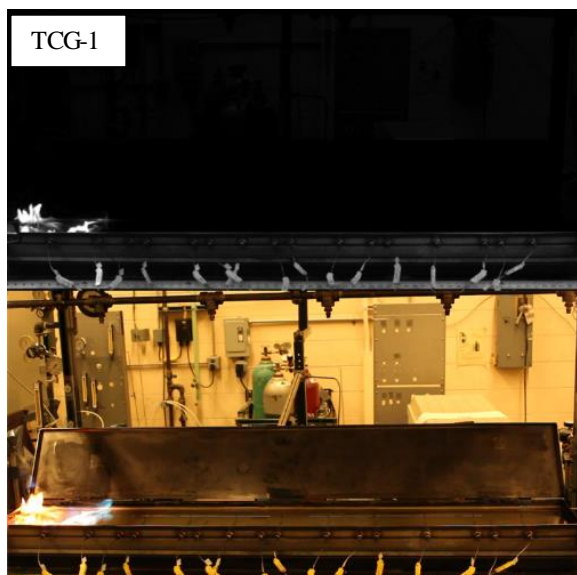
## 6.1 HEFA-50

As described above, Hydro-processed ester fatty acids-50 (HEFA-50) fuel is kerosene-based fuel derived from Camelina. HEFA-50 is a blend of 50% HEFA and 50% Jet-A by volume. The flash-point of HEFA-50 jet fuel is 41°C. The flame spread rate of HEFA-50 is measured for the temperature range of 25-100°C. Results in terms of flame propagation video frames are shown for initial fuel temperatures of 25°C and 80°C as an example. Table 6-7 below shows a comparison of flame arrival time for HEFA-50 (initial fuel temperature = 80°C) as measured by the high-speed camera and the low-speed camera at each of the thermocouple locations.

Table 6-7: Flame arrival time for HEFA-50 at 80°C initial temperature

Flame location	Flame arrival time (seconds)	
	High-Speed Camera	Regular Visible Camera
TCG_1	0	0
TCG_2	0.12	0.13
TCG_3	0.22	0.23
TCG_4	0.34	0.33
TCG_5	0.43	0.43
TCG_6	0.54	0.53
TCG_7	0.63	0.63
TCG_8	0.73	0.73
TCG_9	0.82	0.83

Based on the data in Table 6-7, flame spread rate for HEFA-50 fuel at the initial fuel temperature of 80°C is estimated to be 146.3 cm/sec from the high-speed camera measurement and 144 cm/sec from the low-speed camera measurements. The flame spread speed are comparable allowing us to conclude that both camera speeds are adequate for comparing the effects of fuel type and fuel temperature on the flame spread rate within the range considered here. Figure 6-2 below shows the flame propagation as recorded by black-white high-speed camera and regular DSLR at identical times.



High-speed  $t = 0$  sec, Regular  $t = 0$  sec



High-speed  $t = 0.22$  sec, Regular  $t = 0.23$  sec



High-speed  $t = 0.43$  sec, for Regular  $t = 0.43$  sec



High-speed  $t = 0.82$  sec, Regular  $t = 0.83$  sec

Figure 6-2: Pairs of high-speed (top) and regular (bottom) at identical times for HEFA-50 at 80°C

It should be noticed that there is a blue precursor flame is being followed by the main yellow flame. This is a unique observation and was observed for all test cases with initial temperature higher than the closed-cup flash point temperature. SC6100 FLIR infrared camera is also used as an additional source to record and measure the flame spread for HEFA-50 and SIP fuels. Figure 6-3

shows four different IR camera frames for flame approaching specific thermocouple location as specified in the images. Arrival time of the flame tip as captured by IR camera at each thermocouple location was used in order to measure the flame spread rate knowing the distance between each gas phase thermocouple as 15 cm. The flame tip represented in the IR images might not show the actual luminous flame tip as IR camera captured the radiation intensity from CO<sub>2</sub> and soot using the specific filter for each test. Table 6-8 shows the specifications of the filter that was used for the IR camera recordings.

Table 6-8: Infrared camera filter specifications

Filter number	Filter type	cwl (μm)	HWHM(μm)	Max Transmission	Half max transmission
S9	Narrow bandpass	4.3773	0.0772	0.523	0.2615

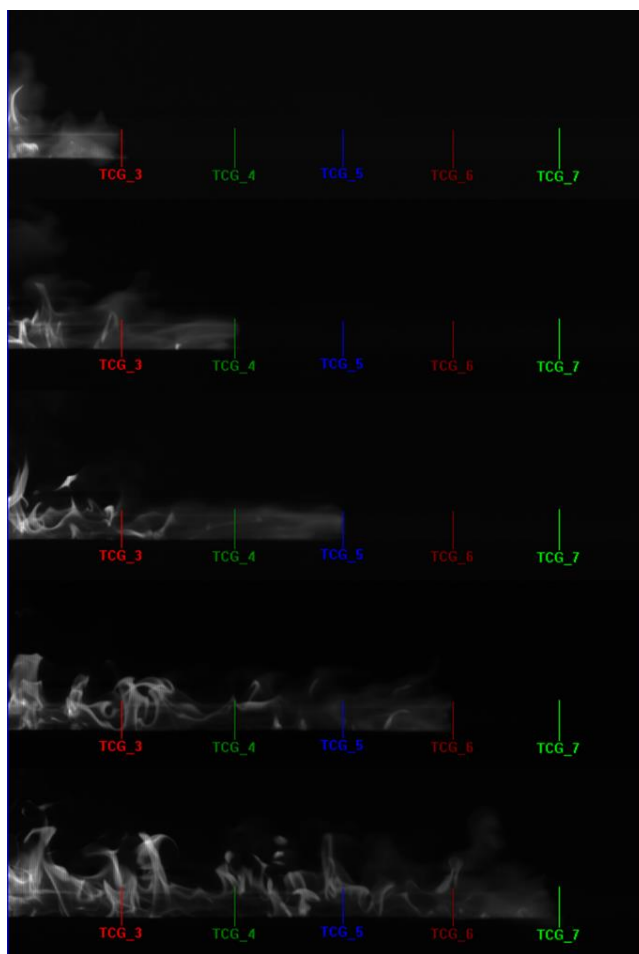


Figure 6-3: Infrared camera images showing flame propagation at few specific thermocouple locations for HEFA-50 at initial temperature 80°C

Figure 6-4 shows the responses of the three liquid phase thermocouples installed in the HEFA-50 fuel pool at an initial fuel temperature at 80°C. The depth of the fuel was maintained to be 25 mm for every test, the tip of liquid phase thermocouples is located at 10 mm below the liquid fuel surface, and the tip of gas-phase thermocouples were located at 12 mm above the liquid fuel surface. Figure 6-4 shows that liquid phase temperature does not vary significantly during the test period.

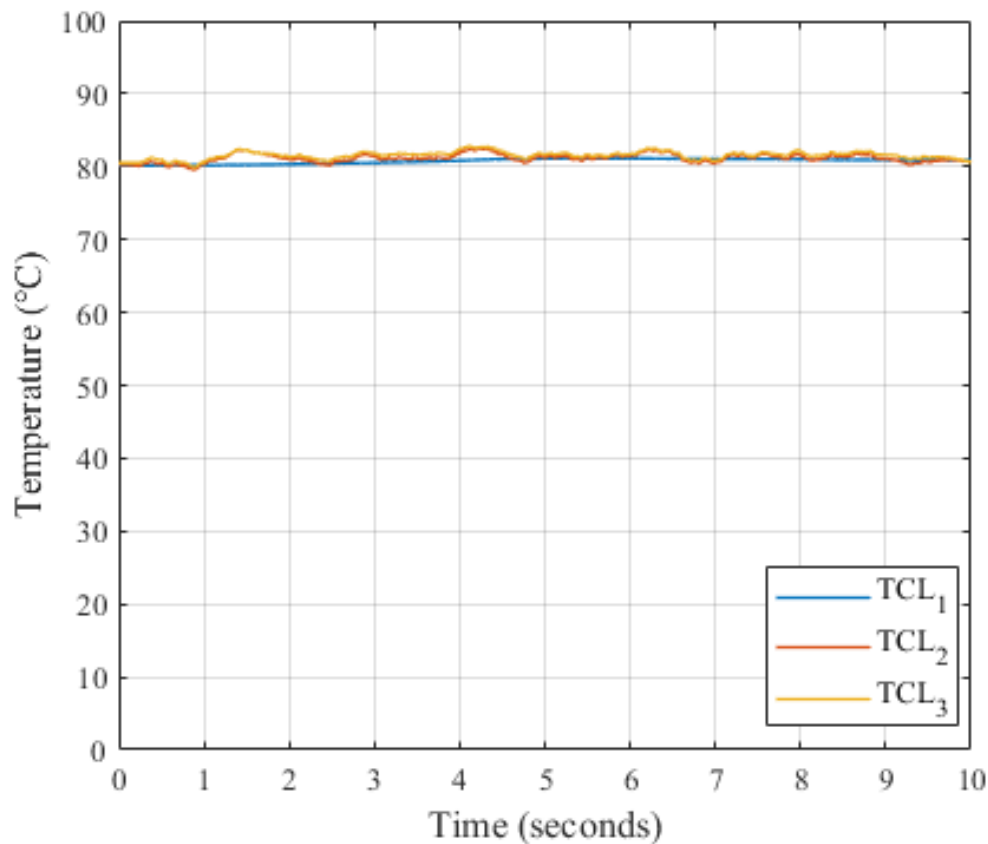


Figure 6-4: Liquid phase thermocouple responses for HEFA-50 fuel at 80°C

Figure 6-5 shows the responses of the nine gas-phase thermocouples for the HEFA-50 fuel at an initial fuel temperature at 80°C. It can be observed that no significant temperature fluctuations could be observed as the gas phase propagation is dominant above flashpoint, in which fuel-air mixture over the liquid-fuel surface burns quickly without significant heat transfer into the liquid fuel. This can also be seen from Figure 6-4 as liquid temperature remains almost around the initial temperature indicating that there is no significant heat transfer from the flame to the liquid fuel for this case.

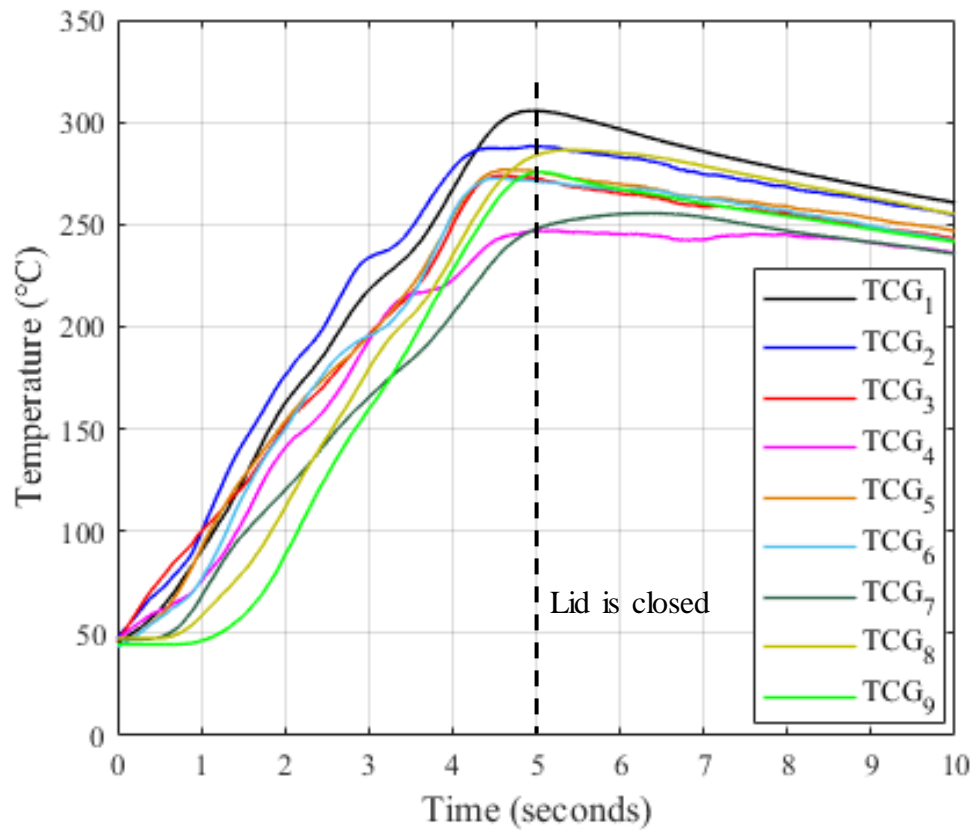


Figure 6-5: Gas-phase thermocouple responses for HEFA-50 fuel at 80°C

Also, it should be noticed that the flame-propagation time is ~1 second for the initial fuel temperature of 80°C. Thermocouples' response is not fast in comparison to flame propagation speed as the temperature rise is not consistent. Hence, thermocouple data for temperatures above the fuel's flashpoint is not pertinent for flame spread rate calculations.

For the tests at room temperature, gas phase thermocouple results are useful to calculate the flame spread rate as the flame spread is slow with respect to thermocouple response time and easily distinguishable temperature rise for each gas-phase thermocouple is observed. Although for few test cases, thermocouple responses are inadequate as rise of the successive gas-phase thermocouple was before the previous thermocouple. However, for flame spread rate determination, first and last gas-phase thermocouple responses are used to determine the flame spread rate and compare with high-speed, regular-speed and infrared video data. Figure 6-6 below shows the liquid phase versus time history for HEFA-50 test with initial fuel temperature to be room temperature.

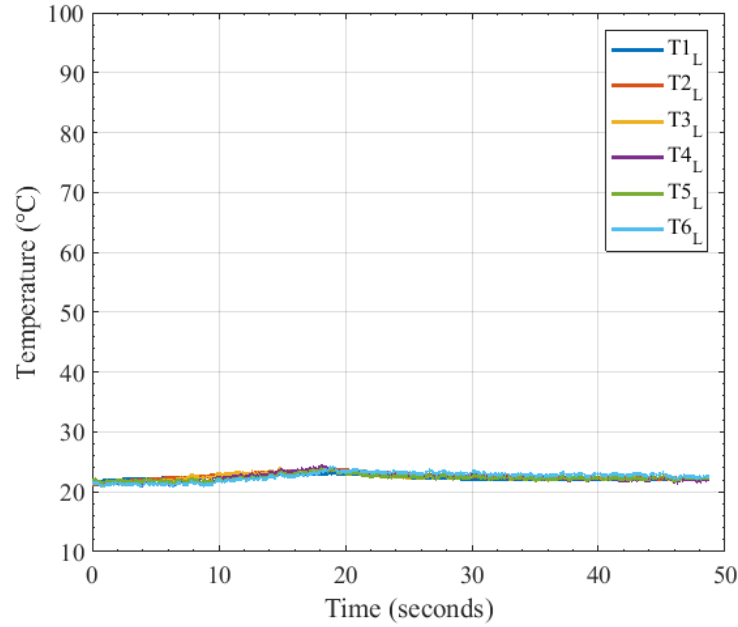


Figure 6-6: Liquid phase thermocouple responses for HEFA-50 fuel at room temperature

Figure 6-7 below shows the gas-phase thermocouple response for flame propagation over HEFA-50 liquid fuel at room temperature. As the flame propagates, a consistent rise in gas-phase temperature can be observed. The temperature rise response from the gas phase thermocouple 1 (located at  $x = 30$  cm) is adjusted to  $t = 0$  seconds and accordingly thermocouple 9 (located at  $x = 156$  cm) shows a temperature rise at  $t = 23$  seconds. The flame spread rate from these data is calculated to be 5.47 cm/sec.

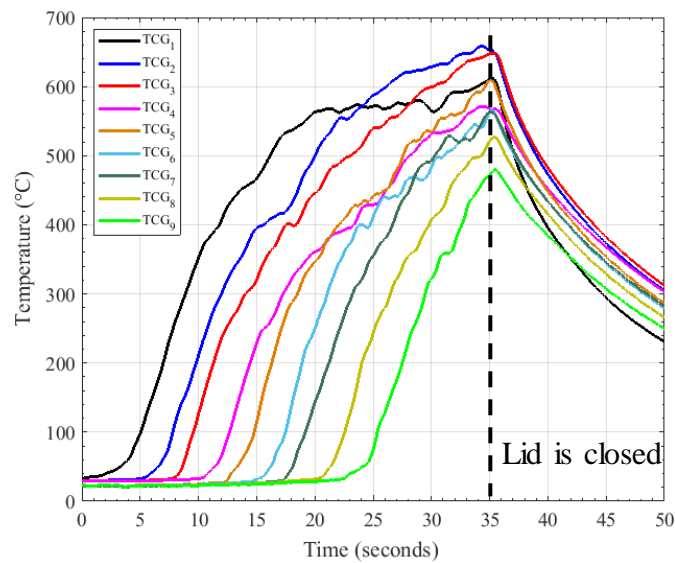


Figure 6-7: Gas-phase thermocouple responses for HEFA-50 fuel at room temperature



Also, as the flame reached the other end of the test pan, the lid is closed around 35 seconds and gas-phase temperature reduces as the fire is extinguished.

Figure 6-8 represents the low-speed and high-speed camera frames respectively for HEFA-50 fuel at room temperature at the specific time as noted at the corner of each frame. Time (t) was set to zero seconds at the arrival time of the flame to the first gas phase thermocouple. From high speed and low-speed data, the flame spread rate for the HEFA-50 fuel is calculated to be 5.16 cm/sec 5.21 cm/sec respectively, which is in good agreement with the thermocouple data (5.47 cm/sec). Pulsation of the flame back and forth was also observed at this temperature, which requires further study.

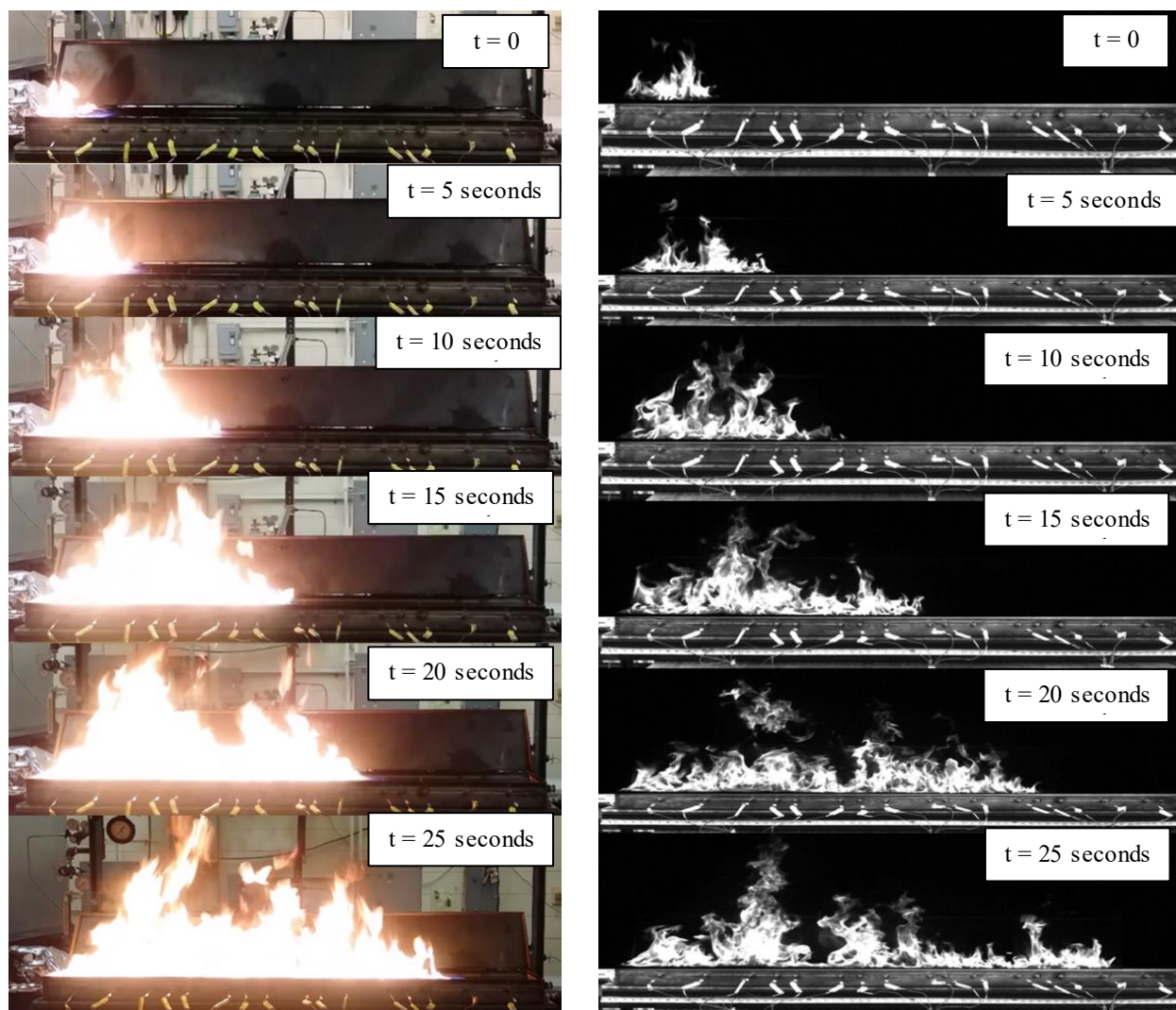


Figure 6-8: Regular (left) and high-speed (right) camera video frames for HEFA-50 fuel at initial temperature 25°C and time-steps between 0 to 25 seconds

Figure 6-9 highlights the effects of initial fuel temperature on the progress of the main yellow flame. It can be observed that precursor blue flame spread rate is almost the same at different initial fuel temperatures; however, the spread rate of the main yellow flame front slowly rises by increasing the initial fuel temperature and eventually catching up with the precursor flame for the super-flash stoichiometric conditions.

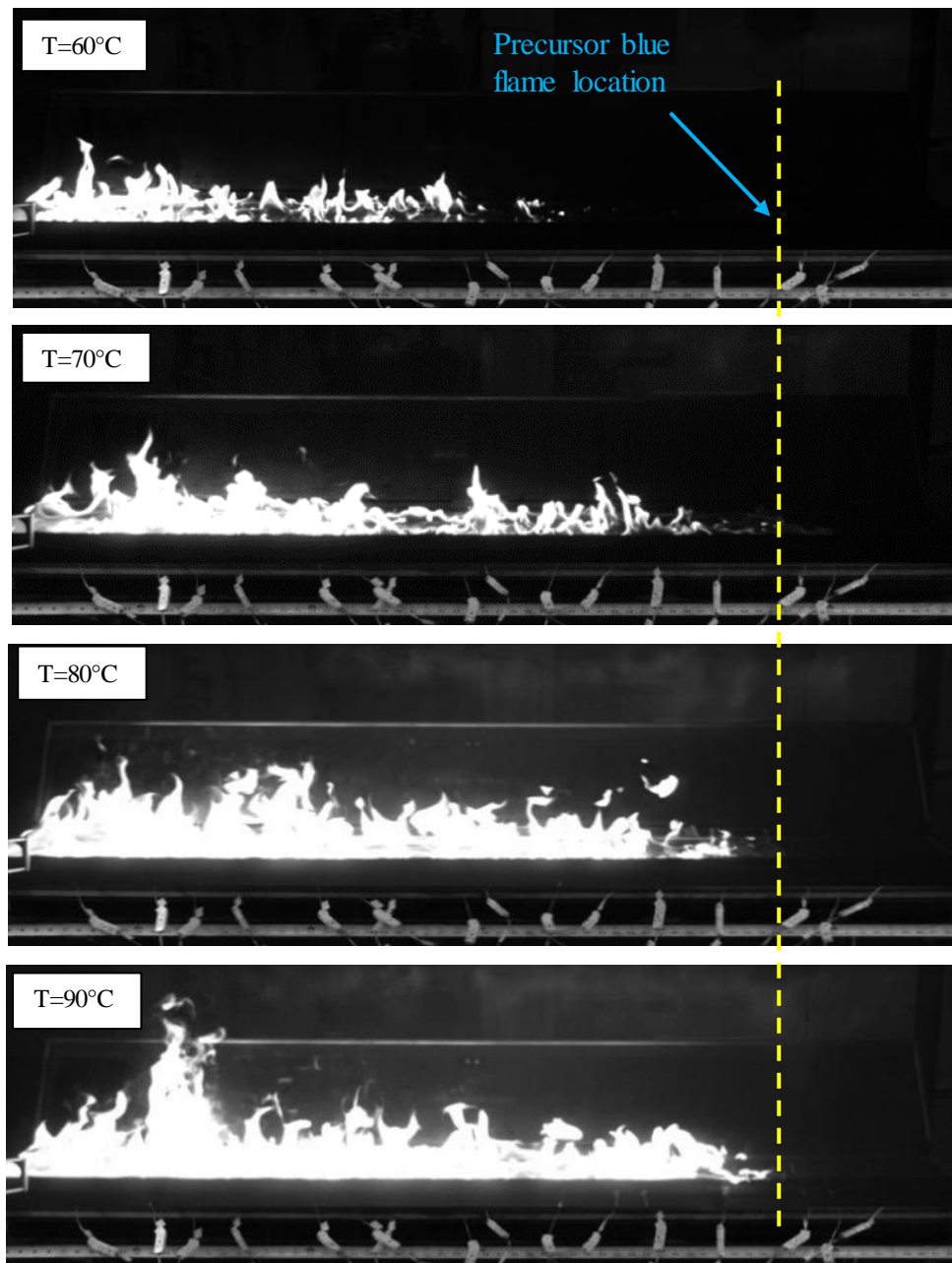


Figure 6-9: High-speed video frames of flame propagation over HEFA-50 fuel surface for different initial temperatures at 0.8 seconds



Figure 6-10 shows the flame spread rates for HEFA-50 fuel for different initial fuel temperatures.

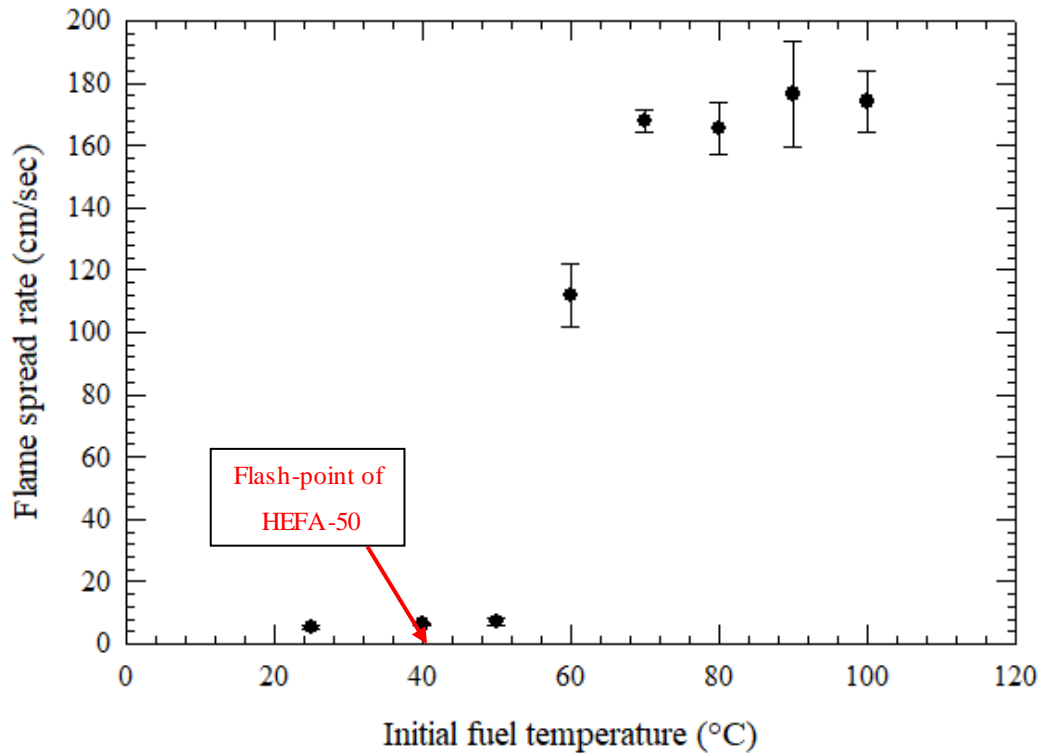
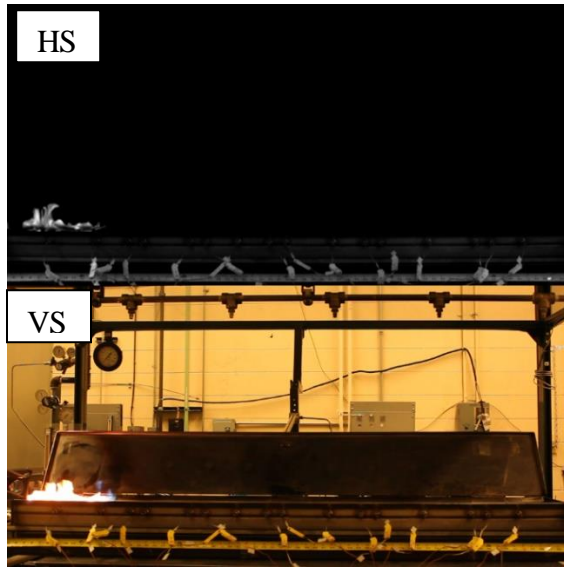


Figure 6-10: Flame spread rate for HEFA-50 fuel for different initial fuel temperatures

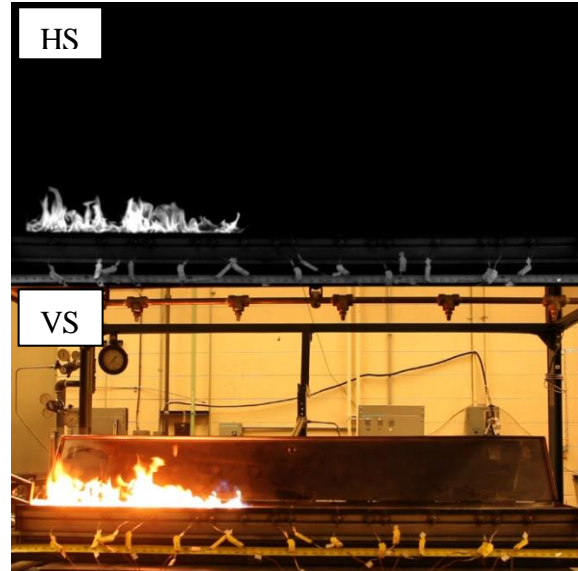
Flame spread rate is ~5 cm/sec for all initial fuel temperatures below and slightly above the closed-cup flashpoint temperature of HEFA-50, which is 38°C. For 60°C initial fuel temperature, there is a jump in flame spread rate to ~100 cm/sec. On further heating the fuel to higher temperatures, flame spread rate increases to ~150 cm/sec and remains within 10 cm/sec of the mean value of 160 cm/sec.

## 6.2 Jet-A

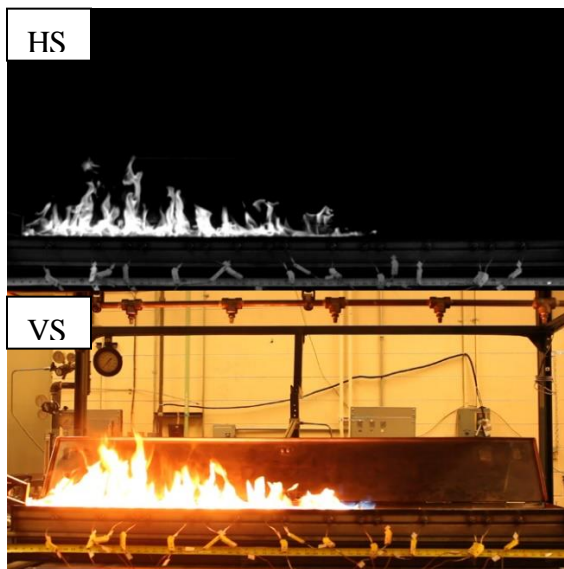
Flame spread rate for Jet-A is measured for the initial temperature range of 25-100°C. Figure 6-11 shows high-speed and regular camera frames of flame propagation across the heated Jet-A pool at 80°C.



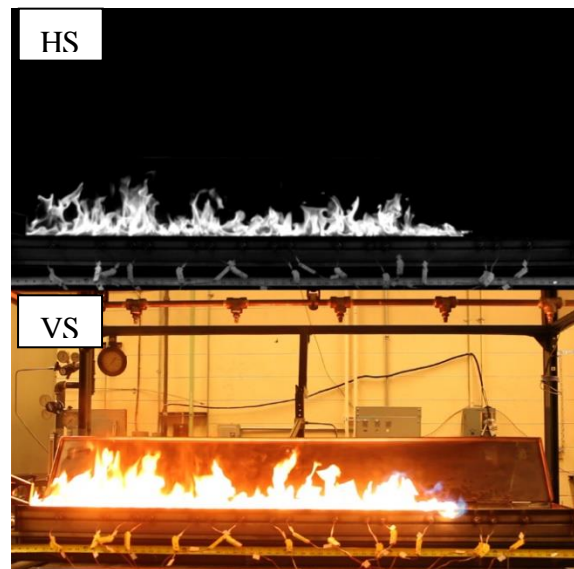
High-speed  $t = 0$  sec, Regular  $t = 0$  sec



High-speed  $t = 0.335$  sec, Regular  $t = 0.36$  sec



High-speed  $t = 0.605$  sec, Regular  $t = 0.62$  sec



High-speed  $t = 0.775$  sec, Regular  $t = 0.77$  sec

Figure 6-11: Pairs of high-speed (*top*) and regular (*bottom*) frames at identical times of flame propagation over Jet-A at initial temperature of 80°C

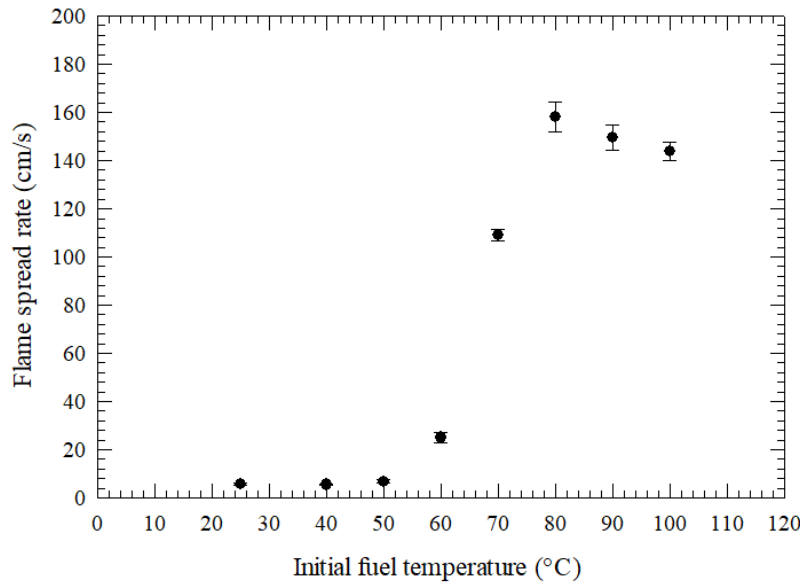


Figure 6-12: Flame spread rate for Jet-A fuel for different initial fuel temperatures

Flame spread rate is ~5 cm/sec for all initial fuel temperatures below and slightly above the closed-cup flashpoint temperature of Jet-A, which is 43°C. For 55°C initial fuel temperature, there is a jump in flame spread rate to ~30 cm/sec. On further heating the fuel to higher temperatures, flame spread rate increases to ~120 cm/sec and remains within 10 cm/sec of the mean value of 140 cm/sec. Figure 6-13 compares the flame spread rate of Jet-A measured in the study with JP-8 (military grade of Jet-A) as measured by White et al. As can be seen in the plot, flame spread rate in both cases are in good agreement.

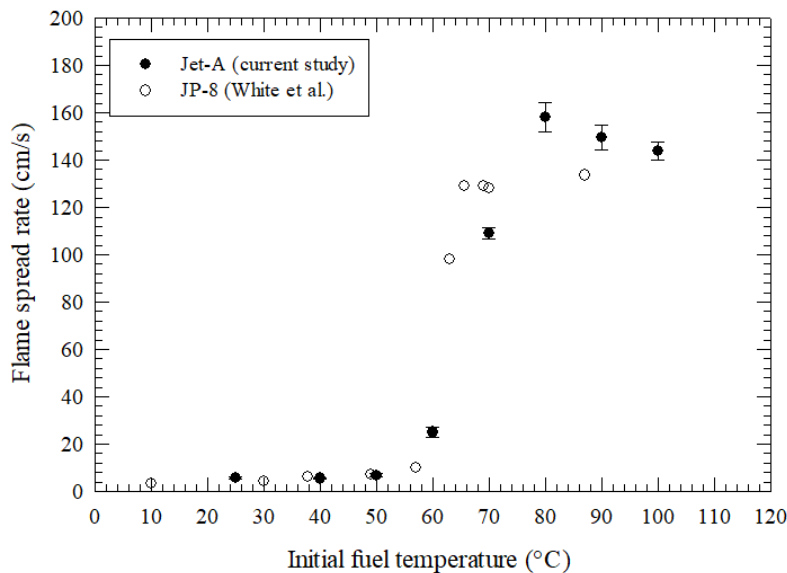


Figure 6-13: Flame spread rate comparison of Jet-A with JP-8 (White et al.)

### 6.3 Fischer Tropsch-IPK (FT-IPK)

Flame spread rate for FT-IPK is measured for the initial temperature range of 25-100°C. Figure 6-14 shows the flame-spread rate of FT-IPK for different initial temperatures.

Similar to HEF-50 and Jet-A, flame spread rate is ~5 cm/sec for all initial fuel temperatures below and slightly above the closed-cup flashpoint temperature of FT-IPK, which is 40°C. For 60°C initial fuel temperature, there is a jump in flame spread rate to ~140 cm/sec. On further heating the fuel to higher temperatures, flame spread rate increases to ~160 cm/sec and remains within 10 cm/sec of the mean value of 150 cm/sec.

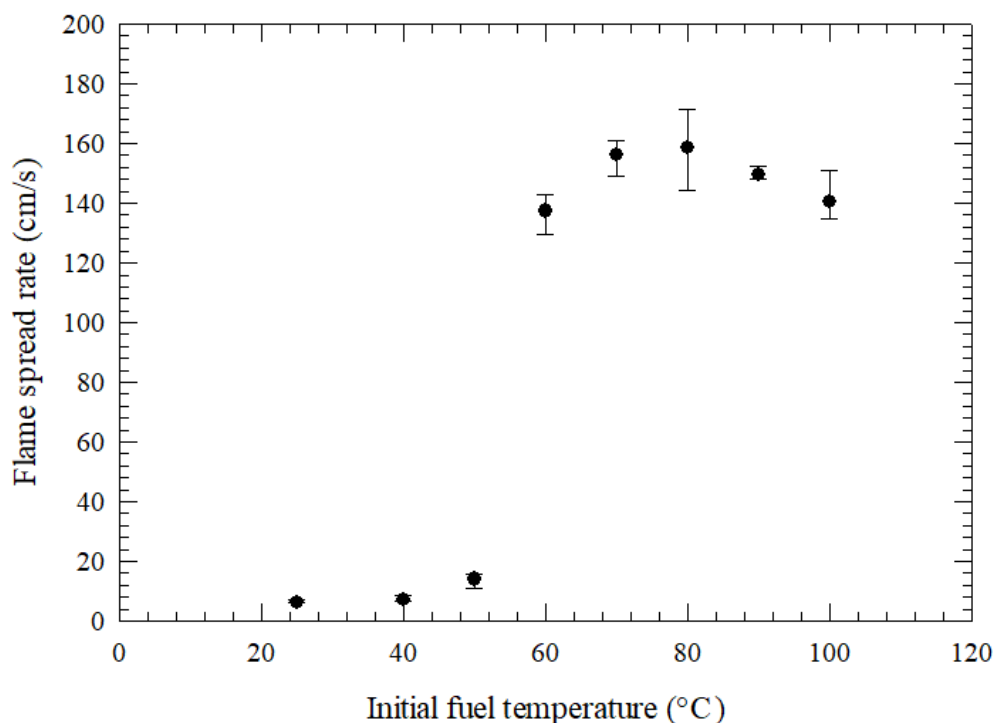


Figure 6-14: Flame spread rate for FT-IPK fuel for different initial fuel temperatures

### 6.4 Synthetic Iso-paraffin (SIP)

Flame spread rate for SIP is measured for the initial temperature range of 80-140°C. Figure 6-14 shows the flame-spread rate of SIP for different initial temperatures. The flash-point of SIP is 110°C, nearly 3 times to that of Jet-A, HEFA-50 and FT-IPK. Due to higher flash-point, induction

time at room temperature is ~5 minutes and needs propane torch to be held for the same time over the SIP fuel pool.

Similar to other fuels, the flame spread rate is ~5 cm/sec for all initial fuel temperatures below and at the closed-cup flashpoint temperature of SIP, which is 110°C. For 120°C initial fuel temperature, there is a jump in flame spread rate to ~150 cm/sec. On further heating the fuel to higher temperatures, flame spread rate increases to ~170 cm/sec and remains within 15 cm/sec of the mean value of 160 cm/sec.

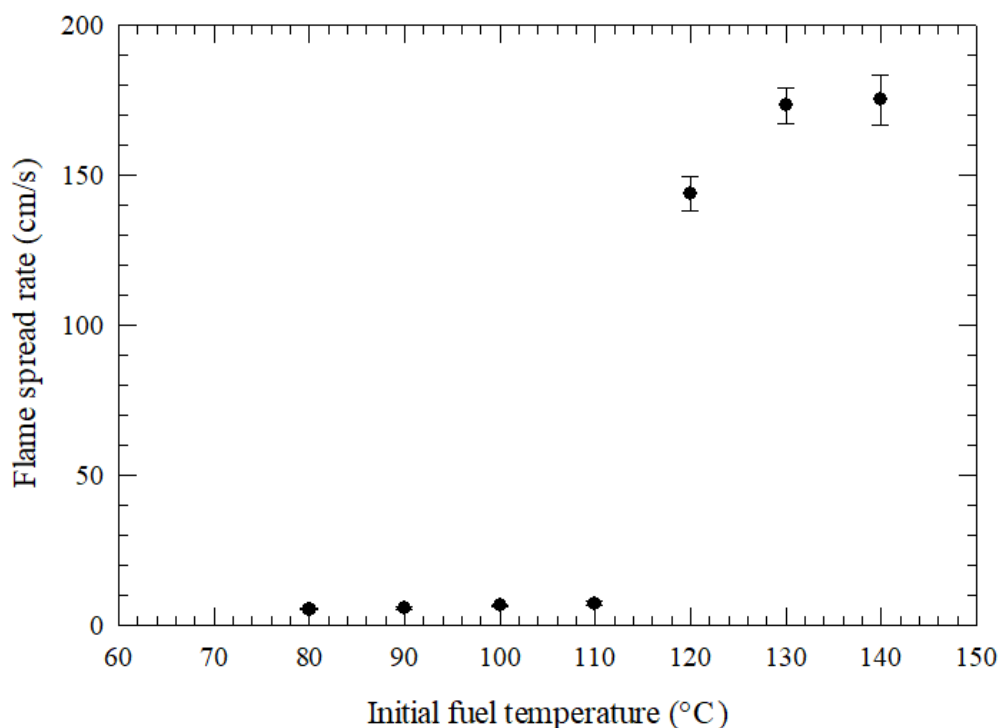


Figure 6-15: Flame spread rate for SIP fuel for different initial fuel temperatures

### **Comparison of flame spread rates of test fuels**

Figure 6-16 shows the flame spread rates for Jet-A, HEFA-50, FT-IPK, and SIP at different initial temperatures. Jet-A, HEFA-50 and FT-IPK with the flashpoints 38°C, 38°C and 40°C respectively show close results compared to each other because of the flashpoint similarities. However, SIP fuel is deviated from the other three fuels because of its flashpoint which is 110°C.

The lowest temperature for the sustained laser-induced spark ignition was 52°C for FT-IPK, 54°C for Jet-A and 58°C for HEFA-50. Flame spread rate for all four fuels was stabilized after certain threshold temperature between 140 cm/sec and 160 cm/sec. That transition temperature could be described as the transition from super-flash lean regime to super-flash stoichiometric regime as described by Li et. al. and it is around 60°C for Jet-A, HEFA-50 and FT-IPK and around 112°C for SIP.

Before the transition temperature, flame spread rates for Jet-A, HEFA-50, and FT-IPK at 25°C 5 cm/sec. It is the region where the flame spread was driven by a liquid motion below the fuel surface. Post the transition temperature, the flame spread rate increases to mean value of ~150 cm/sec.

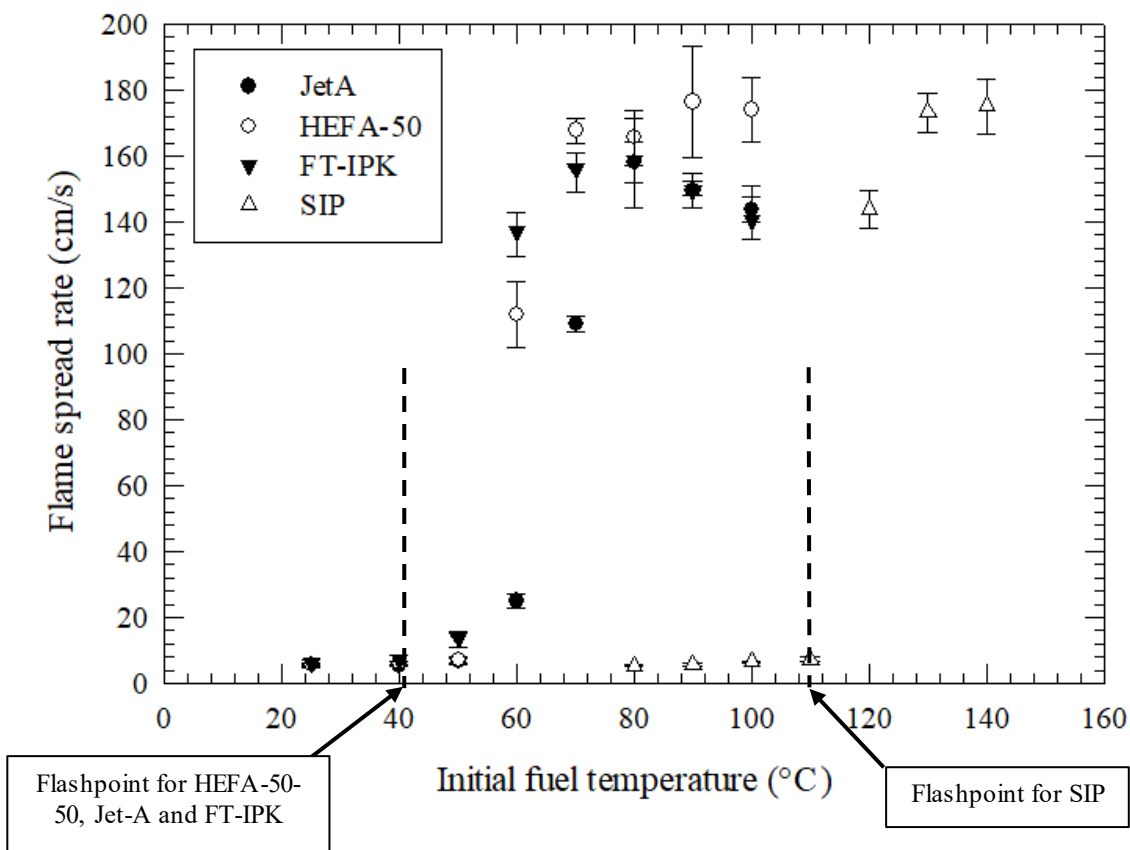


Figure 6-16: Flame spread rates for Jet-A, HEFA-50, FT-IPK and SIP fuels at different initial temperatures

Based on the flame-spread rate pattern for all fuels, a general trend of flame spread rate variation with initial fuel temperature is sketched and shown in Figure 6-17. For temperatures below the flash-point, the flame spread is relatively slow. The slow flame spread is attributed to the type

of flame propagation that occurs at these temperatures. This type of flame propagation is liquid-phase controlled and depicted in Figure 6-18.

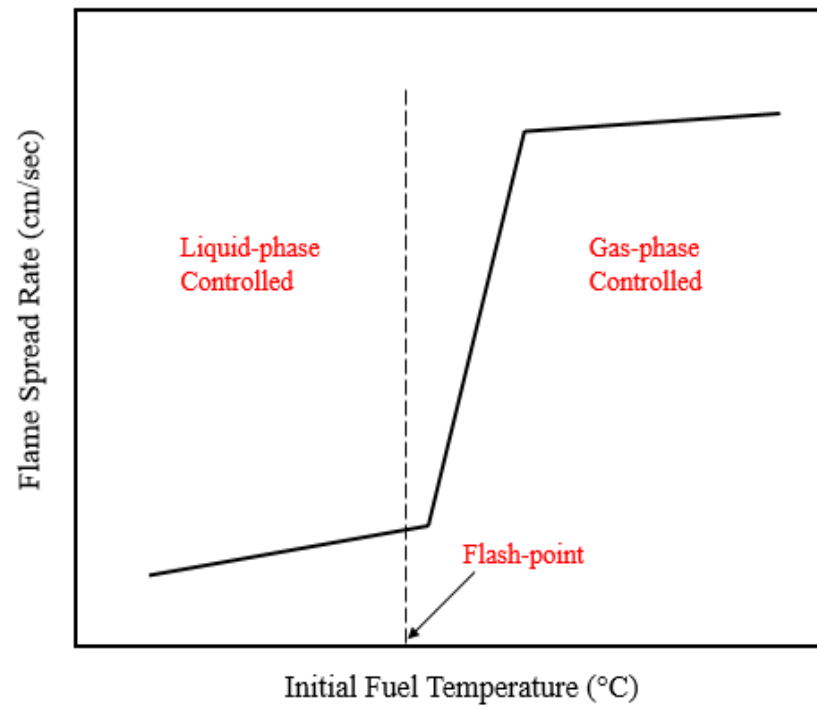


Figure 6-17: Flame-spread regimes based on initial fuel temperatures

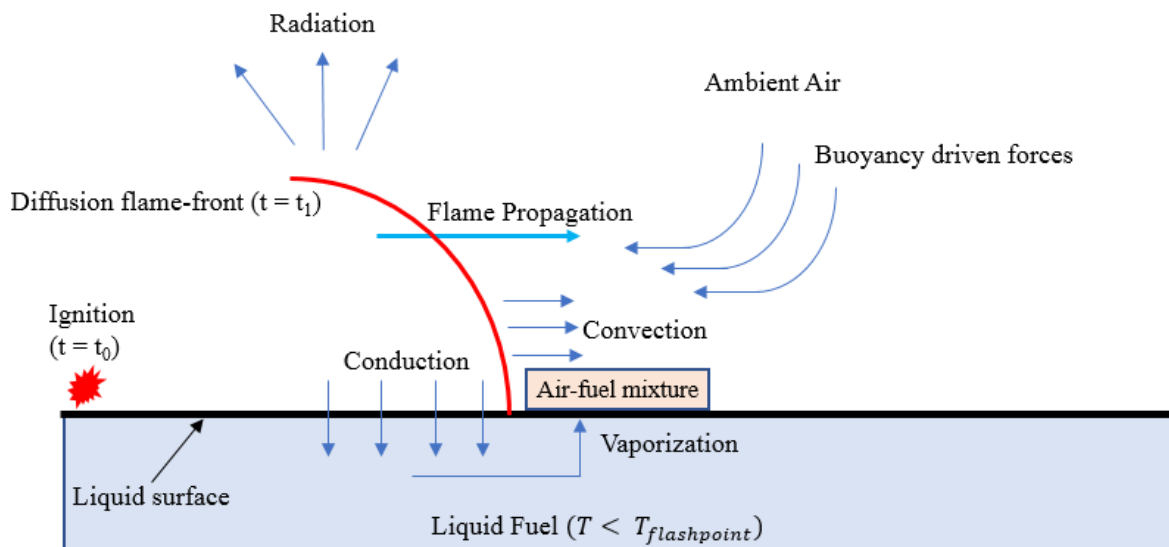


Figure 6-18: Liquid phase controlled flame propagation

For these initial temperatures, the flame propagates as a diffusion flame. The heat from the ignition source turns liquid fuel to fuel vapors and creates an air-fuel mixture. Under adequate conditions, the air-fuel mixture combusts and the flame first stabilizes and then propagates. As flame propagates, due to conduction and convection it heats up the succeeding the fuel into vapors forming air-fuel mixture and combusting under adequate conditions. Thus, in this type of flame propagation, the flame propagation significantly depends on the fuel heating via conduction and convection from the flame and hence named liquid-phase controlled propagation.

For temperatures slightly above the flash-point, the flame spread is relatively significantly higher in comparison to liquid-phase controlled propagation. This type of flame propagation is gas-phase controlled and is depicted in Figure 6-19.

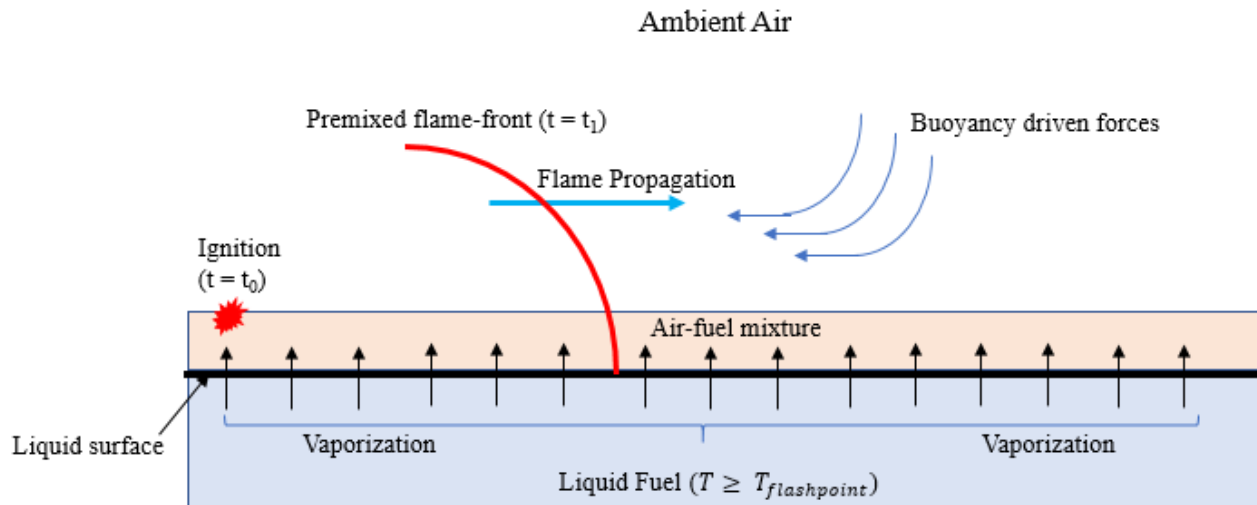


Figure 6-19: Gas-phase controlled flame propagation

For these initial temperatures, the flame propagates as a premixed flame. Above the flash-point, fuel vapors are formed and accumulate above the liquid surface and forms air-fuel mixture. On supplying sufficient ignition energy, the flame propagates as a premixed flame and spread is faster as the air-fuel mixture exists across the pool.



## 7. FLAME PROPAGATION ANALYSIS

In chapter-6, flame spread rate of four fuels namely Jet-A, HEFA-50, SIP, and FT-IPK for different initial fuel temperatures is reported. It was also observed that in the flame spread process a main yellow flame and a precursor blue flame exist over the fuel surface. In this chapter, these two components of the flame are studied.

### 7.1 Critical Transition Temperatures

The critical transition temperature is the temperature of the fuel at or above which the flame spread rate mechanism shifts from liquid-phase propagation to gas-phase propagation. This temperature is important from the safety point of view as at or above this temperature the flame spreads with the rate of ~150-160 cm/s. Figure 7-1 shows the critical temperature range highlighted for SIP fuel as observed in the flame spread rate tests. For Jet-A, HEFA-50, and FT-IPK the critical temperature range is 60-70°C whereas for SIP this range is from 110-120°C.

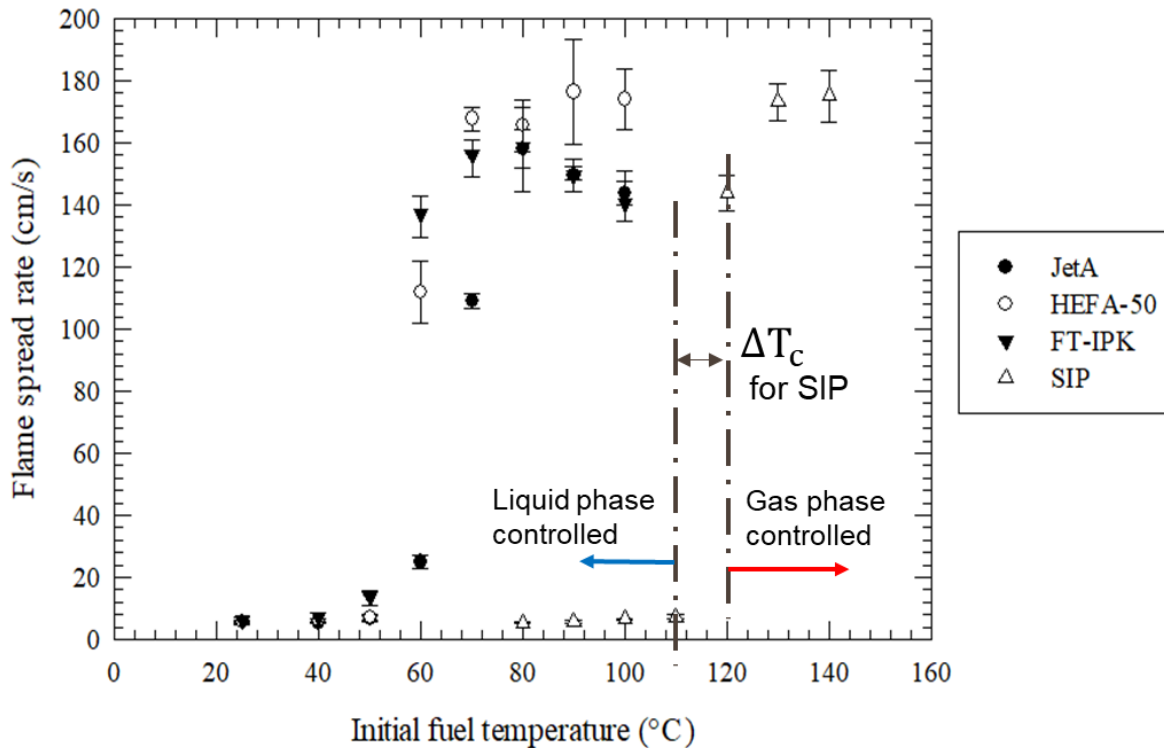


Figure 7-1: Critical transition temperature range for all fuels

Figure 7-2 below shows that the distance between the precursor blue flame front and the main yellow front decreases with increase in temperature.

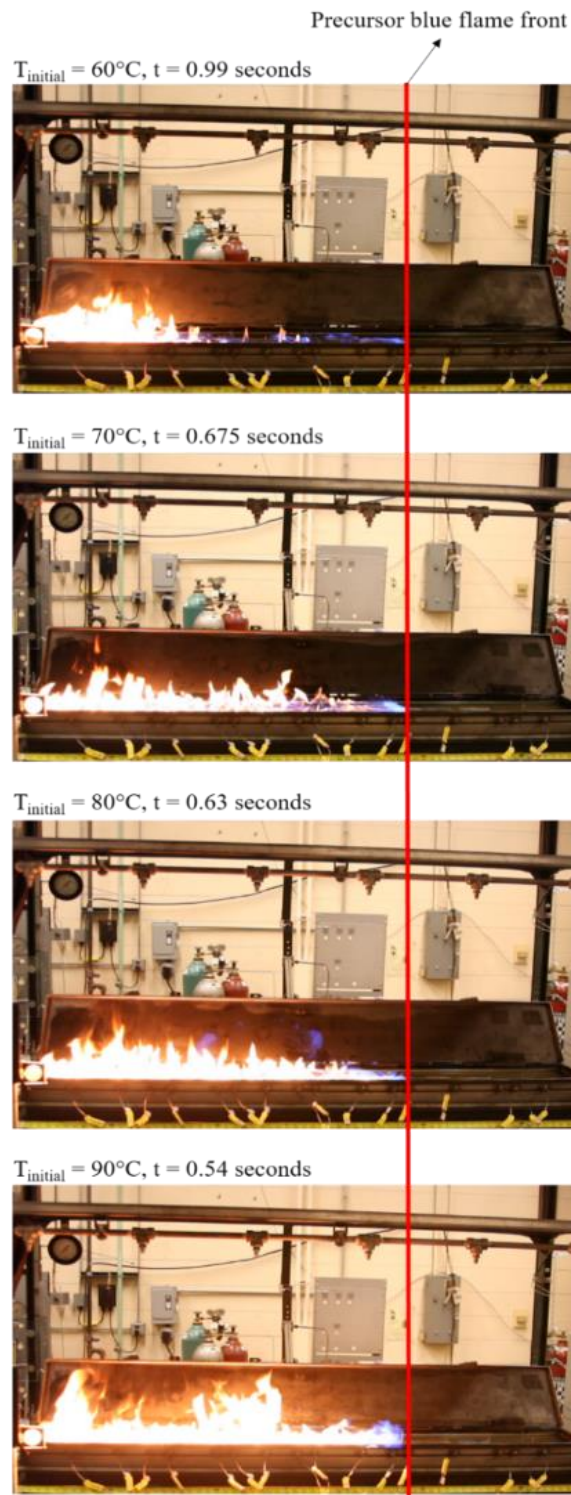


Figure 7-2: Blue flame front image frames for different initial fuel temperatures at same location

After identifying the critical transition temperature range for all fuels, a series of tests are conducted to determine the critical transition temperature for all the test fuels. Table 7-1 shows the test matrix for this study.

Table 7-1: Test matrix to determine the critical transition temperature

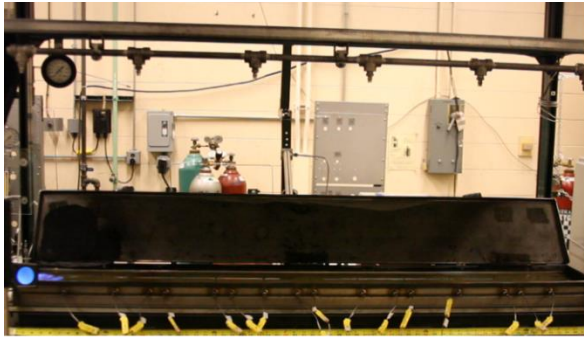
	<b>Initial Fuel Temperature (°C)</b>									
<b>Fuel</b>	<b>Test 1</b>	<b>Test 2</b>	<b>Test 3</b>	<b>Test 4</b>	<b>Test 5</b>	<b>Test 6</b>	<b>Test 7</b>	<b>Test 8</b>	<b>Test 9</b>	<b>Test 10</b>
<b>Jet-A</b>	70	68	66	64	62	60	-	-	-	-
<b>FT-IPK</b>	70	68	66	64	62	60	58	56	54	52
<b>HEFA-50</b>	70	68	66	64	62	60	58	56	-	-
<b>SIP</b>	120	118	116	114	112	110	-	-	-	-

The test matrix starts with a fuel temperature of 70°C for Jet-A, HEFA-50, FT-IPK and 120°C for SIP with stepwise reductions until a point of no ignition is reached. No ignition means that the fuel vapor cannot be ignited by consecutive sparks energized through 800 mJ laser pulses. Nd-YAG laser is used to ignite the fuel pool.

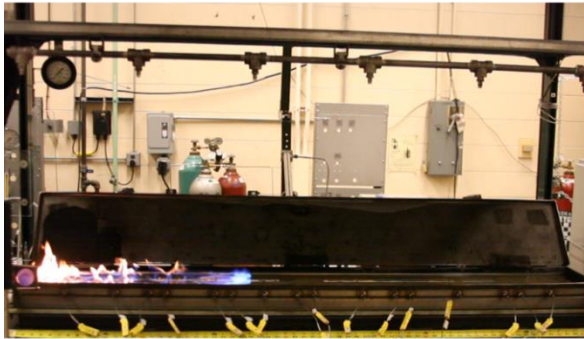
Details of the high-speed and low-speed videos and an interpretation of the results in terms of the flame spread rate for both the blue flame and yellow flame at various initial fuel temperatures are discussed for each fuel. The test procedures for all fuels are identical.

Figure 7-3 shows the precursor blue flame front and the following main yellow flame front over the HEFA-50 fuel surface at identical times. It can be observed that precursor blue flame propagates faster and along the fuel surface whereas the main yellow flame propagates relatively slower and flame height is significantly larger than the blue flame.

Fuel temperature = 70°C



t = 0 seconds



t = 0.40 seconds

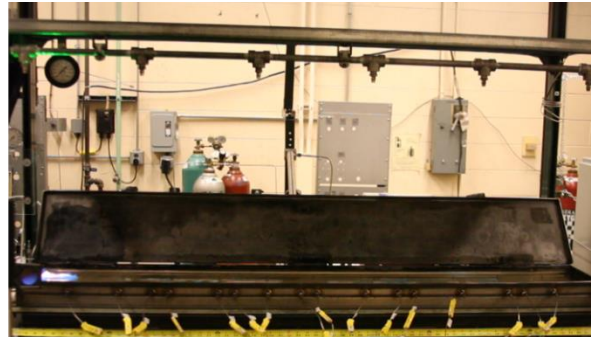


t = 0.81 seconds

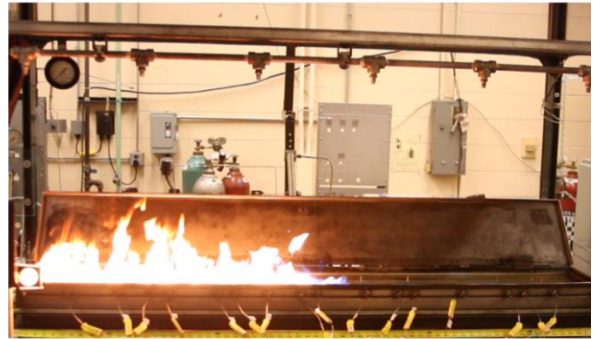


t = 1.21 seconds

Fuel temperature = 90°C



t = 0 seconds



t = 0.40 seconds



t = 0.81 seconds



t = 1.21 seconds

Figure 7-3: Flame front image for 70°C (left) and 90°C (right) initial HEFA-50 fuel temperatures at identical times

Table 7.2 shows the critical transition temperatures for all the fuels. The critical transition temperature of Jet-A is  $64^{\circ}\text{C} \pm 1^{\circ}\text{C}$  and is  $\sim 10^{\circ}\text{C}$  higher than that of FT-IPK and  $\sim 6^{\circ}\text{C}$  higher than that of HEFA-50. Although the flash-point of these fuels is  $\sim 40^{\circ}\text{C}$ , their critical transition temperatures are spread out over a range of  $10^{\circ}\text{C}$ . This difference is probably due to different composition which ultimately affects the evaporation rates of these fuels. Jet-A contains the most heavier compounds and has highest content of aromatic compounds followed by HEFA-50 and FT-IPK. The molecular weight of Jet-A and HEFA-50 is 167 g/mol and 168 g/mol respectively whereas FT-IPK is the lightest among these fuels with molecular weight of 154 g/mol.

Table 7-2: Critical Transition Fuel Initial Temperatures

<b>Fuel</b>	<b>Critical Transition Temperature (<math>^{\circ}\text{C}</math>)</b>
Jet-A	$64 \pm 1$
FT-IPK	$54 \pm 1$
HEFA-50	$58 \pm 1$
SIP	$112 \pm 1$

The critical transition temperature of SIP is  $112^{\circ}\text{C} \pm 1^{\circ}\text{C}$  and is very close to its flash-point of  $110^{\circ}\text{C}$ . SIP is the heaviest amongst all the test fuels and contains no aromatics.

## 7.2 Precursor Blue flame and Main Yellow flame

As discussed in the previous sections, the flame propagation over the liquid fuels contains a precursor blue flame and a main yellow flame. These flames are observed for both liquid-phase propagation and gas-phase propagation. In this section, flame spread rates of blue flame and yellow flame are discussed for fuel temperatures above the critical transition temperatures.



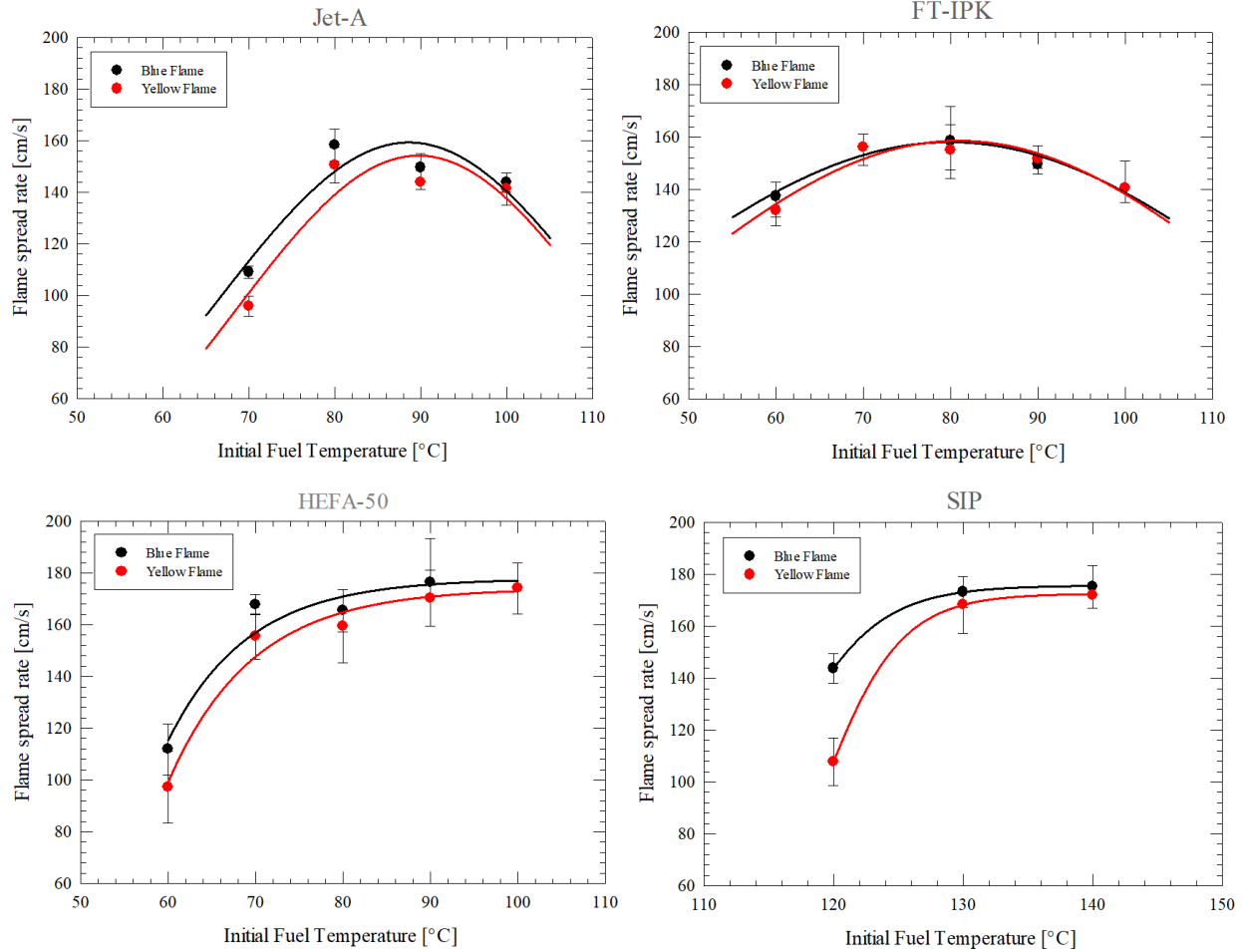


Figure 7-4: Yellow flame and blue flame spread rate over all test fuels

Figure 7-4 above shows the flame spread rates of yellow flame and blue flame over all the test fuels. The difference between flame spread rates of the blue flame and yellow flame is more at lower fuel temperatures and decreases with an increase in fuel temperature. The difference in the flame spread rates between both flames is higher for SIP and least for FT-IPK. FT-IPK is the lightest fuel and for relatively lower temperatures fuel-air mass ratio exceeds the lower flammability limit. For Jet-A and HEFA-50 the difference between the flame spread rates of both fuels looks similar. This is possibly due to similar evaporation rates for these fuels.

## 8. CONCLUSION

Two phenomena namely, hot surface ignition and flame spread rate are studied and reported in this dissertation. Following are the key conclusions,

### **Hot surface ignition**

- Hot surface ignition is a probabilistic event. Ignitions are transient and initiate at random locations on the plate surface. The randomness of these locations depends on the small variations in the initial drop sizes and their vaporization in the transient buoyant plume, the solid surface finish, and small variations in the surface temperature resulting from previous evaporation events.
- The “Ignition range” is often defined as the difference between the temperature of the first measurable probability of HSI and the lowest temperature of the 100% measurable probability of HSI. The ignition range for all the fuels is ~40-100°C.
- The flame propagated in two ways, namely point ignition, as if the ignition event occurred at few discrete locations, and distributed ignition, as if the ignition event is distributed across the plate. For all the fuels except A, the ignition event is distributed ignition. For A, point ignition is observed for ignition temperatures up to 890°C and distributed ignition is observed for temperatures above 890°C.
- Qualitatively, the baseline fuel, 100LL Aviation gasoline appeared to produce slightly higher residues than those produced by other test fuels. However, neither fuel produced measurable quantities of residues for the present test conditions. Specially designed tests would be necessary for quantitatively comparing the residue forming at surface plate temperatures much lower than those observed for the hot surface ignition.

## **Flame Spread Rate**

- A scaled, fuel temperature-controlled pool fire apparatus with flame spread rate diagnostics and visualization using multiple spectral cameras was completed.
- The boundary condition effects are found to be minimal on the measurement of flame spread rate in the current apparatus. Some of the boundary and initial condition effects include the ignition source, the initial pool fire development region, the extinction region, and the extinguishment method.
- Thermocouples embedded in the gas phase above a certain height do not provide a reliable measurement of flame spread rate for the tests above flashpoint of the fuel.
- Visible low-speed, high-speed cameras and IR camera provide consistent measurements of the flame spread rates and is recommended to be used for all related future studies.
- Four aviation fuels such as Jet-A, HEFA-50, FT-IPK, and SIP were tested and showed similarities and differences in their flame spread rates, details of the flame spread process including the precursor blue flame and the main yellow diffusion flame behavior.
- The critical transition temperatures at which flame propagation shifts from liquid-phase propagation to gas-phase propagation are determined for all the fuels.



## REFERENCES

- [1] Ahrens, M. (2010). U.S. Vehicles Fire Trends and Patterns. *National Fire Protection Association Fire Analysis and Research Division*.
- [2] A. E-659 (2000). Standard Test method for Autoignition temperature of liquid chemicals.
- [3] NFPA (2004). *Guide to Fire and Explosions Investigations*.
- [4] Colwell, J. D., & Reza, A. (2005). Hot Surface Ignition of Automotive and Aviation Fluids. *Fire Technology*, 105- 123.
- [5] Davis, S., Kelley, S., & Somandepalli, V. (2010). Hot Surface Ignition of Performance Fuels," *Fire Technology*, 363-374.
- [6] Johnson, A.M., Roth, A.J., Moussa, N.A. (1988). Hot Surface Ignition tests of Aircraft fluids. *Air Force Wright Aeronautical Laboratory, Wright-Patterson Airforce base*.
- [7] Bennett, J.M. (2001). Ignition of Combustible fluids by heated surfaces. *Process safety progress*, vol.20 (1), 229-36.
- [8] Somandepalli, V., Kelley, S., & Davis, S. (2008). Hot surface ignition of ethanol-blended fuels and biodiesel. *SAE world congress*, Detroit, MI, SAE Paper 2008-01-0402.
- [9] Kinbara, T., Surface combustion phenomena of liquids, Rikagaku-Kenkyusho Shuho (Chem. Research (Tokyo)); (Part I) 9, 561-570 (1930); (Part 2) 10, 37-52 (1931); (Part 3) 11, 104-119 (1932); (Part 4---Benzene Combustion) 11, 1192-1200 (1932) (all in Japanese). Bull. Inst. Phys
- [10] Ross, H. D. (1994). Ignition of and flame spread over laboratory-scale pools of pure liquid fuels. *Progress in Energy and Combustion Science*, 20(1), 17-63.
- [11] White, D., Beyler, C. L., Fulper, C., & Leonard, J. (1997). Flame spread on aviation fuels. *Fire safety journal*, 28(1), 1-31.

- [12] Li, M. H., Lu, S. X., Guo, J., & Tsui, K. L. (2014). Study on Flame Spread over Aviation Kerosene and Diesel. In *Advanced Materials Research* (Vol. 1016, pp. 587-591). Trans Tech
- [13] Li, M., Lu, S., Guo, J., Chen, R., & Tsui, K. L. (2015). Flame spread over n-butanol at sub-flash temperature in normal and elevated altitude environments. *Journal of Thermal Analysis and Calorimetry*, 119(1), 401-409.
- [14] Li, M., Lu, S., Guo, J., Chen, R., & Tsui, K. L. (2015). Initial fuel temperature effects on flame spread over aviation kerosene in low-and high-altitude environments. *Fire Technology*, 51(3), 707-721.
- [15] Li, M., Lu, S., Chen, R., & Wang, C. (2017). Pulsating behaviors of flame spread across n-butanol fuel surface. *Applied Thermal Engineering*, 112, 1445-1451.
- [16] Li, M., Wang, C., Yang, S., & Zhang, J. (2017). Precursor flame characteristics of flame spread over aviation fuel. *Applied Thermal Engineering*, 117, 178-184.
- [17] Li, M., Wang, C., Zhang, J., Yang, S., Fan, C., & Liu, X. (2017). Characteristics of gas phase-controlled flame spread over liquid fuels. *Applied Thermal Engineering*.
- [18] Degroote, E., & Garcia-Ybarra, P. L. (2000). Flame spreading over liquid ethanol. *The European Physical Journal B-Condensed Matter and Complex Systems*, 13(2), 381-386.
- [19] Degroote, E., & Garcia Ybarra, P. L. (2005). Flame propagation over liquid alcohols: Part I. Experimental results. *Journal of thermal analysis and calorimetry*, 80(3), 541-548.
- [20] Degroote, E., & Garcia Ybarra, P. L. (2005). Flame propagation over liquid alcohols: Part II. Steady propagation regimes. *Journal of thermal analysis and calorimetry*, 80(3), 549-553.
- [21] Degroote, E., & García Ybarra, P. L. (2005). Flame propagation over liquid alcohols: Part III. Pulsating regime. *Journal of thermal analysis and calorimetry*, 80(3), 555-558.
- [22] Degroote, E. (2007, April). Avalanche-Collapse Process on Flame Spreading Over Liquid Fuels. In *AIP Conference Proceedings* (Vol. 905, No. 1, pp. 140-142). AIP.

- [23] Burgoyne, J. H., Roberts, A. F., & Quinton, P. G. (1968). The spread of flame across a liquid surface. I. The induction period. In *Proceedings of the Royal Society of London A: Mathematical, Physical and Engineering Sciences* (Vol. 308, No. 1492, pp. 39-53). The Royal Society.
- [24] Burgoyne, J. H., & Roberts, A. F. (1968). The spread of flame across a liquid surface. II. Steady-state conditions. In *Proceedings of the Royal Society of London A: Mathematical, Physical and Engineering Sciences* (Vol. 308, No. 1492, pp. 55-68). The Royal Society.
- [25] Burgoyne, J. H., & Roberts, A. F. (1968). The spread of flame across a liquid surface. III. A theoretical model. In *Proceedings of the Royal Society of London A: Mathematical, Physical and Engineering Sciences* (Vol. 308, No. 1492, pp. 69-79). The Royal Society.
- [26] Mackinven, R., Hansel, J. G. & Glassman, I., Influence of laboratory parameters on flame spread across liquid fuels. *Combustion Science and Technology*, 1 (1970) 293-306.
- [27] Torrance, K. E., Subsurface flows preceding flame spread over a liquid fuel. *Combustion Science and Technology*, 3 (1971) 133-143.
- [28] Torrance, K. E. & Mahajan, R. L., Fire spread over liquid fuels: liquid phase parameters. In *Fifteenth Symposium (International) on Combustion*. The Combustion Institute, Pittsburgh, PA, 1975, pp. 281-7.
- [29] Akita, K. (1973, January). Some problems of flame spread along a liquid surface. In *Symposium (International) on Combustion* (Vol. 14, No. 1, pp. 1075-1083). Elsevier.
- [30] Akita, K., & Fujiwara, O. (1971). Pulsating flame spread along the surface of liquid fuels. *Combustion and Flame*, 17(2), 268-269.
- [31] Li, A., Vozka, P., Mastream, A., Kilaz, G., Qiao, Li. (2019). Lean flammability limits of alternative aviation fuels. *Fire Safety Journal*, 108.
- [32] Vozka, P., Kilaz, G. (2019). How to obtain a detailed chemical composition for middle distillates via GC x GC-FID without the need of GC x GC – TOF/MS. *Fuel*, 247, 368-377.

## PUBLICATIONS

- 1) Goyal, V., Kim, J., Lucht, R.P., & Gore, J.P. (2019). Hot Surface Ignition Temperatures of Alternative Aviation Fuels", *11th US National Combustion Meeting*.
- 2) Goyal, V., Kim, J., Lucht, R.P., & Gore, J.P. (2019). Effect of Initial Fuel Temperature on flame spread rate of alternative aviation fuel. *11th US National Combustion Meeting*.
- 3) Roncancio, R., Navarkar, A., Goyal, V., and Jay P. Gore. Effect of carbon nanotubes addition on the Flame Spread Rate over a Jet A pool, *11th US National Combustion Meeting*.
- 4) Goyal, V., Yerbatyr Tursyn, Y., Kim, J., Lucht, R.P., & Gore, J.P. (2017). Flame Spread Measurements of Alternative Aviation fuels. *55th AIAA Aerospace Sciences Meeting*, AIAA SciTech Forum.
- 5) Goyal, V., Carayon, A.B., Simmons, R., Meyer, S., & Gore, J.P. (2017). Hot Surface Ignition Temperatures of Hydrocarbon Fuels. *55th AIAA Aerospace Sciences Meeting*, AIAA SciTech Forum.
- 6) Goyal, V., Hasti, V., Gore, J.P., & Mongia, H.C. (2015). Detached eddy simulation of novel confined swirl-stabilized combustor", *9th US National Combustion Meeting*.

## APPENDIX A – HSI EXPERIMENTAL APPARATUS DESIGN

## Appendix A1 – Copper Plate Design Files

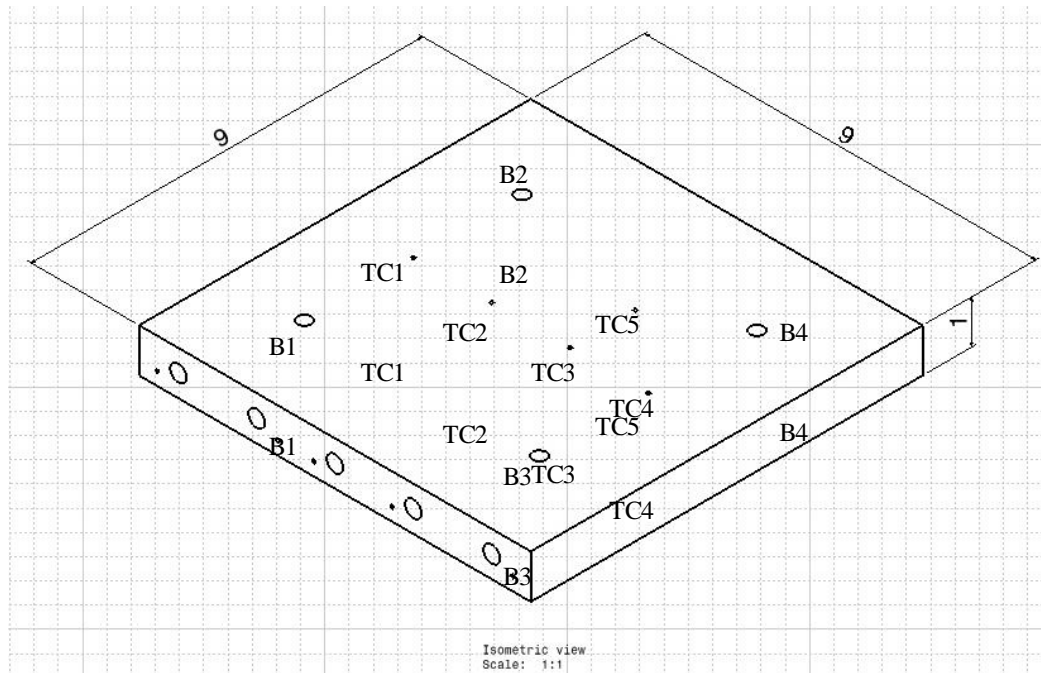


Figure A1: Isometric view of the copper plate

In figure A1, “TC” stands for thermocouple and “B” stands for bolt.

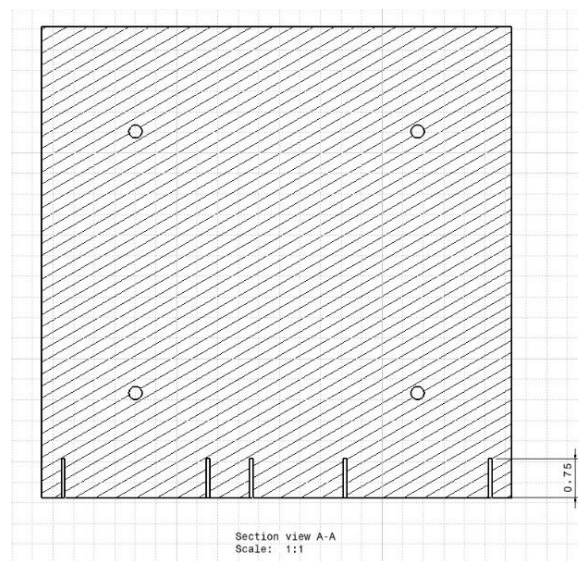


Figure A2: Top view of the copper plate

All dimensions are in inches.

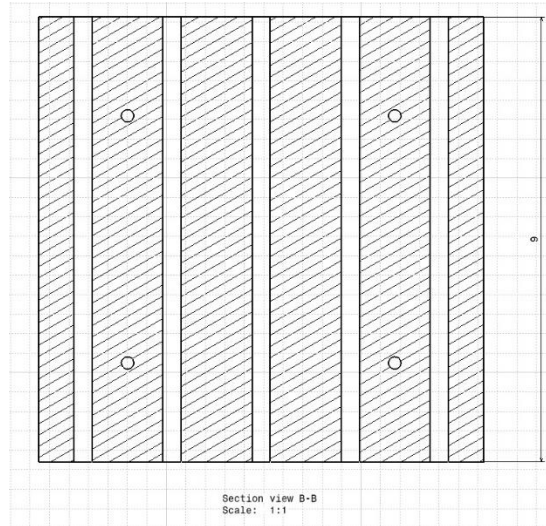


Figure A3: Bottom view of the copper plate

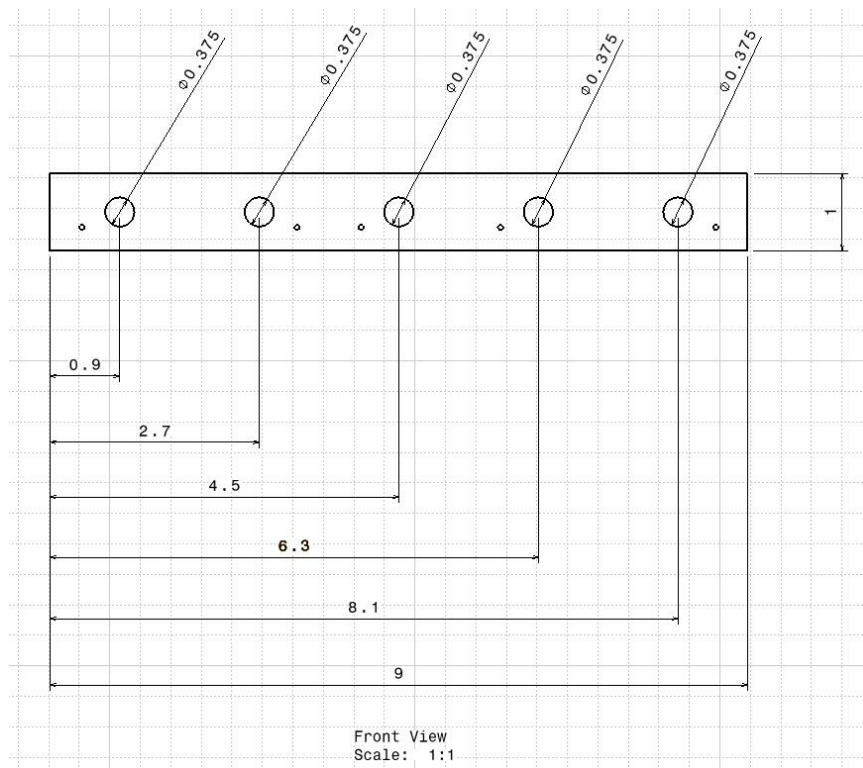


Figure A4: Dimensions and positions of the cartridge heaters' holes

All dimensions are in inches.

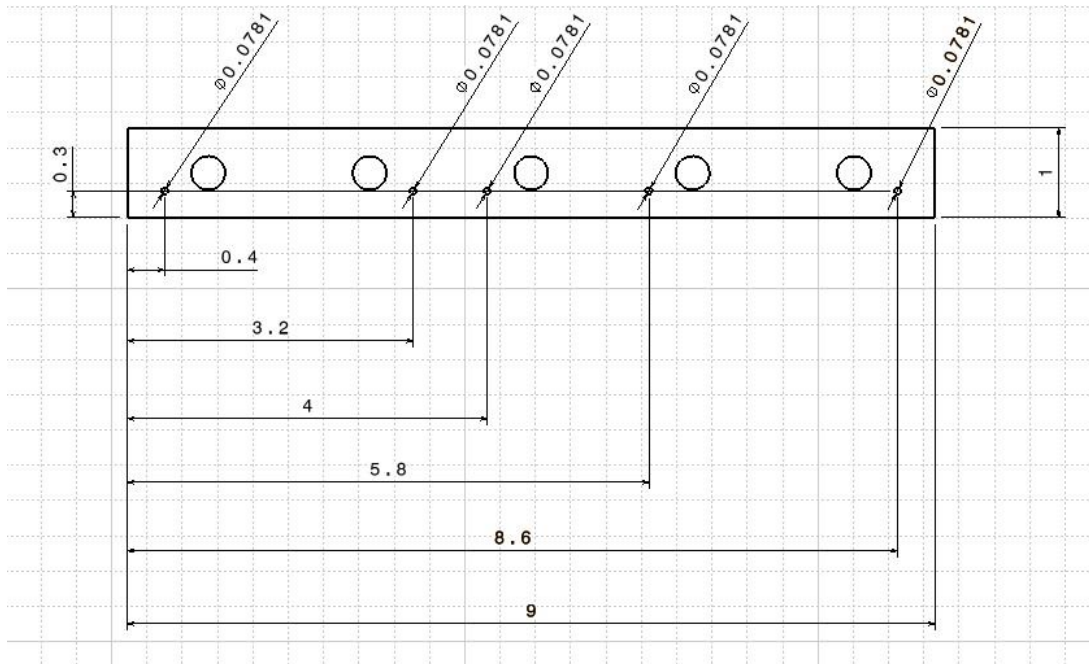


Figure A5: Dimensions and positions of the thermocouples

## Appendix A2 – Stainless Steel Plate Design Files

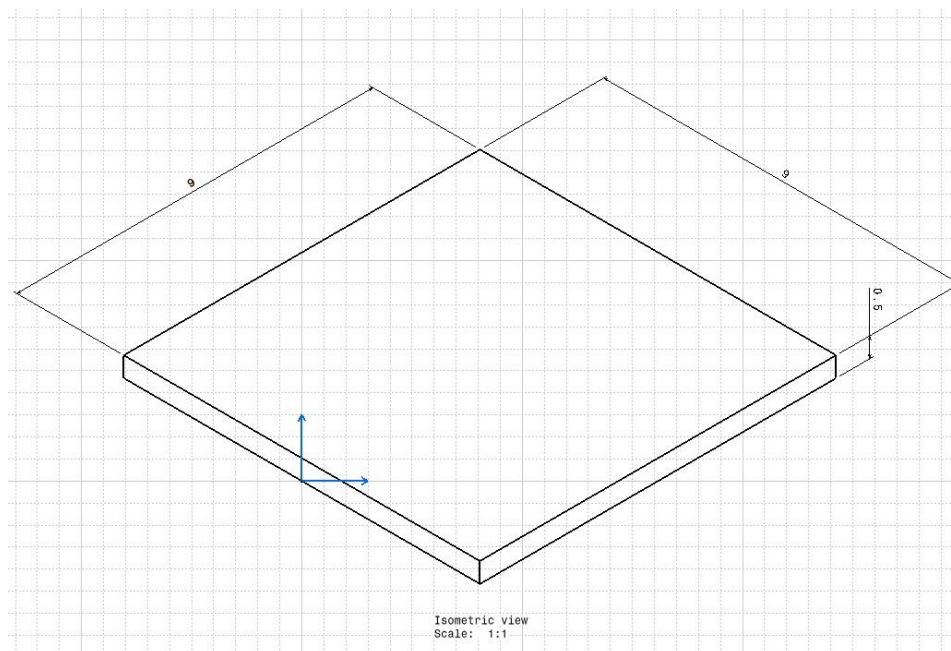


Figure A6: Isometric view of the stainless-steel plate with dimensions

All dimensions are in inches.

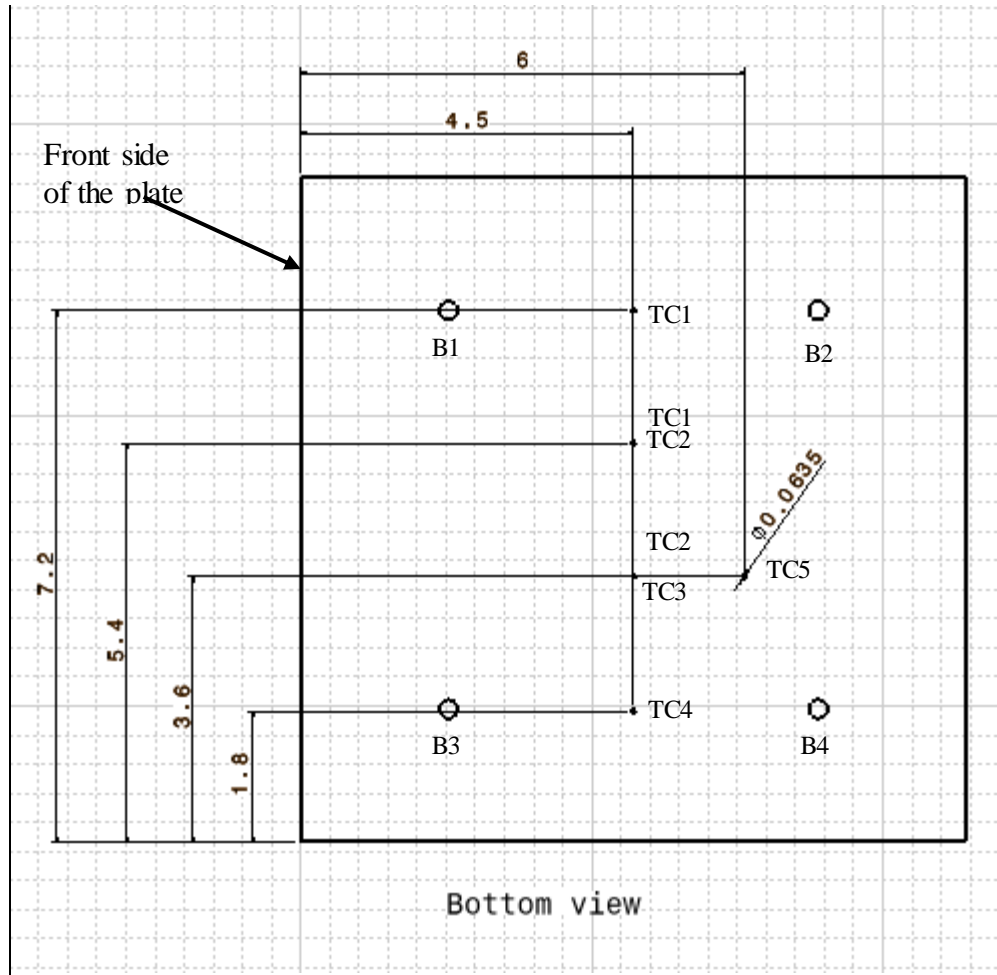


Figure A7: Bottom view of the stainless steel plate showing thermocouples and bolts location

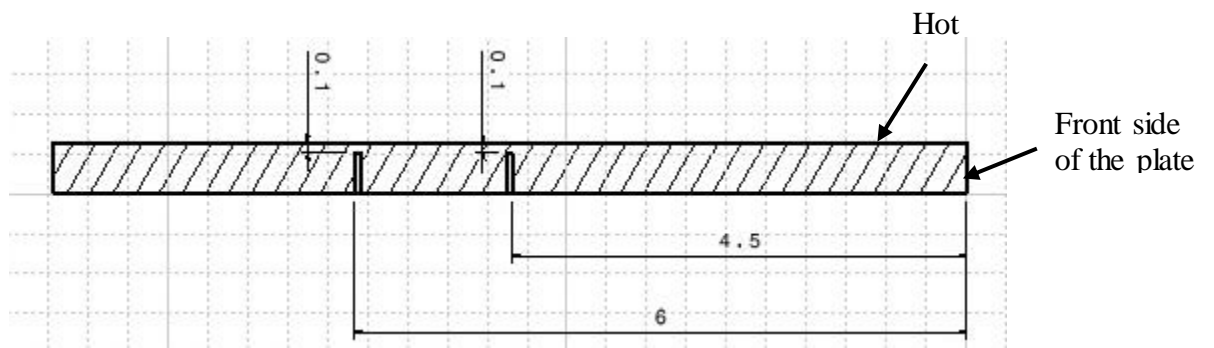


Figure A7: Side view of the stainless steel plate showing thermocouples depth

All dimensions are in inches.



## APPENDIX B – HSI TEST PROCEDURES

<b>0. SAFETY</b>	
0.00	Verify PPE ready for use: safety glasses, nitrile gloves, labcoats, and gloves for heated objects
<b>1. PREPARING THE APPARATUS</b>	
1.00	Take the bolts off and remove the thermocouples from the bottom of the rig
1.01	Take off the used stainless steel plate
1.02	Ensure that the number labeled on the ziplock bags corresponds to the correct fuel
1.03	Bolt the new stainless steel plate to the copper plate, by getting access to the bolts from the bottom of the rig
1.04	Stick the five thermocouples through the insulation and the two plates
1.05	Check the integrity of the ten thermocouples and of the five cartridge heaters (fuses included, using a voltmeter)
1.06	Setup the infrared camera in order to monitor the hot surface temperature
1.07	Setup the high speed camera
1.08	Wear nitrile gloves
1.09	Clean the stainless steel plate using isopropyl alcohol
1.10	Place the insulation surrounding the plates, and fill any potential holes in the insulation with additional high-temperature insulation
1.11	Change nitrile gloves
1.12	Disassemble the syringe and clean it using isopropyl alcohol
1.13	Clean the tube and nozzle using isopropyl alcohol
1.14	Lubricate the syringe o-rings with a small amount of Krytox
1.15	Reassemble the syringe and mount it on the syringe pump
1.17	Align the syringe pump on its stand
1.18	Align the nozzle of the syringe so that the nozzle is 30 cm away from the hot surface
1.19	Change nitrile gloves
1.20	Clean and dry the beaker to be used with isopropyl alcohol
1.21	Rinse a clean and dry beaker using the fuel to be used
1.22	Put 175 mL of fuel in the rinsed beaker properly labeled
1.23	Rinse the syringe with the fuel to be used
1.24	Empty the beaker containing the fuel in a bottle used for the disposable fuel
<b>2. CALIBRATING THE SYRINGE PUMP</b>	
2.00	Put 160 mL of fuel in the clean beaker prepared in 1.17
2.01	Load the .ppl program “NE_8000_nameofthefuel_LOAD” using the software SyringePumpPro
2.02	Load the syringe with the fuel to be tested – this program will load 150 mL of fuel, and will create a small jet to get rid of any air bubble
2.03	Calibrate the syringe pump flow rate in order to deliver a single drop of 0.25 mL

2.04	Check that the drop formed is not followed by a long tail of fuel, using the high speed camera
2.05	Set the syringe pump flow rate in the .ppl program “NE_8000_nameofthefuel_DROP”
2.06	Empty the beaker containing the fuel in a bottle used for the disposable fuel
2.07	Take off the purple nitrile gloves
<b>3. PERFORMING THE IGNITION TESTS</b>	
3.00	Set the plate temperature to 400°C
3.01	Align the nozzle of the syringe so that the nozzle is 30 cm away from the hot surface, and pointing towards the center of the plate (4.5” from the borders)
3.02	Load the .ppl program “NE_8000_nameofthefuel_DROP” using the software SyringePumpPro
3.03	Check if the temperature profile in the stainless steel plate is uniform using the thermocouples located in the stainless steel plate
3.04	Run one sequence of the syringe pump program to ensure that 20 successive drops are formed
3.05	Note the initial temperature shown by the thermocouples inside the stainless steel plate
3.06	Drop 1 drop of fuel onto the hot surface every 10 seconds* using the syringe pump software (20 drops total)
3.07	Report if ignition occurred for each drop
3.08	Increase the plate temperature by 50°C*
3.09	Repeat the steps from 3.05 to 3.08 until one ignition is observed
3.10	Reduce the plate temperature by 40°C after first ignition is observed
3.11	Check if the temperature profile in the stainless steel plate is uniform using the thermocouples located in the stainless steel plate
3.12	Note the initial temperature shown by the thermocouples inside the stainless steel plate, using the LabVIEW interface
3.13	Drop 1 drop of fuel onto the hot surface every 10 seconds* using the syringe pump software (20 drops total)
3.14	Report if ignition occurred for each drop
3.15	Increase the plate temperature by 10°C
3.16	Repeat the steps from 3.12 to 3.15 until 20 successive ignitions are observed
3.17	Visually assess the presence of residues once the tests are over
<b>4. POST-TEST PROCEDURE</b>	
4.00	Turn off the power going to the cartridge heaters
4.01	Turn on the fan, pointing towards the stainless steel plate
4.02	Put on purple nitrile gloves
4.03	Set the syringe pump on “manual” mode
4.04	Ensure that there is no fuel left in the syringe
4.05	Fill up the syringe with isopropyl alcohol and empty it in a labeled beaker – repeat this process 3 times
4.06	Empty the beaker containing the fuel in a bottle used for the disposable fuel

## APPENDIX C – ADDITIONAL TEST DATA: HSI

### Appendix C1 - AVIATION GASOLINE 100LL

Set temperature in the copper plate (°C)	Mean temperature in the stainless steel plate (°C)	# of ignitions	P(I) (measured)	P(I) (interpolated from curve fit)	Drop Number																			
					1	2	3	4	5	6	7	8	9	10	11	12	13	14	15	16	17	18	19	20
400	396	0	0.00	0.00	X	X	X	X	X	X	X	X	X	X	X	X	X	X	X	X	X	X	X	X
500	495	0	0.00	0.00	X	X	X	X	X	X	X	X	X	X	X	X	X	X	X	X	X	X	X	X
600	592	0	0.00	0.00	X	X	X	X	X	X	X	X	X	X	X	X	X	X	X	X	X	X	X	X
700	691	0	0.00	0.00	X	X	X	X	X	X	X	X	X	X	X	X	X	X	X	X	X	X	X	X
750	741	0	0.00	0.00	X	X	X	X	X	X	X	X	X	X	X	X	X	X	X	X	X	X	X	X
760	748	0	0.00	0.01	X	X	X	X	X	X	X	X	X	X	X	X	X	X	X	X	X	X	X	X
770	758	0	0.00	0.05	X	X	X	X	X	X	X	X	X	X	X	X	X	X	X	X	X	X	X	X
780	768	3	0.15	0.15	X	X	X	X	X	X	X	X	X	X	X	X	X	X	X	X	X	X	X	X
790	778	5	0.25	0.37	X	O	X	O	X	X	X	X	X	O	X	X	X	X	O	X	X	X	X	X
800	788	14	0.70	0.67	O	O	O	O	O	O	O	O	O	X	O	O	X	O	O	X	O	X	X	O
810	797	17	0.85	0.85	O	O	O	O	O	X	X	O	O	O	O	O	O	X	O	O	O	O	O	O
820	806	20	1.00	0.97	O	O	O	O	O	O	O	O	O	O	O	O	O	O	O	O	O	O	O	O
830	815	20	1.00	0.99	O	O	O	O	O	O	O	O	O	O	O	O	O	O	O	O	O	O	O	O

**X:** no ignition; **O:** ignition

Here, “set temperature” is the temperature set on the temperature controller. The “mean temperature” is the average temperature recorded by the thermocouples, TC2, TC3 and TC5, which are near the center in the stainless-steel plate. The “# of ignitions” is the number of drops that ignited out of the 20 drops dropped on the hot surface. “P(I) (measured)” is the measured ignition probability and “P(I) (interpolated from curve fit)” is the interpolated ignition probability value from the logistics curve fit.

## Appendix C2 - TEST FUEL A

Set temperature in the copper plate (°C)	Mean temperature in the stainless-steel plate (°C)	# of Ignitions	P(I) (measured)	P(I) (interpolated from curve fit)	Drop Number																			
					1	2	3	4	5	6	7	8	9	10	11	12	13	14	15	16	17	18	19	20
300	294	0	0.00	0.00	X	X	X	X	X	X	X	X	X	X	X	X	X	X	X	X	X	X	X	X
500	494	0	0.00	0.00	X	X	X	X	X	X	X	X	X	X	X	X	X	X	X	X	X	X	X	X
700	688	0	0.00	0.00	X	X	X	X	X	X	X	X	X	X	X	X	X	X	X	X	X	X	X	X
750	738	0	0.00	0.00	X	X	X	X	X	X	X	X	X	X	X	X	X	X	X	X	X	X	X	X
800	789	0	0.00	0.00	X	X	X	X	X	X	X	X	X	X	X	X	X	X	X	X	X	X	X	X
820	807	0	0.00	0.00	X	X	X	X	X	X	X	X	X	X	X	X	X	X	X	X	X	X	X	X
840	827	0	0.00	0.02	X	X	X	X	X	X	X	X	X	X	X	X	X	X	X	X	X	X	X	X
850	834	1	0.05	0.05	X	X	X	X	X	X	X	X	X	X	X	X	X	X	X	X	X	X	O	X
860	842	6	0.30	0.14	X	X	X	O	X	X	O	X	O	X	X	O	X	X	X	X	O	X	O	X
870	851	8	0.40	0.38	X	O	O	X	O	O	O	O	X	X	X	X	X	X	X	X	X	O	X	X
880	858	11	0.55	0.63	X	X	O	X	O	X	O	X	X	O	O	O	X	O	X	O	O	O	X	O
890	866	17	0.85	0.85	O	O	O	O	O	O	X	X	X	O	O	O	O	O	O	O	O	O	O	O
900	874	20	1.00	0.96	O	O	O	O	O	O	O	O	O	O	O	O	O	O	O	O	O	O	O	O
910	882	20	1.00	0.99	O	O	O	O	O	O	O	O	O	O	O	O	O	O	O	O	O	O	O	O

X: no ignition; O: ignition

Here, “set temperature” is the temperature set on the temperature controller. The “mean temperature” is the average temperature recorded by the thermocouples, TC2, TC3 and TC5, which are near the center in the stainless-steel plate. The “# of ignitions” is the number of drops that ignited out of the 20 drops dropped on the hot surface. “P(I) (measured)” is the measured ignition probability and “P(I) (interpolated from curve fit)” is the interpolated ignition probability value from the logistics curve fit.

## Appendix C3 - TEST FUEL B

Set temperature in the copper plate (°C)	Mean temperature in the stainless steel plate (°C)	# of Ignitions	P(I) (measured)	P(I) (interpolated from the curve fit)	Drop Number																			
					1	2	3	4	5	6	7	8	9	10	11	12	13	14	15	16	17	18	19	20
400	400	0	0.00	0.00	X	X	X	X	X	X	X	X	X	X	X	X	X	X	X	X	X	X	X	X
500	500	0	0.00	0.00	X	X	X	X	X	X	X	X	X	X	X	X	X	X	X	X	X	X	X	X
600	600	0	0.00	0.00	X	X	X	X	X	X	X	X	X	X	X	X	X	X	X	X	X	X	X	X
650	650	0	0.00	0.04	X	X	X	X	X	X	X	X	X	X	X	X	X	X	X	X	X	X	X	X
660	660	0	0.00	0.06	X	X	X	X	X	X	X	X	X	X	X	X	X	X	X	X	X	X	X	X
670	669	2	0.10	0.10	X	X	X	X	X	X	X	X	X	X	X	X	X	X	X	X	X	X	X	X
680	679	5	0.25	0.17	X	X	X	X	X	X	X	X	X	X	X	X	X	X	X	X	X	X	X	X
690	688	12	0.60	0.23	X	X	X	X	X	X	X	X	X	X	X	X	X	X	X	X	X	X	X	X
700	698	13	0.65	0.33	X	X	X	X	X	X	X	X	X	X	X	X	X	X	X	X	X	X	X	X
710	708	12	0.60	0.45	X	X	X	X	X	X	X	X	X	X	X	X	X	X	X	X	X	X	X	X
720	717	9	0.45	0.57	X	X	X	X	X	X	X	X	X	X	X	X	X	X	X	X	X	X	X	X
730	727	10	0.50	0.69	X	X	X	X	X	X	X	X	X	X	X	X	X	X	X	X	X	X	X	X
740	736	10	0.50	0.77	X	X	X	X	X	X	X	X	X	X	X	X	X	X	X	X	X	X	X	X
750	745	14	0.70	0.84	X	X	X	X	X	X	X	X	X	X	X	X	X	X	X	X	X	X	X	X
760	754	18	0.90	0.90	X	X	X	X	X	X	X	X	X	X	X	X	X	X	X	X	X	X	X	X
770	764	20	1.00	0.95	X	X	X	X	X	X	X	X	X	X	X	X	X	X	X	X	X	X	X	X
780	773	20	1.00	0.97	X	X	X	X	X	X	X	X	X	X	X	X	X	X	X	X	X	X	X	X

X: no ignition; O: ignition

Here, “set temperature” is the temperature set on the temperature controller. The “mean temperature” is the average temperature recorded by the thermocouples, TC2, TC3 and TC5, which are near the center in the stainless-steel plate. The “# of ignitions” is the number of drops that ignited out of the 20 drops dropped on the hot surface. “P(I) (measured)” is the measured ignition probability and “P(I) (interpolated from curve fit)” is the interpolated ignition probability value from the logistics curve fit.

## Appendix C4 - TEST FUEL C

Set temperature in the copper plate (°C)	Mean temperature in the stainless steel plate (°C)	# of ignitions	P(I) (measured)	P(I) (interpolated from the curve fit)	Drop Number																			
					1	2	3	4	5	6	7	8	9	10	11	12	13	14	15	16	17	18	19	20
400	398	0	0.00	0.00	X	X	X	X	X	X	X	X	X	X	X	X	X	X	X	X	X	X	X	X
500	497	0	0.00	0.00	X	X	X	X	X	X	X	X	X	X	X	X	X	X	X	X	X	X	X	X
600	597	0	0.00	0.00	X	X	X	X	X	X	X	X	X	X	X	X	X	X	X	X	X	X	X	X
650	647	0	0.00	0.00	X	X	X	X	X	X	X	X	X	X	X	X	X	X	X	X	X	X	X	X
700	696	0	0.00	0.00	X	X	X	X	X	X	X	X	X	X	X	X	X	X	X	X	X	X	X	X
750	745	0	0.00	0.07	X	X	X	X	X	X	X	X	X	X	X	X	X	X	X	X	X	X	X	X
760	755	3	0.15	0.15	X	X	X	X	X	X	X	X	X	X	X	X	X	X	X	X	X	X	X	X
770	765	6	0.30	0.29	X	X	X	X	X	X	X	X	X	X	X	X	X	X	X	X	X	X	X	X
780	774	6	0.30	0.46	X	X	X	X	X	X	X	X	X	X	X	X	X	X	X	X	X	X	X	X
790	786	11	0.55	0.70	X	X	X	X	X	X	X	X	X	X	X	X	X	X	X	X	X	X	X	X
800	791	12	0.60	0.78	X	X	X	X	X	X	X	X	X	X	X	X	X	X	X	X	X	X	X	X
810	799	12	0.60	0.87	X	X	X	X	X	X	X	X	X	X	X	X	X	X	X	X	X	X	X	X
820	811	19	0.95	0.95	X	X	X	X	X	X	X	X	X	X	X	X	X	X	X	X	X	X	X	X
830	817	18	0.90	0.97	X	X	X	X	X	X	X	X	X	X	X	X	X	X	X	X	X	X	X	X
840	825	20	1.00	0.98	X	X	X	X	X	X	X	X	X	X	X	X	X	X	X	X	X	X	X	X
850	832	20	1.00	0.99	X	X	X	X	X	X	X	X	X	X	X	X	X	X	X	X	X	X	X	X

**X:** no ignition; **O:** ignition

Here, “set temperature” is the temperature set on the temperature controller. The “mean temperature” is the average temperature recorded by the thermocouples, TC2, TC3 and TC5, which are near the center in the stainless-steel plate. The “# of ignitions” is the number of drops that ignited out of the 20 drops dropped on the hot surface. “P(I) (measured)” is the measured ignition probability and “P(I) (interpolated from curve fit)” is the interpolated ignition probability value from the logistics curve fit.

## Appendix C5 - TEST FUEL D

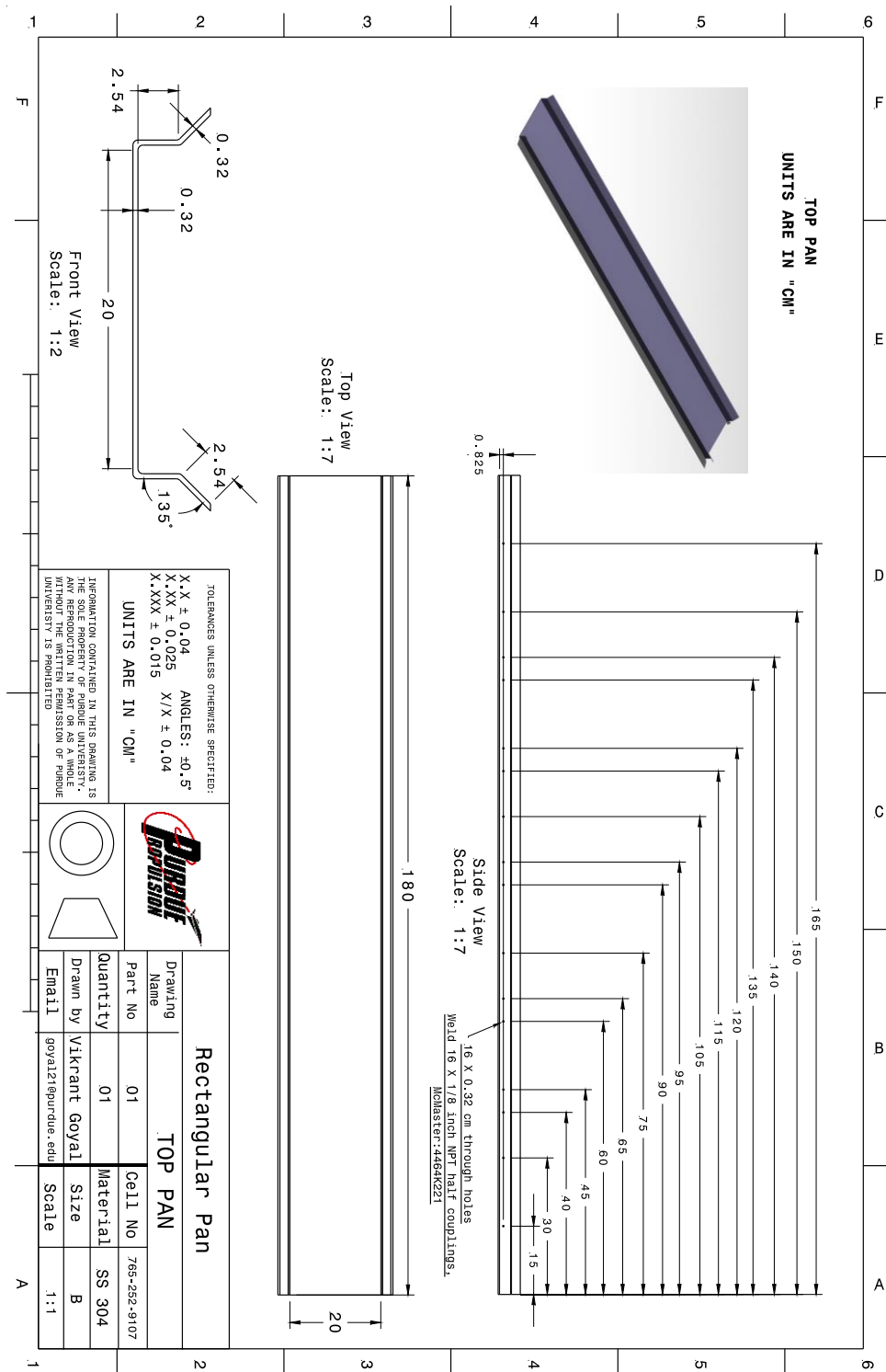
Set temperature in the copper plate (°C)	Mean temperature in the stainless steel plate (°C)	# of ignitions	P(I) (measured)	P(I) (interpolated from the curve fit)	Drop Number																			
					1	2	3	4	5	6	7	8	9	10	11	12	13	14	15	16	17	18	19	20
400	400	0	0.00	0.00	X	X	X	X	X	X	X	X	X	X	X	X	X	X	X	X	X	X	X	X
500	500	0	0.00	0.00	X	X	X	X	X	X	X	X	X	X	X	X	X	X	X	X	X	X	X	X
600	599	0	0.00	0.00	X	X	X	X	X	X	X	X	X	X	X	X	X	X	X	X	X	X	X	X
700	697	1	0.05	0.05	X	X	X	X	X	X	X	X	X	X	X	X	X	○	X	X	X	X	X	X
710	706	4	0.20	0.09	X	X	X	X	X	X	○	X	X	○	X	X	○	X	X	X	X	X	X	X
720	716	3	0.15	0.15	X	○	X	X	○	X	X	○	X	X	X	X	X	X	X	X	X	X	X	X
730	726	2	0.10	0.25	X	○	X	X	X	X	X	X	X	X	X	X	X	X	○	X	X	X	X	X
740	736	3	0.15	0.39	○	X	X	○	X	X	X	○	X	X	X	X	X	X	X	X	X	X	X	X
750	745	1	0.05	0.53	X	X	X	X	X	○	X	X	X	X	X	X	X	X	X	X	X	X	X	X
760	754	1	0.05	0.67	X	X	X	X	X	X	X	X	X	X	X	X	X	X	X	X	X	X	X	X
770	763	3	0.15	0.78	X	X	X	X	X	X	X	○	X	X	○	X	X	X	X	X	X	X	X	○
780	772	9	0.45	0.87	○	○	○	○	○	X	X	X	○	X	○	X	X	○	X	X	X	X	X	○
790	781	8	0.40	0.92	X	X	X	○	○	X	○	X	X	○	X	X	X	○	X	○	○	○	○	X
800	789	19	0.95	0.95	○	○	○	○	○	○	○	○	○	○	○	○	X	○	○	○	○	○	○	○
810	793	20	1.00	0.97	○	○	○	○	○	○	○	○	○	○	○	○	○	○	○	○	○	○	○	○
820	799	20	1.00	0.99	○	○	○	○	○	○	○	○	○	○	○	○	○	○	○	○	○	○	○	○

**X**: no ignition; **○**: ignition

Here, “set temperature” is the temperature set on the temperature controller. The “mean temperature” is the average temperature recorded by the thermocouples, TC2, TC3 and TC5, which are near the center in the stainless-steel plate. The “# of ignitions” is the number of drops that ignited out of the 20 drops dropped on the hot surface. “P(I) (measured)” is the measured ignition probability and “P(I) (interpolated from curve fit)” is the interpolated ignition probability value from the logistics curve fit.

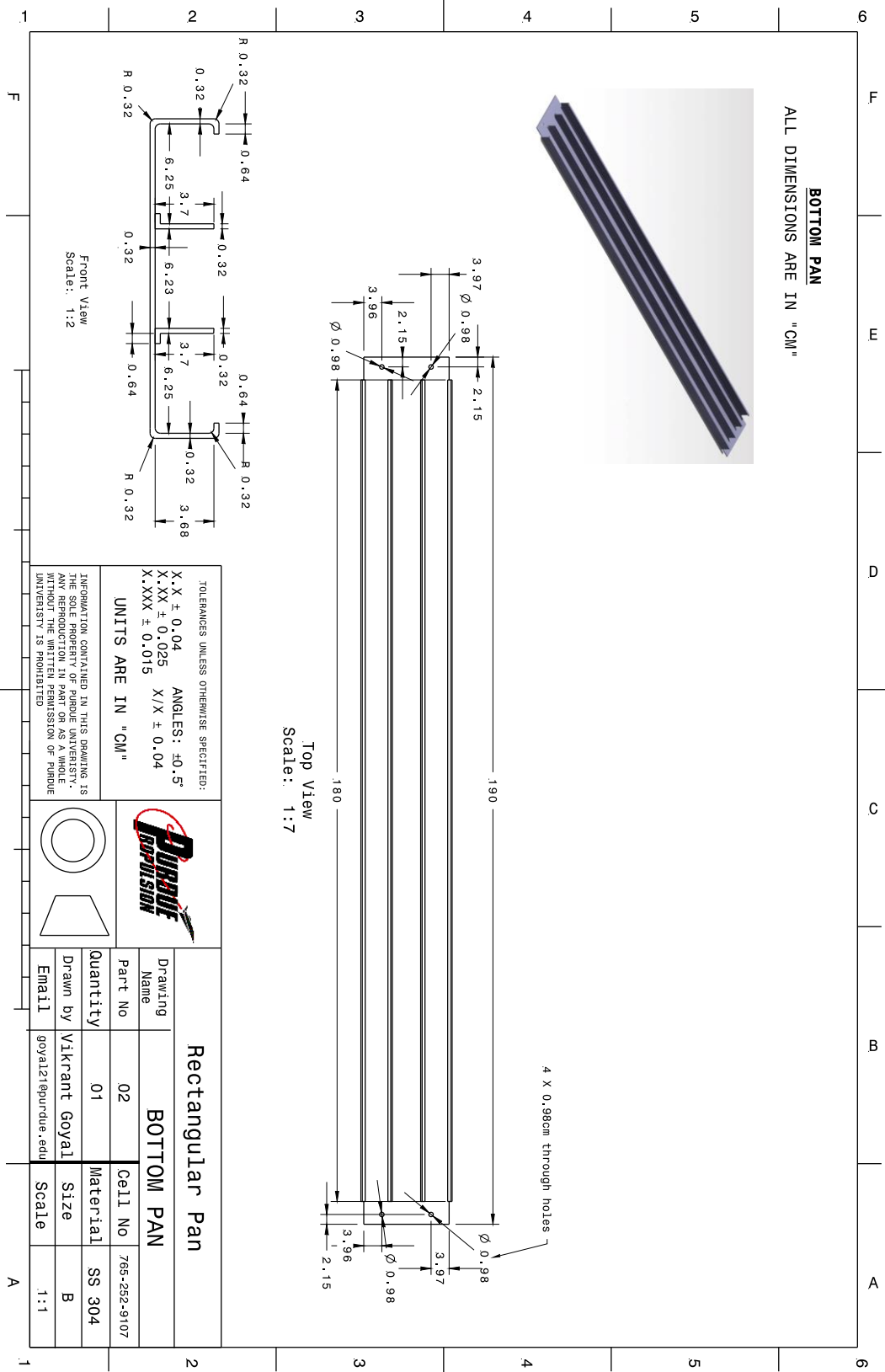
APPENDIX D – POOL FIRE APPARATUS DESIGN FILES

Appendix D1-Top Pan CAD drawing

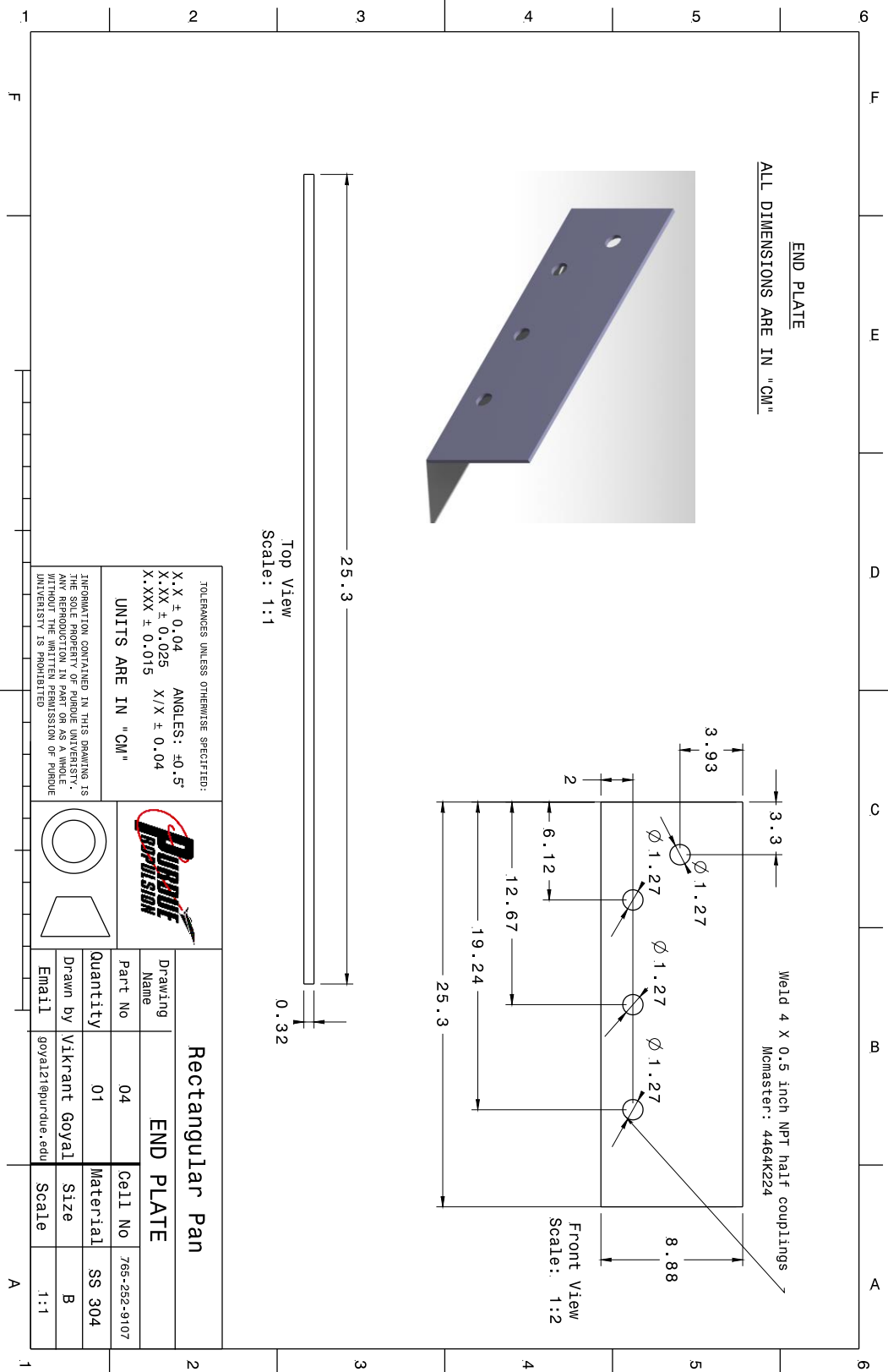




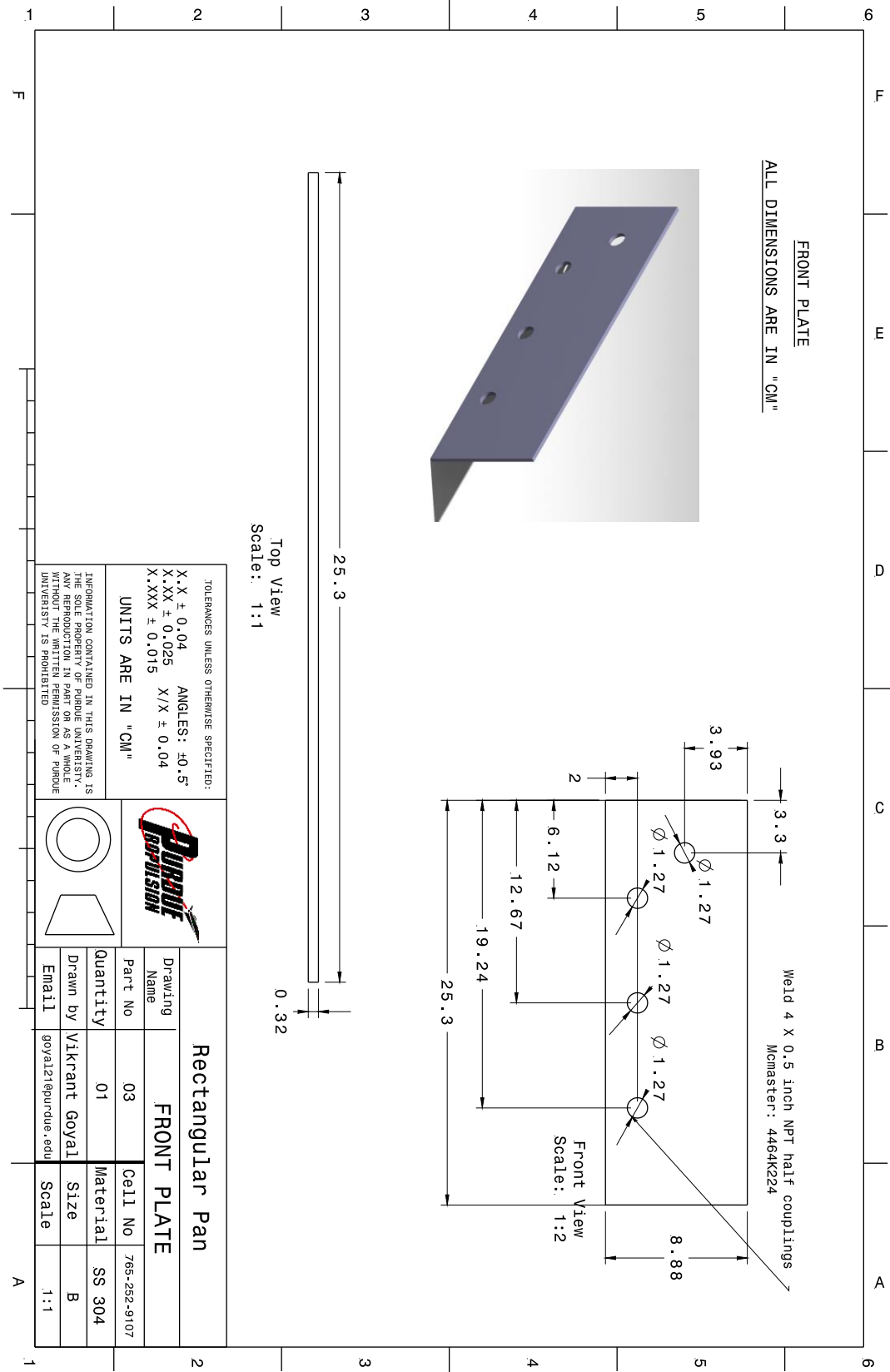
Appendix D2-Bottom Pan CAD drawing



Appendix D3-End Plate CAD drawing



Appendix D4-Front Plate CAD drawing



**LID**

ALL DIMENSIONS ARE IN "CM"

**Top View**  
Scale: 1:6

**Side View**  
Scale: 1:6

Dimensions: 182.27, 87.37, 26.13, 4.5, 20, 1.8, 1.8, 5, 4, 0.32, 0.63 [4 X 0.635 (0.25 inch) through holes]

Labels: HANDLE LOCATION, HANDLE LOCATION

**Rectangular Pan**

**DURPURE CORPORATION**

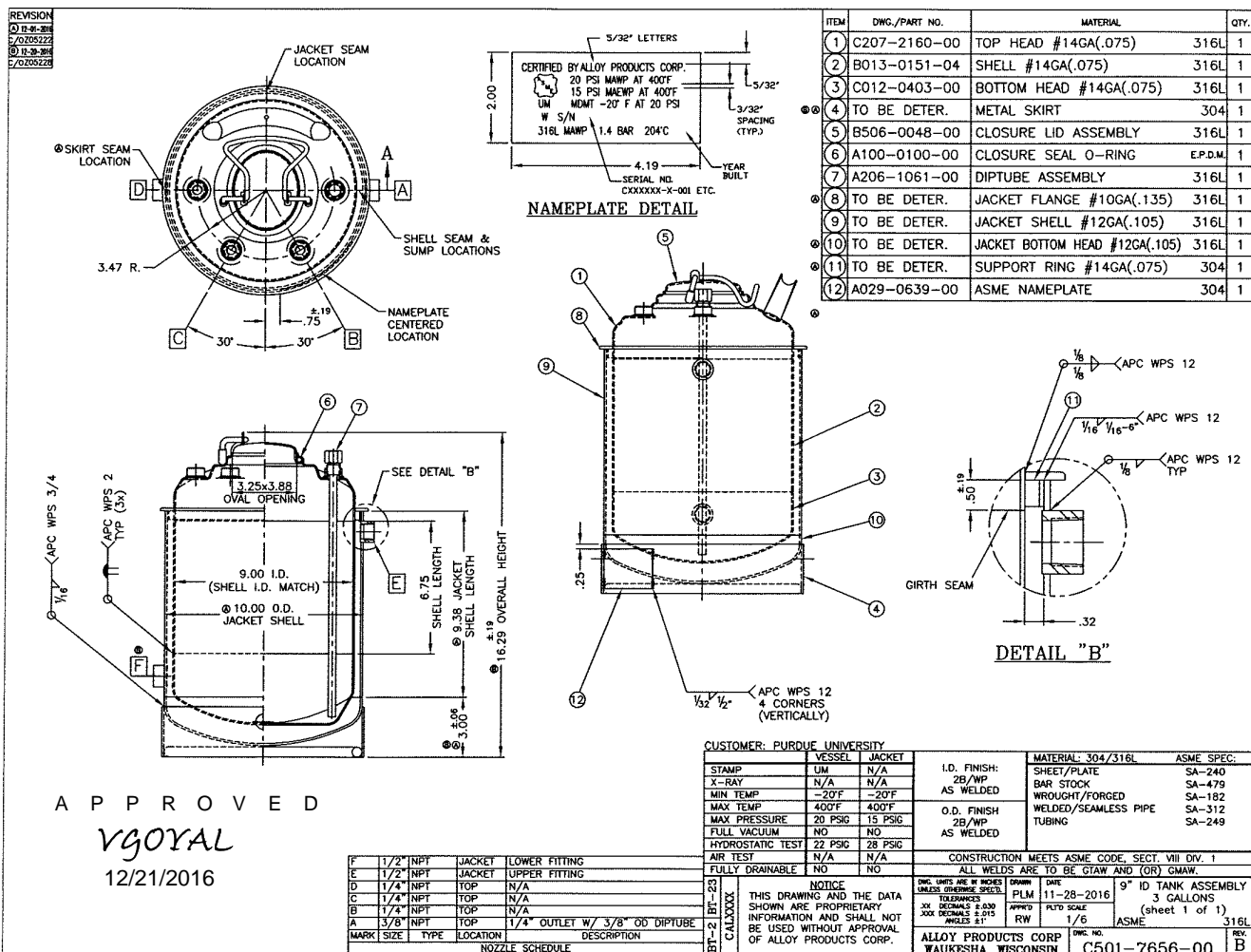
Drawing Name		LID	
Part No	05	Cell No	765-252-9107
Quantity	01	Material	SS 304
Drawn by	Vikrant Goyal	Size	B
Email	goyal21@purdue.edu	Scale	1:1

TOLERANCES UNLESS OTHERWISE SPECIFIED:  
X.X ± 0.04 ANGLES: ±0.5°  
X.XX ± 0.025 X/X ± 0.04  
X.XXX ± 0.015

UNITS ARE IN "CM"

INFORMATION CONTAINED IN THIS DRAWING IS THE SOLE PROPERTY OF PURDUE UNIVERSITY. IT IS TO BE USED FOR THE PROJECT AND NOT BE REPRODUCED OR TRANSMITTED IN ANY FORM OR BY ANY MEANS WITHOUT THE WRITTEN PERMISSION OF PURDUE UNIVERSITY IS PROHIBITED.

## Appendix D6-Fuel Heating Vessel



## APPENDIX E – POOL FIRE EXPERIMENT TEST PROCEDURES

0. SAFETY	
0	Verify Personal Protective Equipment (PPE) ready for use:
	Wear Safety Glasses
	Wear Nitrile Gloves
	Wear Respirator
	Wear Fire-safety coats
1. TRANSPORTING TEST FUEL FROM TEST FUEL DRUM	
1.00	Wear Nitrile gloves
1.01	Wear Safety Glasses
1.02	Take a 5 gallon kerosene can and wash it with isopropyl alcohol
1.03	Dump the used isopropyl solution into another 5 gallon kerosene can
1.04	Take kerosene can and isopropyl alcohol bottle to the backyard of ZL3 where all fuel drums are placed and
	identify the test fuel drum ( All test fuel drums are named accurately)
1.05	Take bung tool from high pressure lab machine shop to open the test fuel drum plug
1.06	Take siphon from fuel drum shed and wash it with isopropyl alcohol
1.07	Open the test fuel drum plug
1.08	Siphon ~3 gallons of test fuel from 55 gal test fuel drum into kerosene tank
1.09	Close test fuel drum plug
1.1	Wash siphon with isopropyl alcohol and keep siphon back in fuels' drum shed
1.11	Put back bung tool in high pressure lab machine shop
1.12	Bring back kerosene tank filled with test fuel to 121A.
1.13	Remove nitrile gloves
2. PREPARING THE RIG	
2.00	Turn on laser warning lights outside both doors of 121A
2.01	Turn on exhaust fan to the maximum
2.02	Put on nitrile gloves and a respirator
2.03	Check all connections – bolts, nuts, cylinders & valves
2.04	Start-up Quanta-Ray laser
2.04.1	Turn on tap water valve to laser for external cooling (water pressure should be around 40 psi)
2.04.2	Turn on N <sub>2</sub> to laser (N <sub>2</sub> flow rate should be at 0.03). Never operate the laser without N <sub>2</sub> flushing
2.04.3	Check cable connections (match colors between cables and cable plugs)
2.04.4	Check the power supply front panel CIRCUIT BREAKER is turned on

2.04.5	Turn on the power supply front panel KEY switch
2.04.6	Set the remote REP RATE SOURCE to EXT
2.04.7	Set the remote Q-SWITCH MODE to EXT
2.04.8	Set the remote INT/COMPUTER to INT
2.04.9	Set the remote LAMP ON/INHIBIT to LAMP ON
2.04.10	Verify all covers are on
2.04.11	Temporarily push out the ENABLE switch
2.04.12	Warm up the laser for 15 minutes
2.05	Software Settings for the laser
	Turn on the computer for the laser
	Turn on the software "Insight" and open "default configuration"
	Set TRIGGER mode and SEQUENCE mode
	Set a number of sequence as what you want
	Click laser shooting button two times
	Slowly increase OSC(or AMP or both based on required ignition energy) LAMP ENERGY to the level at the remote
	Once you check there is a spark, Click laser stop button one time. Then, Q-switch will be off and flash lamps will keep running
2.06	Check operation of lid-actuation system
	Open manual valve connected to shop-air supply
	Adjust shop-air pressure to 50 psi
	Press the push-button to open the lid ( push-button should be continuously pressed)
	Release the push button to close the lid
	Adjust the shop-air pressure to 0 psig
	Open the lid manually
2.07	Check operation of CO2 fire extinguisher system
	Fully open the CO2 cylinder valve
	Check for any leakages in pipeline
	Open the ball valve installed in CO2 pipeline
	Check manually for low CO2 spray velocity from nozzles
	Close the CO2 cylinder valve
	Close the ball valve installed in CO2 pipeline
2.08	Thermocouple Connections
	Check all thermocouples' connections
	Use a Vernier caliper and adjust gas-phase thermocouples tip at 10 mm above test pan bend
	Use Vernier caliper and adjust liquid-phase thermocouples tip at 3 mm below the test pan bend
	Switch on Lenovo laptop placed inside DAQ control box
	Remotely connect personal laptop to Lenovo laptop using "Remote Desktop Connection" options in Windows

	Connect to Lenovo system using credentials - Username: Test Operator and Pwd: lfdag
	Open "Top level GUI" and load "Pool fire.ini" file
	Check response of all thermocouples
2.09	High Speed Camera installation
2.09.1	Open high speed camera box and take out camera, Ethernet cable, power cord and camera lens
2.09.2	Place tripod at 8 feet distance from rectangular pan on a table placed opposite to pool.
2.09.3	Adjust height of tripod 28 inches from table surface and 7 inches from table left side when viewed while facing the table.
2.09.4	Mount the camera on tripod
2.09.5	Connect power cord to camera
2.09.6	Mount camera lens
2.09.7	Open laptop that comes along with high speed camera and open Phantom camera control (PCC) software
2.09.8	Connect Ethernet cable from camera to the laptop and connect PCC software to the camera
2.09.9	Make the following adjustments to camera settings
	Camera exposure time : 150 $\mu$ s
	Resolution: 800x400
	Frame rate: 100 fps (vary fps depending on flame spread rate and high speed camera frame number)
2.10	Regular Camera installation
2.10.1	Open regular camera box and take out camera and power cord
2.10.2	Place tripod at 6.5 feet distance from rectangular pan in front of the table placed opposite to pool
2.10.3	Adjust height of tripod 20.5 inches from table surface and 1 inch from table left side when viewed while facing the table
2.10.4	Mount the camera on tripod
2.10.5	Connect power cord to camera
2.10.6	Make the following adjustments to camera settings
	Camera exposure time : Auto-exposure
	Resolution: 640 x 512
	Frame rate: 30 fps
2.11	Open the exhaust speed at speed number 8
2.12	Fuel heater operation and fuel filling procedure
2.12.1	Check if all the valves connected to the stainless steel vessel and the bottom pan are closed.
2.12.2	Pour 3 gallons of fuel into the stainless steel vessel
2.12.3	Open the N2 cylinder valve
2.12.4	Open the manual valve MV_N01



2.12.5	Adjust N2 downstream pressure to 10 psi
2.12.6	Open all the manual valves connected to the bottom pan and stainless steel heating vessel
2.12.7	Turn on the fuel re-circulator heater
2.12.8	Set the oil temperature to desired temperature
2.12.9	Press "OK" button on the fuel re-circulator heater, it will start the circulation and heating process
2.12.10	Monitor the pan temperature via 3 surface thermocouple probes
2.12.11	Monitor fuel temperature in the stainless steel vessel using k-type calibrated thermocouple meter
2.12.12	After desired temperature is reached, open valve MV_F01 and MV_F03
2.12.13	After test pan is filled with fuel, close MV_F01 and MV_F03
2.13	Remove nitrile gloves
3. CONDUCTING THE TEST	
3.00	Wear Fire-safety coats
3.00	Open the CO2 cylinder valve - Operator 1
3.01	Press the push-button switch to open the lid - Operator 1
3.02	Start recording camera videos - Operator 2
3.03	Start recording thermocouple data - Operator 2
3.04	Click capture button one time at Insight computer software for laser ignition
	If Ignition does not happen, redo 3.04. Make it sure the video recording still have enough number of frame to record the event
3.05	Record flame spread event with all cameras until flame reaches the other end of the pool
3.06	Release the push-button switch to close the lid after lead operator signal- Operator 1
3.07	Look around the edges of the pool-lid to ensure that there are no residual flames emerging from these edges
3.08	Open the CO2 ball-valve to extinguish the fire, if fire is not extinguished after closing the lid - Operator 1
3.09	Close the CO2 ball valve
3.10	Close the CO2 cylinder valve
3.11	Take off fire-safety coats
4. POST-TEST PROCEDURES	
4.00	Adjust shop air pressure to 0 psig connected to solenoid valve for lid operation
4.01	Open the lid manually
4.02	Shut-off Quanta-Ray laser
4.02.1	Block the laser beam with a beam trap ( or a laser shield)
4.02.2	Click laser shooting button once. The laser will be firing
4.02.3	Reduce slowly the laser power to zero by turning LAMP ENERGY control to START

4.02.4	Click laser stop button twice
4.02.5	Allow the laser the current status for 30 minutes to cool down the flash lamps, the rod, and the crystal
4.02.6	After 30 minutes, press the STOP button at the remote
4.02.7	Turn off the power supply front panel KEY switch
4.02.8	Leave CIRCUIT BREAKER as turned on. This keeps watching the crystal's temperature inside the laser
4.02.9	Leave N2 cylinder and the valve as opened. Close these after at least 24 hours
4.03	Reduce the set temperature point of the thermal fluid to 20°C to initiate effective cooling
4.04	Check the fuel pool temperature from installed liquid-phase thermocouples
4.05	Wait for fuel pool to cool down to room temperature
4.06	Open the valve MV_F03 and MV_F02 to dispense tested fuel into kerosene tank
4.07	Stop pumping the thermal fluid
4.08	Close all the valves connected to the stainless-steel vessel and re-circulator heater.
4.09	Close N2 cylinder valve, and open the manual valve MV_F01 and MV_N01 in order to remove N2 in the tube
4.10	Clean the test pan, stainless steel vessel with iso-propyl alcohol
4.11	Copy the recorded camera data into hard-drive for analysis
4.12	Copy thermocouple data into hard-drive for analysis
4.13	Packing High Speed Camera
4.13.1	Close the PCC software
4.13.2	Disconnect Ethernet cable from laptop and camera
4.13.3	Disconnect power cord from high speed camera
4.13.4	Unmount high speed camera from tripod
4.13.5	Pack the camera box
4.14	Packing Regular Camera
4.14.1	Disconnect power cord from high speed camera
4.14.2	Unmount high speed camera from tripod
4.14.3	Pack the camera box
4.14	Close the exhaust fan
4.15	Dump the tested fuel into 55 gallon kerosene waste fuel tank placed at backyard of ZL3

## **Appendix E1-Laser Safety and Operation Procedures**

### **DANGER: INVISIBLE LASER RADIATION**

Class 4 – High Power Lasers are safety and fire hazards. Take necessary precautions when working with the laser to avoid accidental exposure to both direct and reflected beams. Severe eye or skin damage may result from diffuse or specular beam reflections. Infrared radiation passes easily through the cornea and when focused on the retina can instantaneously cause permanent damages. Below two laser models are equipped with the current system.

1. Quanta-Ray GCR-series Nd:YAG Laser

### **DANGER: HIGH VOLTAGE**

The operating conditions of the laser head and power supply require electrical circuits to operate at lethal voltage and current levels. When possible, it is important to disconnect the power line to the power supply before removing protective covers. A bleed off time of 10 minutes is recommended. However, if the covers must be off when operating the laser, be extremely careful to avoid contact with high voltage terminals and components.

### **Precaution for Safe Operation**

1. Wear Personal Protective Eyewear (PPE) at all time – Eyewear selection will depend on wavelength and intensity of radiation. Proper eyewear is available in the Lab 121A for this type laser; 1064nm OD 5+, 532nm OD 6+, and 266nm OD 6+. Also, Proper lab coats, gloves, and respirators are available in the Lab 121A.
2. Keep protective cover on the laser head always.
3. Avoid looking at the output beam.
4. Avoid wearing reflective jewelry.
5. Operate the laser at the lowest beam intensity possible – given the requirements of the operation.
6. Operation in the “long pulse” mode whenever possible.
7. Avoid blocking the output beam or its reflection with any part of the body.
8. To avoid damage to the laser, minimize back-reflections of its output beam.

## Test Procedure

Step #	Action
<b>Pre-test procedure</b>	
<b>Safety</b>	
1	Turn on laser warning lights outside both doors of 121A.
<b>Start-up laser (Quanta-Ray laser)</b>	
2	Turn on tap water valve to laser for external cooling, it is the one by the corner (water pressure should be around 40 psi, usually open already)
3	Turn on SLOWLY N2 to laser
4	Make sure N2 flow rate is around 0.03 scfh (Floating around zero). Never operate the laser without N2 flushing.
5	On the remote, turn the LAMP ENERGY knob to START
6	Check cable connections. Match colors between cables and cable plugs, remember for pool both cables should be black. For PIV, one should be yellow and the other green.
7	Check the power supply front panel CIRCUIT BREAKER is turned on
8	Turn on the power supply from front panel KEY switch
9	Set the remote REP RATE SOURCE to EXT
10	Set the remote Q-SWITCH MODE to EXT
11	Set the remote INT/COMPUTER to INT
12	Set the remote LAMP ON/INHIBIT to LAMP ON
13	Verify all covers are on
14	Temporarily press the ENABLE switch (if the laser does not start press on STOP and try again)
15	Warm up the laser for 15 minutes
<b>Optics Cleaning</b>	
16	Use the squishy air blower to remove dust from all the lens to be used
17	Fold a cleaning tissue and wet it with 2-3 drops of methanol
18	While holding the tissue with the scissors gently clean one by one all the lenses. Remember to wipe the lens only in one direction.
19	Change the tissue or the side every time you clean a new lens (Pay greater attention to clean the center of the lens). Make sure the lens is clean by illuminating it with a flashlight.
<b>Software</b>	
20	Turn on the computer for the laser
21	Turn on the Synchronizer LaserPulse
22	Turn on the software "Insight" and open "default configuration" under the tab "experiment"
23	Set TRIGGER or FLAME STRADDLE mode and SEQUENCE mode
24	Set the number of sequences that you want and save to disk, click apply.
25	Click the laser shooting button two times
26	Slowly increase OSC knob (or AMP or both based on required ignition energy) under LAMP ENERGY at the remote to attain the required energy level.

27	Once you check there is a spark, Click laser stop button one time. Then, Q-switch will be off and flash lamps will keep running
<b>Test procedure</b>	
<b>A measurement</b>	
28	Click in the camera button to start capturing images.
29	Save the images after capture completed.
<b>Shut down procedure</b>	
<b>Shut-off laser</b>	
30	Block the laser beam path with a beam trap (or a laser shield)
31	Click laser shooting button once. The laser will be firing
32	Reduce slowly the laser power to zero by turning LAMP ENERGY control to START
33	Click laser stop button twice
34	Turn off the computer and the Synchronizer LaserPulse
35	Maintain the laser in the current status for 30 minutes to cool down the flashlamps, the rod, and the crystal
36	After 30 minutes, press the STOP button at the remote
37	Turn off the power supply front panel KEY switch
38	Leave CIRCUIT BREAKER as turned on. This keeps watching the crystal's temperature inside the laser
39	Leave the N2 flowing for 24 hr to allow further cooling.
<b>Safety</b>	
40	Turn off laser warning lights
41	After 24 hr, return to the lab and close the N2 flow.

## MAINTENANCE

1. Allow a small N<sub>2</sub> purge flow through the laser head to maintain a positive pressure inside. This will prevent the soot particles floating around in the lab from entering the head and getting deposited on the optics. **FAILURE TO DO THIS MAY RESULT IN THE OPTICAL LENSES GETTING CRACKED WHEN OPERATING THE LASER.**
2. Circulate water through the system for 30 minutes every week when the laser is not in use. Failure to do this may result in the flashlamp and electric component inside laser head getting damaged when operating the laser.

## CAUTION

Do not place anything on top of the laser head cover and/or close the flap of the head forcefully. There is very little clearance between the cover and the horizontal lever that controls the alignment of the HG crystal and doing so might cause the laser to go out of alignment.